



**EXPERIMENTAL AND NUMERICAL INVESTIGATION OF
AERODYNAMIC PERFORMANCE FOR AN EJECTOR –
SHROUDED HORIZONTAL AXIS WIND TURBINE**

THESIS

**SUBMITTED TO THE DEPARTMENT OF MECHANICAL
ENGINEERING TECHNIQUES OF POWER
IN PARTIAL FULFILLMENT OF THE REQUIREMENTS FOR
THE DEGREE OF MASTER THERMAL TECHNOLOGIES
IN MECHANICAL ENGINEERING TECHNIQUES OF POWER (M.TECH.)**

BY

Mohanad Mohammed Naji

(B.Sc. in Mechanical Engineering 2016)

Supervised by:

Dr. Balasem Abdulameer Jabbar Al-quraishi

2023 October

بِسْمِ اللَّهِ الرَّحْمَنِ الرَّحِيمِ

﴿ اقْرَأْ بِاسْمِ رَبِّكَ الَّذِي خَلَقَ (١) خَلَقَ الْإِنْسَانَ مِنْ

خَلْقٍ (٢) اقْرَأْ وَرَبُّكَ الْأَكْرَمُ (٣) الَّذِي عَلَّمَ بِالْقَلَمِ

(٤) عَلَّمَ الْإِنْسَانَ مَا لَمْ يَعْلَمْ (٥) ﴾

صَلَّى اللَّهُ عَلَى الْعَلِيِّ الْعَظِيمِ

سورة العلق : الآية ١-٥

Supervisor Certification

I certify that this thesis entitled " **Experimental and Numerical Investigation of Aerodynamic Performance For an Ejector –Shrouded Horizontal Axis Wind Turbine**" was prepared under my supervision at College of Engineering /University of Anbar in partial fulfillment of the requirements for the degree of Master of Science in Applied Mechanical Engineering.

Signature:

Dr. Balasem Abdulameer Jabbar Al-quraishi

Supervisor

// 2023

In view of the available recommendation, I forward this thesis for debate by the Examining Committee.

Signature:

Asst.Prof. Dr. Adel A. Eidan

Head of Mechanical Eng. Tech of Power Dept.

Date: / / 2023

Linguist Certification

This is to certify that I have read the thesis titled “**experimental and simulation study the aerodynamic performance of an ejector - shrouded horizontal axis wind turbine**” and corrected any grammatical mistake I found. The thesis is therefore qualified for debate as far as language is concerned.

Signature:

Date: / / 2023

Committee Certificate

We certify, as an Examining Committee, that we have read this thesis entitled "**Experimental and Simulation Study the Aerodynamic Performance of An Ejector -Shrouded Horizontal Axis Wind Turbine**" and examined the student "Mohanad Mohammed Naji" in its content and what related to it, and found it adequate for the standard of a thesis for the degree of Master of Science in Mechanical Engineering.

Asst. Prof. Dr. -----

(Chairman)

// 2023

Asst. Prof. Dr. -----

(member)

//2023

Asst. Prof. Dr. -----

(member)

//2023

Dr. Balasem Abdulameer Jabbar Al-quraishi

(Supervisor and Member)

//2023

Approved by Engineering Technical Collage of Najaf

Asst. Prof. Dr. Adel A. Edan **Prof. Dr. Hassanain Ghani Hameed**

Head of the Mechanical Eng. Depart.
Engineering

/ /2023

Acting Dean of the College of

/ /2023

Declaration

I hereby declare that no portion of the work referred to in the thesis has been submitted in support of an application for another degree or qualification to this or any other university or other institutes.

July 2023

Mohanad Mohammed Naji

Acknowledgment

First of all, thanks to the great merciful ALLAH who gives me health, strength, and patience to accomplish this study... (**Alhamdulillah**)

I would like to express my deep thanks and sincere gratitude to my supervisor **Dr. BALASEM ABDULAMEER JABBAR** for his assistance, guidance, encouragement, and endless help throughout the steps of this study.

I would also like to thank head of department and all staff of Engineering Technical Department of Power for their assistance in every step of my career in building my dissertation. Sincere thanks are also expressed to the Engineering Technical College of Najaf staff. Special thanks to my friend Dr. Mustafa Al-Maliki for help me.

Mohanad Mohammed Naji

DEDICATION

To the source of pride and inspiration in my life...my father

To the source of love and tenderness... My dear mother

To my dear wife and children

To those whose support surrounded me every moment, my brothers and sisters

To my brother and friend Dr. Mustafa Al-Maliki and his wife

For those who have exhausted me with their love and devotion, my friends

To everyone who taught me

Great thanks to my family for the patience and support.

Finally, I would like to thank everyone who helped me directly or indirectly to achieve this study.

Mohanad Mohammed Naji

ABSTRACT

Wind energy technology, as represented by wind turbines, is one of the most important alternative energy, particularly the horizontal axis wind turbine (HAWT). As wind turbine power a faction to wind speed, so collecting more winds led to increase the power produced this can be satisfy by enclosing HAWT in a shroud . The primary goal of this work is to present and developed a shroud for a small-scale HAWT suitable for a low and medium wind speeds area. The shroud is a diffuser, with involved the HAWT called diffuser augmented wind turbine (DAWT). The study included two phases to improve performance; First, development of a diffuser design (BD) by improving the geometrical parameters in order to compact it to get Optimum design of flanged diffuser (OFD) model. The second phase, a diffuser with ejector has been presented by attaching the Optimum design diffuser without flange (OD) to an ejector for getting a shroud which has been called ODE model. The development of diffuser model carried out using CFD simulation based on the $k-\omega$ SST that validated experimentally. By combination the OFD and ODE with a rotor, produced a two wind turbines models these are FDAWT model and ESAWT model, respectively. The experimental study was conducted in an open-loop wind blower has been manufactured. Power, torque, and aerodynamic coefficients, for evaluate the performance. The study was revealed the FDAWT that have a diffuser with a flange angle of 50° (OFD) outperformed on the other FD configurations significantly, which satisfied an increase in power coefficient by 91.5 % over BHAWT. As well as, FDAWT with OFD has a simple, inexpensive, and compact when compared to alternative flange designs. The last findings revealed that ESAWT achieved a noticeable increase of power coefficient up to 7.5 % more than FDAWT, hence, the ESAWT model achieved about 98.3% more compare to BHAWT.

CONTENTS

ABSTRACT	I
List of contents	Iii
LIST OF FIGURES	V
LIST OF TABLES	Viii
LIST OF SYMBOLS AND ABBREVIATIONS	Ix

List of contents

CHAPTER ONE		
1.1	Background about wind turbines	1
1.2	Genesis and Development of Wind Turbine	3
1.3	Wind Turbines Classification	4
1.4	HAWT performance parameters	5
1.5	Power Augmentation concepts of HAWT	6
1.6	Diffuser and ejector shroud augmented wind turbine	7
1.7	Problem statement	8
1.8	Objectives of study	9
1.9	Scopes of Study	10
1.1	Thesis outline	11
Chapter Two Literature Review		
2.1	Introduction	13
2.2	DAWT Concept	14
2.2.1	ESAWT concept	18
2.2.2	The evolution of Diffuser geometrical design	21
2.3	Summary	29
Chapter Three Methodology		
3.1	Introduction	31
3.2	Fabrication of the Low-Speed Blower (LSB)	33
3.3	Fabrication of diffuser (base design model)	35
3.4	Simulation work	36
3.4.1	Simulation of the diffuser model	36
3.4.1.1	Grid independence test for diffuser domain	
3.4.1.2	Boundary conditions of diffuser domain	
3.4.2	Develop the Diffuser's Geometrical Specifications	39
3.4.3	Optimum Diffuser with Ejector ODE	42
3.4.4	Rotor model	45
3.5	Experimental work	49
3.5.1	Fabrication of Medium Speed Blower (MSB)	49
3.5.2	Fabrication the ODE model	50
3.5.3	Fabrication the Load control panel	51
3.5.4	Experimental setup for (BHAWT, FDAWT, and ESAWT)	52
3.6	Wind turbine performance and power calculations	54

Chapter Four Result and discussion		
4.1	Introduction	57
4.2	Diffuser results for OFD model	57
4.2.1	Effect of flange angle on velocity ratio	58
4.2.2	Effect of diffuser flange height	59
4.3	Comparing of BD and OFD models	60
4.3.1	Results of ODE	62
4.3.2	Visualization of diffuser models	63
4.4	Validation of the diffuser models	67
4.5	Experimental analysis of FDAWT and ESAWT	69
4.6	Evaluation of mechanical torque	71
4.7	Evaluate of aerodynamic coefficients	73
4.8	Simulation evaluation the shrouded turbines performance.	76
4.9	CFD Simulation validation for the models	80
4.10	Summary	81
5	Chapter Five Conclusion and Recommendations	82
5.1	Introduction	83
5.2	Conclusion	83
5.3	Contribution of the Study	85
5.4	Suggestions for future work	85
APPENDIX A	List of Publications	
APPENDIX B	Table 1 and Table 2	
APPENDIX C	Velocity contour of geometrical diffuser Parameters	
APPENDIX D	Visualization of (BHAWT, FDAWT and ESAWT)	
APPENDIX E	The specification of measurements equipment	

LIST OF FIGURES

Figures	Name	page
Figure 1-1	Wind farmer [9]	2
Figure 1-2	Global wind power capacity and yearly additions, 2012-2022[10]	3
Figure 1-3	Typical Wind turbine classification based on orientation and rotor axis of rotation [15]	5
Figure 1-4	The power coefficient (C_p) as a function of tip speed ratio (γ)	6
Figure 1-5	Shrouded horizontal axis wind turbine: (a) DAWT, (b) ESAWT [17, 18]	8
Figure 2-1	Flow around a wind turbine [20]	14
Figure 2-2	Artist interpretations of BAW. From left to right: beside a building, between airfoil-shaped buildings (visualization Lourens Aaden, DHV), and in a building duct [25].	16
Figure 2-3	One-stage HAWT with a shroud and lobed ejector [32].	20
Figure 2-4	Diffuser (a) without inlet shroud (b) with inlet shroud [35].	21
Figure 2-5	Design Diffuser and flange with simulation [36].	22
Figure 2-6	Different models of the diffuser (a) Plane diffuser, (b) Plane diffuser with inlet shroud, (c) Flanged diffuser, (d) Flanged diffuser with Inlet Shroud [37]	23
Figure 3-1	Present work flow chart	32
Figure 3-2	Low-Speed Blower with its compounds	33
Figure 3-3	LSB compounds with dimensions	34
Figure 3-4	Stages of manufacturing LSB and testing of BD model.	34
Figure 3-5	The BD during the test	35
Figure 3-6	Computational Domain of BD model	37
Figure 3-7	Mesh Generation for BD model	37
Figure 3-8	Skewness and orthogonal mesh spectrum [62]	39
Figure 3-9	Optimum design of flanged diffuser OFD	42
Figure 3-10	Mesh of Optimum design of flanged diffuser with domain	42
Figure 3-11	Optimum diffuser with ejector ODE	44
Figure 3-12	Mesh of Optimum diffuser with ejector ODE	44

Figure 3-13	Fan reverse engineering process	45
Figure 3-14	Details of the fan.	46
Figure 3-15	Procedures of CFX for ESAWT	48
Figure 3-16	Mesh of ESAWT	48
Figure 3-17	Medium Speed Blower with its compounds	49
Figure 3-18	Stages of fabrication of the MSB.	50
Figure 3-19	Stages of fabrication of ODE model	50
Figure 3-20	The load control board for calculating turbine power	51
Figure 3-21	Virtual diagram of LSB rig for empty diffuser testing	52
Figure 3-22	Virtual diagram of MSB for testing of FDAWT and ESAWT	53
Figure 3-23	Actual MSB for Experimental test of FDAWT and ESAWT	53
Figure 4-1	History of Optimization Diffuser	57
Figure 4-2	Effect of flange angle on velocity ratio.	58
Figure 4-3	Effect of flange height on the mean entry velocity at a flange angle of 50 degree	59
Figure 4-4	position of Pitot tube for readings taken at each section of the BD model	60
Figure 4-5	position of Pitot tube for readings taken at each section of the Optimum research diffuser.	61
Figure 4-6	Comparison between the two diffuser models	62
Figure 4-7	Velocity ratio for different ODE models	63
Figure 4-8	Velocity contours at upstream wind flow of 5 m/s for (A): BD, (B): OFD, (C): ODE	64
Figure 4-9	Velocity streamlines at upstream wind flow of 5 m/s for (A): BD, (B): OFD, (C): ODE	65
Figure 4-10	Pressure contours at upstream wind flow of 5 m/s for (A): BD, (B): OFD, (C): ODE	66
Figure 4-11	Validation of OFD and ODE models in range of wind velocity	68
Figure 4-12	Comparing of max power output for (BHAWT, FDAWT, and ESAWT) in terms of rotational speed	70
Figure 4-13	Comparing of max power output for (BHAWT, FDAWT, and ESAWT) in terms of wind velocity.	71
Figure 4-14	Comparing of max torque output for (BHAWT, FDAWT, and ESAWT) in terms of wind velocity	72

Figure 4-15	Comparing of max power coefficient for (BHAWT, FDAWT, and ESAWT) in terms of wind velocity	72
Figure 4-16	Power coefficient's validity as a function of tip speed at $V = 5$ m/s.	75
Figure 4-17	Power output validity as a function of rotational speed at $V=5$ m/s	76
Figure 4-18	Power coefficient's validity as a function of tip speed ratio at $V = 5$ m/s	78
Figure 4-19	power output validity as a function of rotational speed at $V=5$ m/s	79
Figure 4-20	Torque coefficient's validity as a function of tip speed ratio at $V=5$ m/s.	79
Figure 4-21	Validation of power coefficient as a function of tip speed at $V_{\infty}= 5$ m/s	80

LIST OF TABLES

Table	Name	Page
Table 2-1	shows the summary of DAWT for the previous literature	24
Table 2-3	The summary of ESAWT for the previous literature	27
Table 3-1	Statistic grid independence for 3-D diffuser domain	38
Table 3-2	The achieved values of (ϵ) as a function of the geometrical parameters of an empty flanged diffuser	40
Table 3-3	The OFD model with different ranges of flange angle.	41
Table 3-4	The achieved values of (ϵ) as a function of the geometrical parameters of an empty flanged diffuser	43
Table 4-1	The diffuser was specified by the variable values.	57
Table 4-2	Comparison of factors that distinguish two forms of diffuser.	62
Table 4-3	The measured wind velocity values for diffuser configurations	68
Table 4-4	Experimental the performance results of BHAWT, FDAWT and ESAWT	70
Table 4-5	BHAWT Torque, Power and Power Factor Data at V_{∞} of 5 m/s	74
Table 4-6	FDAWT Torque, Power and Power Factor Data at V_{∞} of 5 m/s	75
Table 4-7	BHAWT Torque, Power, and Power coefficient Data at V_{∞} of 5 m/s	75
Table 4-8	FDAWT Torque, Power, and Power coefficient Data at V_{∞} of 5 m/s	78
Table 4-9	ESAWT Torque, Power, and Power coefficient Data at V_{∞} of 5 m/s	78

LIST OF SYMBOLS AND ABBREVIATIONS

Symbols	Meaning	Units
C_T	Torque coefficient for bare turbine	-
Ω	Angular velocity of the rotor	rad / s
P	Output power for the bare turbine	W
T	Rotor torque	N.m
R	Radius of the turbine	m
Re	Reynolds number	-
V_1, V_2	Wind velocity at rotor plane	m/s
V_3	Wind velocity at diffuser exit	m/s
V_∞	Upstream wind velocity	m/s
l	Shroud length (inlet section)	m
α	Shroud angle	degree
Γ	Flange angle	degree
θ	Diffuser angle	degree
H	Flange height	m
D	Diffuser diameter	m
Dr	Rotor diameter	m
L	Diffuser length	m
ϵ	Ratio of maximum axial to upstream wind velocity in the diffuser	-
η_c, η_g	Conversion and generator efficiency	-
λ	Tip speed ratio (TSR)	-
μ	Dynamic viscosity of air	kg /m. s
ρ	Air density	kg/ m^3
$\bar{\omega}$	Standard deviation	-

σ	Accuracy of measurements	-
A	Swept area	m^2
BEM	Blade element momentum theory	-
C_p	Power coefficient	-
I	Current	A
V	Voltage	V

Symbols	Abbreviations
BD	Base design model
BHAWT	Bare horizontal axis wind turbine
CFD	Computational fluid dynamic
DAWT	Diffuser augmented wind turbine
EFD	Empty flanged diffuser
ESAWT	Ejector Shroud Augmented Wind Turbine
ETCN	Engineering Technical College of Najaf
EXP	EXPERIMENTAL
FD	Flanged diffuser
FDAWT	Flanged diffuser augmented wind turbine
LSB	Lower Speed air Blower
MSB	Medium Speed Blower
NACA	National Advisory Committee for Aeronautics
ODE	Optimum Diffuser with Ejector
OFD	Optimum design of flanged diffuser
OD	Optimum design diffuser without flange
RPM	Revolution per minute
SIM	SIMULATION

SAWT	Shroud Augmented Wind Turbine
SST	Shear stress transport
TSR	Tip speed ratio

CHAPTER ONE

INTRODUCTION

1.1 Background about wind turbines

Wind energy is one of the most important renewable energy sources due to its low environmental impact and easy access. Compared to carbon-emitting fossil resources, wind energy is renewable and readily available to the general public, making it an important green energy source. Therefore, it is necessary for energy production to keep up with these rising needs. It is imperative to look for alternate and sustainable energy sources due to the quick depletion of fossil fuels.

Nowadays, the demand for energy is increasing dramatically and is increasing in all parts of the world, and the reason for this is the advancement of technology in all fields. It has become necessary to search for an inexhaustible virtual resource [1-4]. From this standpoint, compared to conventional energy sources, wind power systems, symbolized by wind turbines, have long piqued the curiosity of scientists and researchers. The flow of wind through the turbine rotor produces mechanical energy, which may be used in a variety of purposes, namely the generation of electricity, but compared to the growing global energy demand, wind power is still very poor, mainly due to the Betz limit and the high cost of turbines [5].

Wind power is generally known to grow with the cube of wind velocity. The greater power production is due to the increased flow velocity of the wind across the rotor. [6, 7]. Generally, wind vitality was used in windmills as well as within the maker of sails and wind pumps, and nowadays it is utilized to produce power through wind turbine ranches that are associated to the electric control transmission organize as show in Figure 1-1.

Unused coastal wind turbine ranches are cheaper than gas or coal plants. This asset was researched since it can make our world superior and cleaner. It will to boost financial and residential development. The turbines are a productive speculation in expanding the country's GDP. So far, analysts have been working on increasing capacity, so that more wind power can be used during times when there isn't much wind [8].



Figure 1-1: Wind farmer [9]

1.2 Genesis and Development of Wind Turbine

Since the first century, when wind-powered grinding stones were used, wind power has had a long history. Windmills were first employed in Persia in the ninth century, then in Northern Europe in the 12th century. Because wind turbines are revolving equipment that converts wind energy into mechanical energy, they are the most common method of utilizing wind energy to produce electricity. Researchers are currently working on increasing the capacity of wind energy, so that wind energy can be stored for times when there is not much wind[10-13]. Global wind power capacity has grown significantly over the past decade, from 283 GW in 2012 to 906 GW in 2022. Each year, new capacity has been added to the grid, with annual addition 77 GW added in 2022, as shown in Figure 1-2[10]. The growth in wind power capacity has been driven by a combination of factors, including declining costs, policy support, and increasing demand for renewable energy.

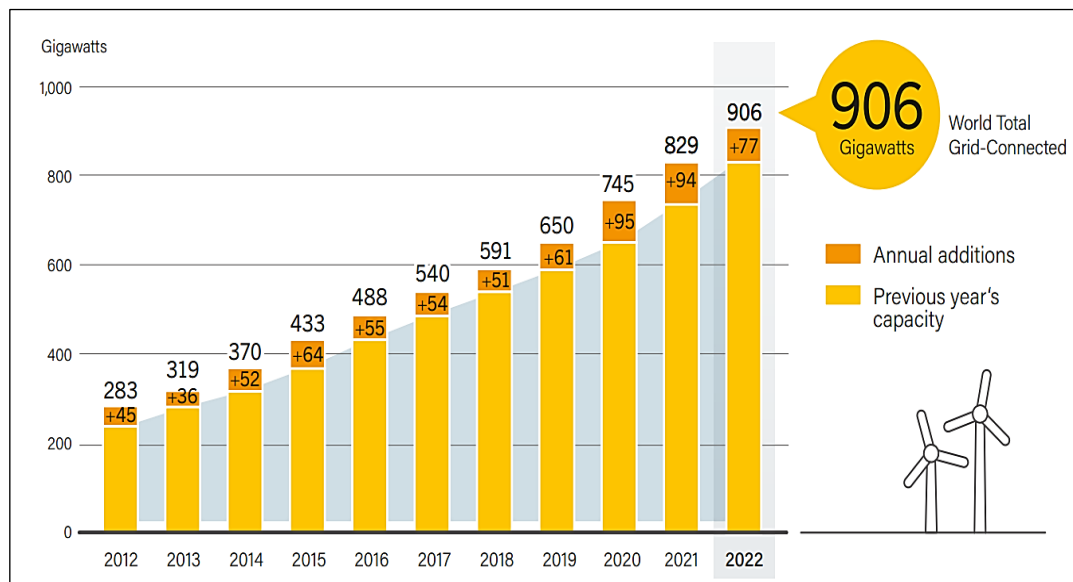


Figure 1-2: Global wind power capacity and yearly additions, 2012-2022[10].

1.3 Wind Turbines Classification

A windmill or turbine is an extended turbine machine that operates at relatively low speeds. To get the highest performance, wind turbines have gone through a series of upgrades and great innovation in their design. Wind turbines are divided into two types. The first is known as a horizontal axis wind turbine (HAWT) It is one of the most common machines, and the concept of using HAWT [11]. HAWT has undergone several procedures and improvements aimed at obtaining the best performance.

HAWT uses pneumatic blades mounted on the rotor, which can be placed as either one or more blades, depending on the design of the turbine. The function of these purpose of the blades is to harvest energy from the wind. The rotor axis is parallel to the ground and operates and rotate as a result of aerodynamic lift. Wind turbines with the horizontal axis receive a lot of attention, research, and development by researchers [12]. HAWT Because of its design, which allows it to fully rotate the blades when positioned in wind flow, it is more efficient than Vertical Axis Wind Turbine (VAWT) for harvesting energy from wind [13].

VAWT is one that rotates perpendicular to the wind direction. In current, the tower's central axis is linked to a speed-escalating gearbox. This shaft drives a generator, which transforms the rotor's mechanical power to electrical power. There are various VAWT developments in which power is created by either drag (Savonius) or lift (Darrieus) [14], as shown in Figure 1-3 [15].

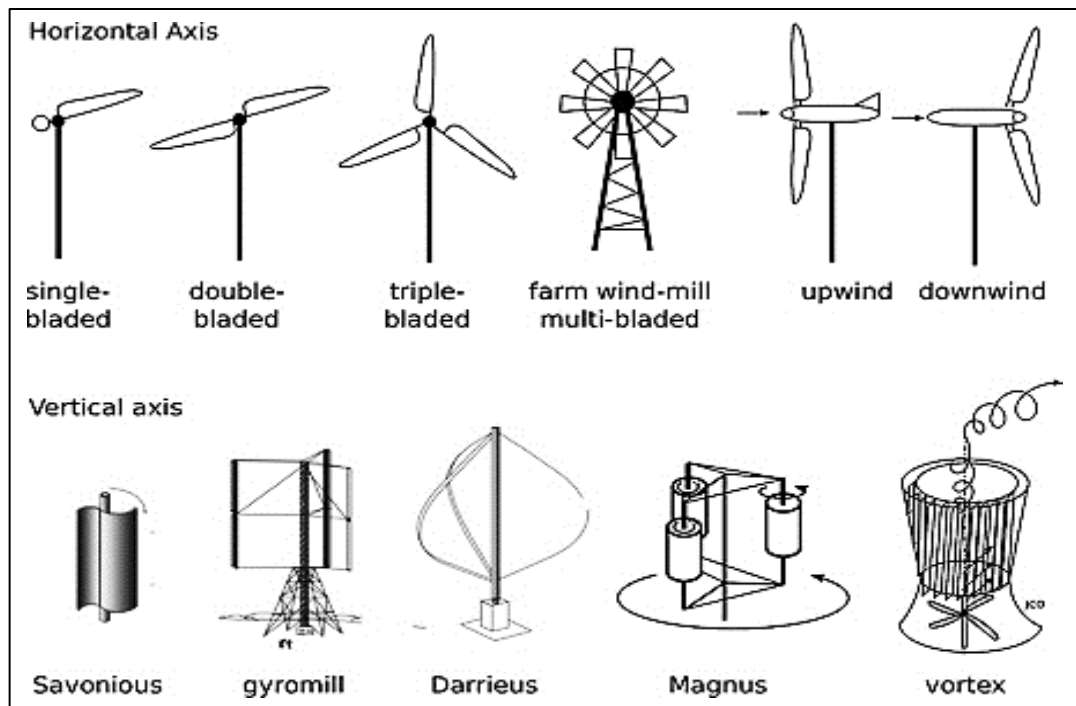


Figure 1-3: Typical Wind turbine classification based on orientation and rotor axis of rotation [15]

1.4 HAWT performance parameters

Due to its effective performance parameters, HAWT are commonly employed to harvest wind energy. The speed ratio (λ), which is defined as the ratio of the rotor tip speed to the wind speed, is a crucial quantity. This parameter is essential for establishing the HAWT's efficiency.

A greater speed ratio enables the rotor to extract more energy from the wind, resulting in more power production. Another important performance metric is the power coefficient (C_p), which indicates the conversion efficiency of wind kinetic energy to electrical power. It is the ratio between the actual power extracted by the turbine and the maximum power that can be extracted from the available wind resource.

A turbine with a higher power coefficient is capable of converting a greater proportion of the wind's energy into usable power. It is essential to optimize both the speed ratio and the power coefficient when developing efficient HAWT capable of producing the highest amount of electricity while reducing energy losses. Figure 1-4 represents a typical plot of power coefficient vs tip speed ratio (C_p , TSR), where (TSR: is the ratio of velocity at rotor tip to upstream wind velocity). The Blade Element Momentum concept, which was first proposed by Glauert in 1935 [16], serves as the basis for the aerodynamic analysis of wind turbine designs.

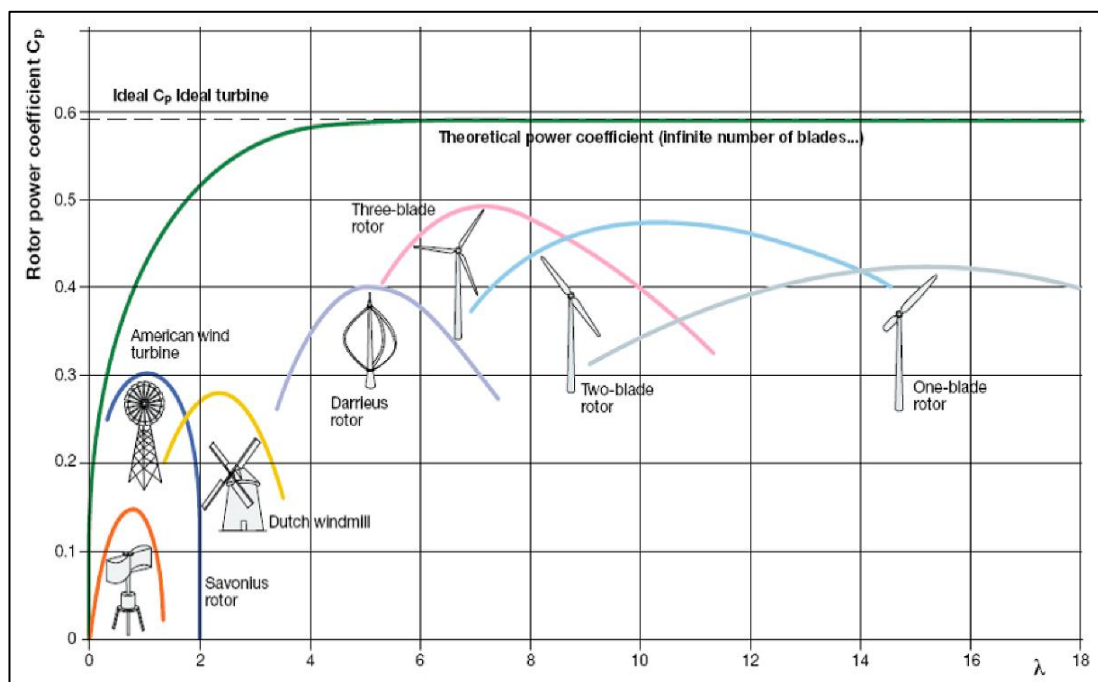


Figure 1-4: The power coefficient (C_p) as a function of tip speed ratio (λ) several types of wind turbines [14]

1.5 Power Augmentation concepts of HAWT

The most activity method to augment more power from HAWT by shroud it. It can be called Shroud Augmented Wind Turbine (SAWT). The Venturi effect explain that: when a fluid travels through a constriction, it experiences a decrease in fluid pressure and an increase in fluid velocity as a result. The diffuser, whose throat a rotor is positioned in, produces the contraction for an enhanced horizontal axis wind turbine. The diffuser cross section perpendicular to the axisymmetric axis, or "throat" plane, is the plane where the area inside the diffuser is least. Betz researched the economic feasibility of enhanced HAWTs in comparison to naked HAWT in the 1920s, which can be credited to the beginning of modern theoretical study. Further studies were undertaken by English and Japanese teams in the 1950s, confirming and quantifying the possibility of the increased mass flow down the diffuser throat [17].

The DAWT concept has drawn unwavering attention as a specialized thought that dominated the contemporary HAWT over the next years up to the present. Because diffuser wind masses and structural cost grow dramatically with size due to advances in analytical modeling, numerical simulation, and lessons gained from failed commercial endeavors like Vortex Energy Limited, DAWT cannot compete with current HAWT on a wide scale. As a result, small scale is now the main focus. Many manufacturers of home wind turbines have now commercialized DAWT. These designs are single-ducted, and some of them are double-ducted Ejector Shroud Augmented Wind Turbine (ESAWT) to enable external flow to enter through the inner side duct and increase the boundary layer in the pressure gradient that develops behind the rotor[18].

1.6 Diffuser and ejector shroud augmented wind turbine

When compared to other notions, the DAWT and ESAWT theories offer better power augmentation[18]. They hardly differ from one another at all. The diffuser geometries and shape, the tow combinations' performance is affected by the blade airfoils and the wind conditions at the mounting site. The primary factors influencing how well DAWT and ESAWT function aerodynamically are the diffuser's geometric characteristics. Diffuser geometrics are defined by dimensions of intake diffuser diameter (D), which are associated by rotor diameter (D_r), diffuser length (L), diffuser angle (θ), flange height (H), and flange angle (α). (if it present), as well as shroud length (inlet section) (l) and shroud angle (γ) as shown in Figure1-5 for (a) DAWT configuration[17]. While (b) show the geometrical parameters for ESAWT[18]. Which are almost the same as those of DAWT with the slight difference that there is no flange and the addition of an ejector at the exit DAWT. Each of these engineering characteristics has an impact on the performance of DAWT and ESAWT, either directly or indirectly.

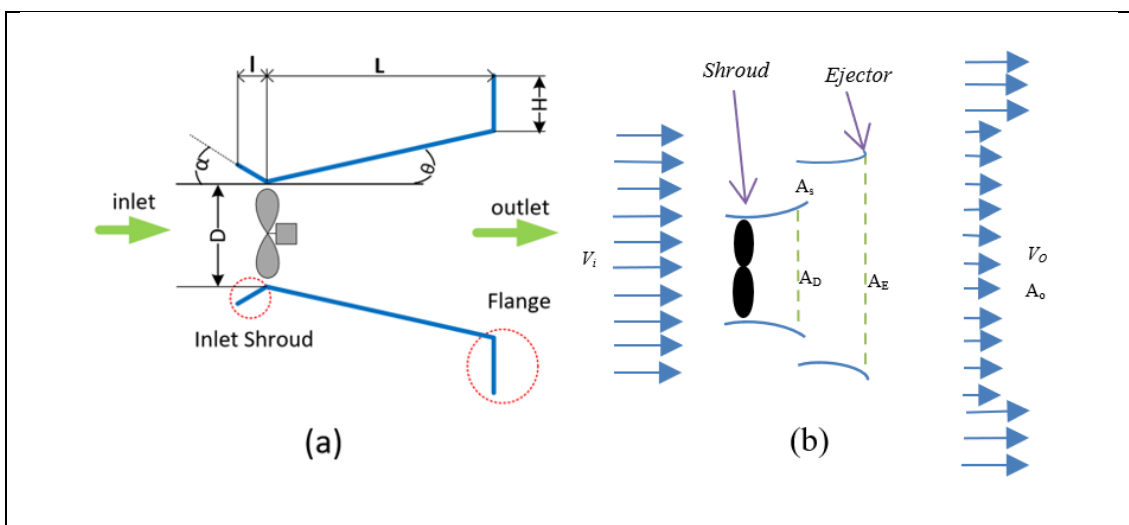


Figure1-5: Shrouded horizontal axis wind turbine: (a) DAWT, (b) ESAWT[17, 18]

1.7 Problem statement

Wind energy is one of the most important sources of renewable energy in the world in the production of electric power. However, they are of little use in areas with low wind speed levels, in other words, wind turbines require open areas to operate efficiently. This necessitates installing wind turbines away from cities, especially in case of HAWT which is characterized by high efficiency compared to other types of wind turbines. Placing HAWT inside a duct (Diffuser) improves the efficiency of wind power production dramatically and this makes it easy for HAWT to be used in urban areas as well as areas with low wind speeds. ESAWT can increase the available pressure drop across the turbine, resulting in drawing more flow, and improving the produced aerodynamic power. A lot of researchers focus on improve the power produced from DAWT by developed the geometrical parameters of the diffuser [1-5]. The researchers Yu Yu et al [19] in there numerical study focus on develop a model of DAWT throw by a ranged of some geometrical parameters of diffuser where they got an increasing of power coefficient up to 55% compare to bare HAWT without mention any effect on velocity ratio (ϵ) at rotor plane. This study continued that effort and focus to curtailment the overall BD size by implementing a numerical approach to discover optimum design parameters (L/D , θ , H/D and γ) in 3D models to achieve the best increment in velocity ratio value at rotor position. Then developing the last design of DAWT to present model of ESAWT. However, obtaining the modified optimum design for ESAWT achieves optimum augmentation in turbine power.

1.8 Objectives of study

1. To develop DAWT performance by modifying geometrical parameters of diffuser length, diffuser angle, flange height, and shroud angle
2. To enhance the performance of modified DAWT by add an ejector at the outlet to present ESAWT model.

1.9 Scopes of Study

1. Fabrication of base design model of diffuser (BD) based on the previous study and testing it using low speed blower. And then calculate wind velocity ratio (ϵ) and pressure difference at flow field.
2. Numerical validation of BD model by using ANSYS CFX.
3. Different models of the modified diffuser in terms of (L , Θ , H , α and γ) are considered in 3D CFD, to achieve optimum performance for DAWT and ESAWT.
4. The HAWT rotor is a Fan with four thin blades of 1mm thickness and diameter of 300 mm made from aluminum.
5. The rotor was modeled using reverse engineering technique as same dimensions helping of Solid Work program for simulation purpose.
6. The 3D CFD domains performed for models of BD, OFD, ODE, and rotor using ANSYS CFX with a turbulence model ($k-\omega$ SST).
7. The performance of FDAWT and ESAWT were evaluated in lab field (medium speed blower tunnel) using a board control load to calculate the power, hence validation of the results using the rotor CFX domain.

1.10 Thesis outline

The structure of this thesis, in brief, was composed of the following five chapters:

Chapter 1: This chapter covered the systems, traits, and varieties of wind turbines, particularly the DAWT, the research challenge, and its goals, as well as the ranges and the importance of carrying out the study.

Chapter 2: The primary and most significant portion of this chapter concentrated on several research conducted to develop the performance utilizing the idea of DAWT in several areas, including the diffuser shape, the method used to assess the performance, and the geometrical parameters of the diffuser model.

Chapter 3: This chapter set out the design of the methodological procedures required for research in two approaches, namely simulation and experimental, in which presented methods, strategies, design theories, and methods of calculation.

Chapter 4: The findings from the methodological stage were provided in this chapter. To make the results easier for readers to understand, they were provided in different sections, beginning with an explanation and discussion of the simulation results of the diffuser model's design. Additionally, validation was provided so that the outcomes could be compared.

Chapter 5: The key points of the study were summarized in this chapter, together with its scope, applicability, concluding remarks, and recommendations for future research.

Chapter Two

Literature Review

2.1 Introduction

Nowadays, the demand for energy is increasing dramatically in all parts of the world, and the reason for this is the advancement of technology in all fields. Because of the significant impacts of global warming and the growing depletion of fossil fuels, the research and implementation of renewable, clean energy has become a major. To overcome the present energy issue, numerous alternative energy sources are being investigated. It has become necessary to search for an inexhaustible virtual resource. In this regard, wind energy technologies have emerged as one of the accessible energy sources with the fastest growth rates worldwide, when compared to traditional energy sources. However, in comparison to the expanding worldwide energy demand, wind power remains relatively low, owing mostly to the Betz limit and the expensive cost of turbines [14]. DAWT is one of wind power augmentation systems since, it used a diffuser to shroud turbine rotor.

The flanged diffuser also produces a drop in atmospheric pressure near the diffuser's exit. This causes a speed boost over the bare turbine. As is well known, wind energy is proportional. to the cube of the speed, so the air turbines supported by the diffuser are able to increase the speed significantly, and thus we will reap high energy. The increase in speed is caused by the cover entry efficiency, pressure recovery coefficient, and basic pressure coefficient, all of which are connected to the shroud [19]. This study focused on improving the power of wind turbines by enclosing them within a duct. In addition, reviews on different designs of DAWT, ESAWT from previous studies included numerical and experimental procedures.

2.2 DAWT Concept

Many studies focused on the advantages of enclosing HAWT in a diffuser to form a device called DAWT [20]. The purpose of a diffuser is to boost the power output of a wind turbine by increasing the velocity of the wind as it approaches the rotor. The diffuser with a flange at the exit at the proper height can increase wind velocity when it is augmented by the power of DAWT. The presence of flange creates pressure drop at diffuser outlet due to vortex formation bringing more draw wind to diffuser. A lower pressure would exist at the back of the wind turbine to function as a vacuum, sucking the wind and accelerating it towards the blades as show in Figure2-1. The region surrounding or near the vortex will normally have lower pressure where the vortex will create the suction force. So, increasing wind velocity approaching at turbine rotor.

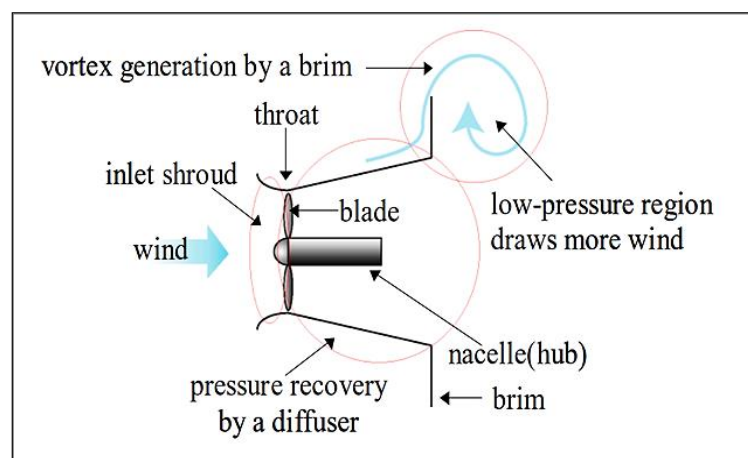


Figure 2-1: Flow around a wind turbine[20]

In previous years, reference was made to reviews recorded in 1956 By Lilley and Rainbird [21]. Where hypotheses concerning the performance of regular windmills vs. covered (tube) windmills were compared. In 1979, the hot topic that took place at the innovative, the development of diffuser-assisted wind turbine engineering was the focus

of the Wind Energy Systems Conference in USA. This conference reached conclusions stating that it is possible to obtain an increase in speed, but the economic application of DAWT is not possible due to the high cost.

Ozer Igra at Ben-Gurion University[22] presented very impressive research in the field of DAWT. It was discovered that for shrouds with effective apex angles greater than 10 deg. Diverting the outside air flow into the shroud's internal boundary layer can result in an increase in r of 20% or more for the examined range of A_e/A_t (shroud without ring-flap).

M. O. L. Hansen Hansen et al[23], simulate the flow through a wind turbine in a diffuser is modeled and validated using an actuator disc CFD model. Furthermore, a 1D analysis shows that the Betz limit can be exceeded by a factor proportionate to the relative increase in mass flow through the rotor caused by the diffuser.

Negin Maftouni and Hoda Parsa[24], present a two different types of wind turbines were studied and analyzed the first type is reinforced with a cover, and the second is naked. The results indicate that the wind turbines covered with a shroud give an increase in energy by 105% compared to the bare.

S. Mertens[25], they published his Ph.D. wind energy conversion in the built environment. It describes the wind resources available in the built environment that can be transformed into electricity by a wind turbine. It focuses on the integration of wind turbine and building in such a way that the building focuses on maximum energy production of the wind turbine. as show in Figure 2-2

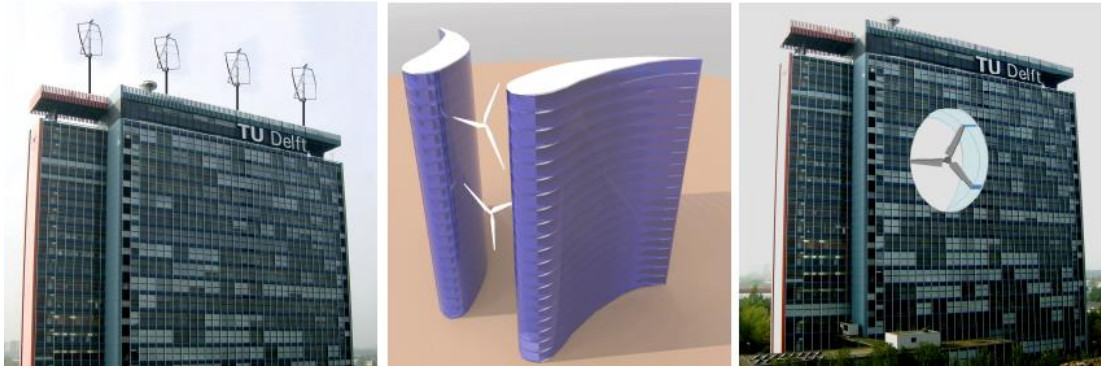


Figure 2-2: Artist interpretations of BAW. From left to right: beside a building, between airfoil-shaped buildings (visualization Lourens Aaden, DHV), and in a building duct [25].

T. Rezek and colleagues[26], they presented an optimization study for building a shrouded turbine diffuser. The goal of the research was to find the geometry of a hydrofoil-shaped diffuser that maximizes a turbine's hydraulic output given a set of constraints. The optimization approach was built using an automated cycle of geometry change, meshing, and CFD analysis of the flow field, which included a loaded diffuser (actuator disk). According to the statistics, the best diffuser has a power coefficient of around 118%. This approach also feeds data into the rotor design process (flow rate and pressure drop).

Y. Y. Maw and M. T. Tun [19], they study the performance of a DAWT with different diffuser shapes. The goal of this study is to employ numerical investigations to create a more efficient diffuser design for a horizontal axis wind turbine. The results indicate that. The performance of new diffuser augmented wind turbine (IND_009) is 50% and 55% higher than the baseline diffuser augmented wind turbine and the horizontal axis wind turbine at rated velocity. The flow visualization of the HAWT, DAWTs are also discussed.

Kosasih and Jafari have designed a wonderful[27], submitted a novel linear wind generator (LWG), is unveiled. The modular and scalable LWG can generate electricity even at low wind velocity conditions, making it an effective and safe power generator in constructed areas. This research demonstrates that Power Window can generate electricity with an acceptable coefficient of performance ($CP \approx 0.15$) in a very low linear velocity ratio ($\lambda \approx 0.2$), which is not possible in most conventional wind turbines of comparable size.

On another side, a wind lens design was established by **M. Takeyeldin, and T. M. Lazim**[28], they study the performance of a horizontal axis wind turbine with a diameter of 0.6 m intended to operate at low Reynolds number is shown in this research. The SD2030 thin airfoil was chosen as a profile section for the turbine blades in this design effort. The Blade Element Momentum (BEM) was used to optimize the taper ratio, section twist angle, and blade angle. The results show that this novel turbine design with the SD2030 airfoil can rotate at a low start-up wind speed of 2.4 m/s, proving that the design is successful and that the turbine is capable of operating at low Reynolds numbers such as 1×10^5 while producing the appropriate output.

Ohya and T. Karasudani[20] introduced a unique wind turbine system that incorporates a diffuser shroud with a wide-rimmed edge and a wind turbine within it in 2010. shows that at the same wind speed and turbine diameter, a shrouded wind turbine with a brimmed diffuser may produce up to two to five times more power than a normal wind turbine. Since a vigorous vortex formation behind the broad brim generates a low-pressure region, more airflow is drawn to the wind turbine inside the diffuser shroud.

also, **M. Lipian et al.[29]**, presented a study to development and validation of a numerical model for the DAWT, a technology aimed at improving wind turbine performance about 40-50%. The model was validated in a wind tunnel before being utilized to improve the diffuser form. According to the findings, DAWT technology has the potential to dramatically boost the power production of wind turbines, perhaps doubling the output when compared to a standard rotor.

Hossam M. El-Bakry et al[30], conducted a test on two models of diffusers. Where the first case was with a dimension of $L/D = 0.15$, while the second case was with a dimension of $L/D = 0.4$, and the angles for both cases were different. The findings indicated that the second model of the diffuser which leads to an increase in power output by 0.26, while the first case had a power of 0.18.

2.2.1 ESAWT concept

There is not much difference between DAWT and ESAWT. The main difference is presented in the ejector at the outlet of a diffuser. Moreover, of limited studies on this topic due to the complex design, but there are some important studies.

F.A. Al-Sulaiman[18], suggest a complete exergoeconomic study of an ejector-augmented shrouded horizontal axial wind turbine was performed. At three ejector inlet area ratios. The cost rate of the electricity generated, exergy loss to cost rate, energetic improvement potential, power produced, and air mass flow rate via the wind turbine are the key exergoeconomic characteristics investigated. The findings demonstrate that the performance of the wind turbine improves as the

ejector inlet area ratio increased, and the cost per kWh of the power produced decreases significantly with wind speed increased from about 2 \$/kWh at 5 m/s to about 0.1 \$/kWh at 15 m/s. On the other hand, the exergy destruction rate is relatively low while the exergy loss is relatively high.

M. Werle and W. Presz Jr[31], they show the new control-volume-based predictions for shrouded propellers have been found to match experimental and computational data, as well as other models. Simple polynomials that can be calculated from the empty shroud's aerodynamic performance serve as the solutions and new correlation parameters. By separating the designs of the shroud and ejector from those of the propeller, the formulation also makes the process of design optimization simpler.

W. Han et al.[32], developed a design concept for a horizontal axis wind turbine with a shroud and a lobed ejector. They employed a one-stage wind turbine with a shroud and a lobed ejector to harness low-speed wind energy, with an efficiency of 66-73% at wind speeds ranging from 2 to 6 m/s. Numerical study was used to validate the suggested wind turbines performance. According to their research, the wind turbine's mass flow was enhanced, resulting in a 240% increase in turbine output. Figure2-3 as you can see fabricating of this structure is so complex.

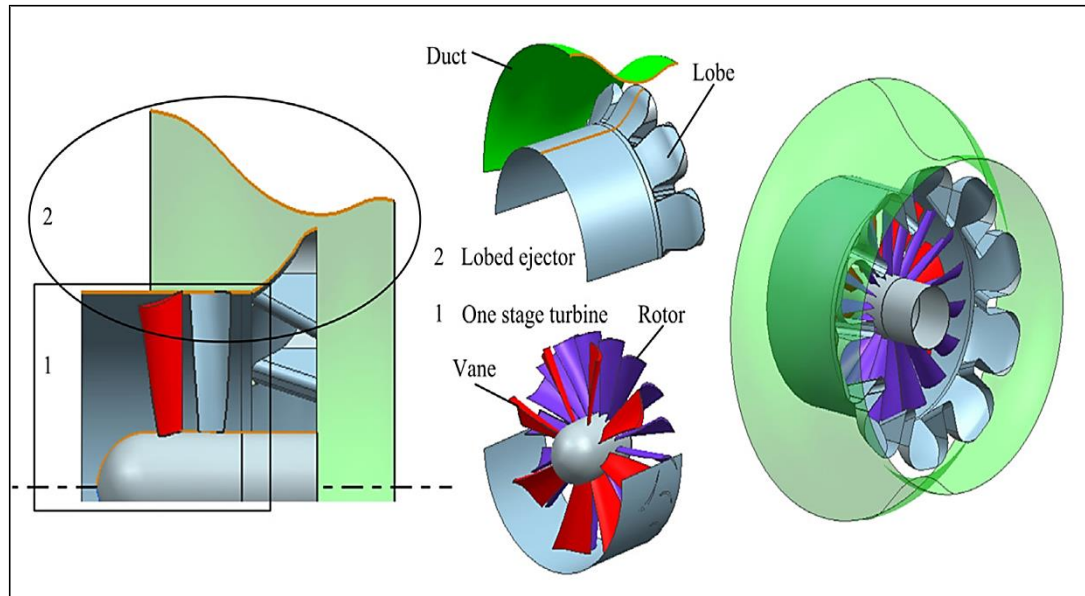


Figure 2-3: One-stage HAWT with a shroud and lobed ejector [32].

R. Schmidt and A. Hupfer[33], in their study at the Institute of Aeronautical Engineering at the Universität der Bundeswehr München focuses on small turbojet engines for unmanned aircraft systems. These engines must meet specific design requirements, such as compactness, reliability, and affordability. However, their low efficiency, high exhaust gas temperature, and loud noise limit their potential use. The ejector nozzle concept offers a solution to these limitations by reducing exhaust gas temperature and increasing thrust. The ejector nozzle has been combined with a special mixer nozzle to enhance performance. In order to optimize the mixing capabilities of the main nozzle, both computational and experimental approaches are applied.

2.2.2 The evolution of Diffuser geometrical design

Indeed, the development of the performance of the shrouded turbine (DAWT and ESAWT) depends on improving the diffuser geometrical design parameters mainly. Recently, DAWT and ESAWT-assisted wind turbines are getting a lot of attention from researchers because of their ability to overcome the Betz limit[34]. It is difficult to list all the research interested in this matter, but the most important and recent studies have been reviewed and due to the design affinity between the two models. Most of the research and studies are presented together in this paragraph.

Riyantoa, etal[35], employed a two alternative DAWT engineering models, as illustrated in Figure 2-4, one without an entrance shroud $L / D = 0.25$ and one with an entrance shroud $L / D = 0.39$. The experiment was carried out in a wind tunnel at a speed of (1-5 m/s). The results revealed that using a diffuser increased the efficiency of wind turbines by 41.1% for the first diffuser and 20.5% for the second diffuser.

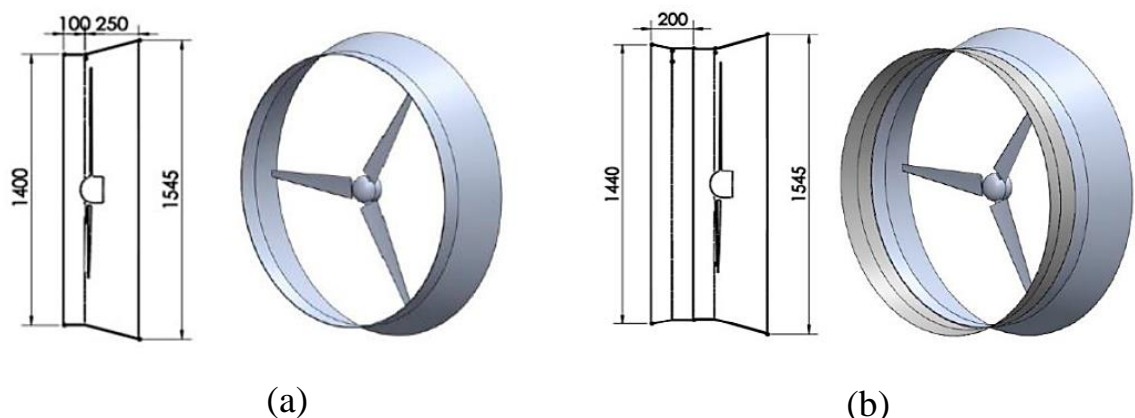


Figure 2-4: Diffuser (a) without inlet shroud (b) with inlet shroud [35].

D. Lokesharun et al. [36], in their study by simulations of diffuser designs were conducted. Using ANSYS Fluent CFD software with a wind inlet velocity of 5 m/s. The outcomes demonstrated that the diffuser with flanges performed at its peak level, with the blades located 0.13 m from the entry of the 1 m long diffuser. The optimized design resulted in a significantly greater generation of power as compared to traditional wind turbines. Shown in Figure 2- 5.

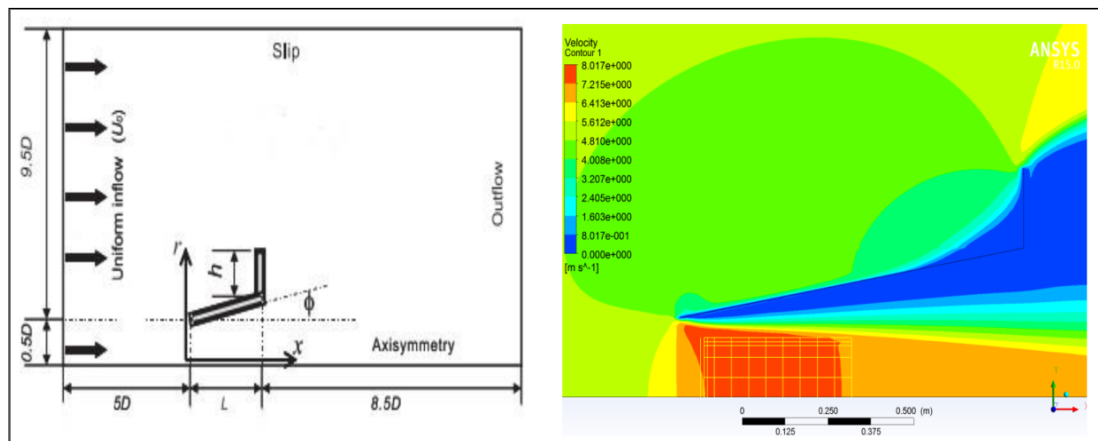


Figure 2-5: Design Diffuser and flange with simulation [36].

Roshan Kumar Chhetri et al.[37], conducted a CFD simulation of four different diffusers design, Plain Diffuser, flanged, with and without inlet shroud Diffuser with geometrical characteristics of Inlet Shroud and ($L/D=0.5$, $\theta =14.5$, $H/D=0.25$, $\gamma =45$, and $l/D=0.111$) as shown in Figure2-6. A comparative analysis of each diffuser was conducted to evaluate velocity increase. The best diffuser, which improved wind velocity by 60% and increased power output by 3.6 times, was discovered to be a flanged diffuser.

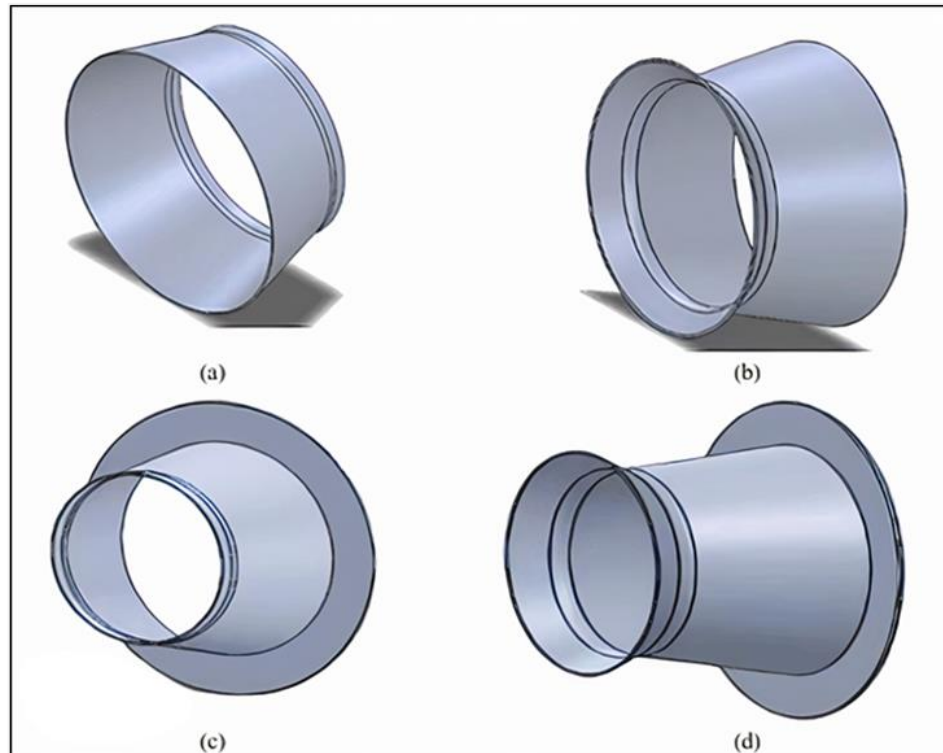


Figure 2-6: Different models of the diffuser (a) Plane diffuser, (b) Plane diffuser with inlet shroud, (c) Flanged diffuser, (d) Flanged diffuser with Inlet Shroud [37]

Takeye et al.[38] presented a CFD study for a DAWT with a lens model of ($L/D=0,226$, $H/D=0.1$, and flange angle in the range of 7, 10, 20, and 30°) at wind velocity of 5m/s. They proved wind lens's usefulness at low wind speeds, where they got an increase in the performance by 30-60% over the bare turbine, especially for flange angle over 10°.

In addition, it has been presented an exhaustive review of contributions in mechanisms of ESAWT and DAWT as summarized in

References	R.M	G. P	Remarks
W.-X. Wang etal.2015[39]	SIM EXP.	$L/D=0.22$ $H/D=1$ $\Theta=Non$ $l/D=Non$	wind turbines with flanged diffusers have substantially higher blade rotational speeds and dynamic strains than those without.

		γ =Non	
H. M. Elbakry et al.2016[30]	SIM	L/D=0.15,0.4 H/D=Non Θ =4,8 l/D=Non γ =Non	The findings indicated that the second model of the diffuser which leads to an increase in power output by 0.26, while the first case had a power ratio of 0.18.
T. A. Khamlaj et al.2018[40]	SIM	L/D=1.25 H/D=0.5 Θ =12 l/D=0.25 γ =Non	The outcomes show that the turbine cover produces excellent performance and a high-power factor.
F. Q. Putra et al.2018[41]	SIM	L/D=0.25,1.25 H/D=0.5 Θ =40,80 l/D=Non γ =Non	The results show that velocity increase reaches up to 2.08 times compared with that of the bare turbine at a wind velocity of 4m/s.
M. I. Maulana et al. 2018[42]	SIM	L/D=2 H/D=0.6 Θ =9 l/D=Non γ =Non	The results showed that increase in wind speed. In terms of the free current, up to 2.15 times.
F. Mardiansah et al. 2018[43]	SIM	L/D=2.5 H/D=0.375 Θ =16 l/D=Non γ =8	The results revealed that the entry speed rose by 85.75 percent when compared to the basic design.
N. A. Pambudi et al.2019[35]	EXP	L/D=0.25,0.39 H/D=Non Θ =16.7 l/D=0.0069 γ =Non	Without shroud. Increase power efficiency 20.5% With an Inletshroud. Increase power efficiency 41.1%
D. Lokesharun et al.2019[36]	SIM	L/D=0.5 H/D=0.2 Θ =12 l/D=Non γ =0	The findings showed that decreased pressure at the diffuser's exit allows the flanged diffuser to boost power output. Additionally, the flange's angle is crucial.
Y. Klistafani et al. 2019[32]	SIM	L/D=7.7 H/D=Non Θ =4 l/D=0.5 γ =0	The best shape is the curved one compared to other shapes, as it achieved a C_p of 84.18% and a suction speed of 9.2 m / s.
S. A. Kale et al. 2019 [44]	SIM	L/D=1 H/D=0.35 Θ =10 l/D=0.15 γ =10	The findings demonstrated that the smallest diameter can yield the maximum speed and a C_p of 1.62.

X. Wang, K. et al.2020[45]	EXP	L/D=Non H/D=Non $\Theta=30$ l/D=Non $\gamma=Non$	The results show an increase in power from 0.38 watts - 0.48 watts.
M. Anbarsooz et al.2020 [46]	SIM EXP	L/D=1.5 H/D=0.5 $\Theta=40$ l/D=Non $\gamma=Non$	The results showed that the flanged diffuser could increase the energy about 3.87 times compared to the HAWT.
S. Surya et al. 2020 [47]	SIM	L/D=0.6-4 H/D=Non $\Theta=Non$ l/D=Non $\gamma=-20$ to20	The results showed an increase in the mass flow rate of 27.4%.
M. Takeyeldein et al 2020[38]	SIM	L/D=0.226 H/D=0.1 $\Theta=7,10,20,30$ l/D=Non $\gamma=0$	Increase C_p by 30-60% at $V=5$, θ over 10
S. K. Thangavelu et al .2020 [48]	SIM	L/D=2 H/D=0.443 $\Theta=12$ l/D=Non $\gamma=14$	The results showed that the diffuser with holes gives an increase in speed of 8.56 m/s over the initial velocity of 4 m/s.
T. Rezek et al .2021[26]	SIM EXP	L/D=0.1,0.137, 0.221,0.37 H/D=0.05,0.10, 0.15,0.20 $\Theta=Non$ l/D=Non $\gamma=Non$	The results revealed a 2–5 increase in energy rate compared to the bare wind turbines
R. K. Chhetri et al.2021 [37]	SIM	L/D=0.5 H/D=0.25 $\Theta=14.5$ l/D=0.11 $\gamma=45$	The results flanged diffuser generates power up to 3.6 times faster than a naked turbine
Y. Y. Mawetet al.2021 [19]	SIM	L/D=1 H/D=0.35 $\Theta=10$ l/D=0.15 $\gamma=0$	The enhanced diffuser (IND-009) achieved 50% higher performance than the basic diffuser design.
A. Susandi et al	SIM	L/D=1.25	The results were that the turbines

2021 [49]		H/D=Non $\Theta=4-16$ l/D=Non $\gamma=Non$	covered with the diffuser produced energy (1.4 - 2.9) times higher than the turbines without the cover
J. R. Vaz et al .2021 [50]	SIM EXP	L/D=1 H/D=Non $\Theta=3.6-4.5$ l/D=Non $\gamma=Non$	The results showed that the maximum difference in speed was about 23.3% at an angle of 4.5 and .1.65% at an angle of 3.6.
A. M. Elsayed 2021 [51]	SIM	L/D=1,4 H/D=0.1,0.4 $\Theta=4.2,16$ l/D=Non $\gamma=-30,15,30$	The results showed an increase in wind speed up to 1.77, as well as an increase in CP from (.76 2 - 26 .5).
K. Watanabe et al. 2021 [52]	EXP	L/D=0.18,1.7 H/D=0.13,0.69 $\Theta=12$ l/D=Non $\gamma=Non$	The results showed a clear increase in the power factor of about 2-5 compared with HAWT.
O. K. J. et al .2022 [53]	SIM	L/D=0.25 H/D=Non $\Theta=12$ l/D=Non $\gamma=Non$	The findings demonstrated that the turbine's location at the diffuser's beginning provides good energy by (20% -14%) compared to where it is at the beginning and conclusion.
B. Heyru et al .2022 [54]	SIM EXP	L/D=1.98 H/D=0.5 $\Theta=10$ l/D=1.5 $\gamma=90$	he results proved that the curved diffuser gives a higher speed than the straight diffuser by 7%
S. Sridhar et al.2022 [55]	SIM EXP	L/D=1.65 H/D=Non $\Theta=15$ l/D=2.7 $\gamma=Non$	The results showed an increase in speed by 46.8% and 27.4% compared to the un-drilled turbine.

NOTE: (R.M) Research method, (EXP) experimental, (SIM) simulation, (G.P)geometrical parameters.

and خطأ! لم يتم العثور على مصدر المرجع. respectively, which illustrated the effects of the most important parameters on wind turbine rotor performance.

Table 2-1: shows the summary of DAWT for the previous literature



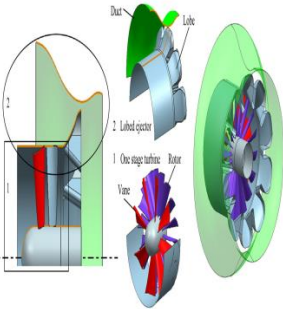
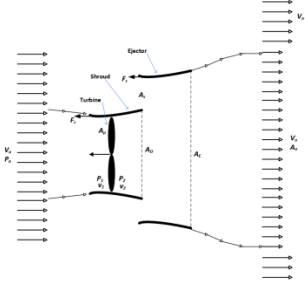

References	R.M	G. P	Remarks
W.-X. Wang et al.2015[39]	SIM EXP.	L/D=0.22 H/D=1 Θ =Non l/D=Non γ =Non	wind turbines with flanged diffusers have substantially higher blade rotational speeds and dynamic strains than those without.
H. M. Elbakry et al.2016[30]	SIM	L/D=0.15,0.4 H/D=Non Θ =4,8 l/D=Non γ =Non	The findings indicated that the second model of the diffuser which leads to an increase in power output by 0.26, while the first case had a power ratio of 0.18.
T. A. Khamlaj et al.2018[40]	SIM	L/D=1.25 H/D=0.5 Θ =12 l/D=0.25 γ =Non	The outcomes show that the turbine cover produces excellent performance and a high-power factor.
F. Q. Putra et al.2018[41]	SIM	L/D=0.25,1.25 H/D=0.5 Θ =40,80 l/D=Non γ =Non	The results show that velocity increase reaches up to 2.08 times compared with that of the bare turbine at a wind velocity of 4m/s.
M. I. Maulana et al. 2018[42]	SIM	L/D=2 H/D=0.6 Θ =9 l/D=Non γ =Non	The results showed that increase in wind speed. In terms of the free current, up to 2.15 times.
F. Mardiansah et al. 2018[43]	SIM	L/D=2.5 H/D=0.375 Θ =16 l/D=Non γ =8	The results revealed that the entry speed rose by 85.75 percent when compared to the basic design.
N. A. Pambudi et al.2019[35]	EXP	L/D=0.25,0.39 H/D=Non Θ =16.7 l/D=0.0069 γ =Non	Without shroud. Increase power efficiency 20.5% With an Inletshroud. Increase power efficiency 41.1%
D. Lokesharun et al.2019[36]	SIM	L/D=0.5 H/D=0.2 Θ =12 l/D=Non γ =0	The findings showed that decreased pressure at the diffuser's exit allows the flanged diffuser to boost power output. Additionally, the flange's angle is crucial.

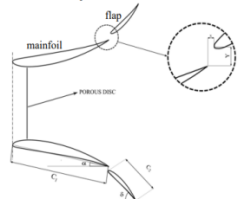
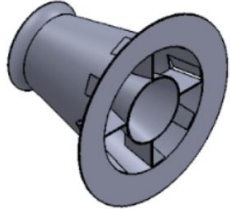
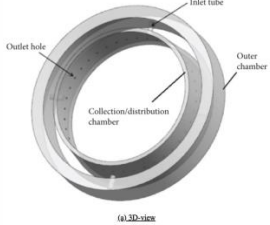
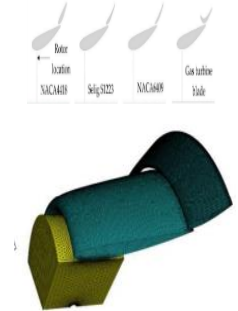

Y. Klistafani et al. 2019[32]	SIM	L/D=7.7 H/D=Non $\Theta=4$ l/D=0.5 $\gamma=0$	The best shape is the curved one compared to other shapes, as it achieved a C_p of 84.18% and a suction speed of 9.2 m / s.
S. A. Kale et al. 2019 [44]	SIM	L/D=1 H/D=0.35 $\Theta=10$ l/D=0.15 $\gamma=10$	The findings demonstrated that the smallest diameter can yield the maximum speed and a C_p of 1.62.
X. Wang, K. et al.2020[45]	EXP	L/D=Non H/D=Non $\Theta=30$ l/D=Non $\gamma=Non$	The results show an increase in power from 0.38 watts - 0.48 watts.
M. Anbarsooz et al.2020 [46]	SIM EXP	L/D=1.5 H/D=0.5 $\Theta=40$ l/D=Non $\gamma=Non$	The results showed that the flanged diffuser could increase the energy about 3.87 times compared to the HAWT.
S. Surya et al. 2020 [47]	SIM	L/D=0.6-4 H/D=Non $\Theta=Non$ l/D=Non $\gamma=-20$ to20	The results showed an increase in the mass flow rate of 27.4%.
M. Takeyeldein et al 2020[38]	SIM	L/D=0.226 H/D=0.1 $\Theta=7,10,20,30$ l/D=Non $\gamma=0$	Increase C_p by 30-60% at $V=5$, θ over 10
S. K. Thangavelu et al .2020 [48]	SIM	L/D=2 H/D=0.443 $\Theta=12$ l/D=Non $\gamma=14$	The results showed that the diffuser with holes gives an increase in speed of 8.56 m/s over the initial velocity of 4 m/s.
T. Rezek et al .2021[26]	SIM EXP	L/D=0.1,0.137, 0.221,0.37 H/D=0.05,0.10, 0.15,0.20 $\Theta=Non$ l/D=Non $\gamma=Non$	The results revealed a 2–5 increase in energy rate compared to the bare wind turbines

R. K. Chhetri et al.2021 [37]	SIM	L/D=0.5 H/D=0.25 $\Theta=14.5$ l/D=0.11 $\gamma=45$	The results flanged diffuser generates power up to 3.6 times faster than a naked turbine
Y. Y. Mawetet al.2021 [19]	SIM	L/D=1 H/D=0.35 $\Theta=10$ l/D=0.15 $\gamma=0$	The enhanced diffuser (IND-009) achieved 50% higher performance than the basic diffuser design.
A. Susandi et al 2021 [49]	SIM	L/D=1.25 H/D=Non $\Theta=4-16$ l/D=Non $\gamma=Non$	The results were that the turbines covered with the diffuser produced energy (1.4 - 2.9) times higher than the turbines without the cover
J. R. Vaz et al .2021 [50]	SIM EXP	L/D=1 H/D=Non $\Theta=3.6-4.5$ l/D=Non $\gamma=Non$	The results showed that the maximum difference in speed was about 23.3% at an angle of 4.5 and .1.65% at an angle of 3.6.
A. M. Elsayed 2021 [51]	SIM	L/D=1,4 H/D=0.1,0.4 $\Theta=4.2,16$ l/D=Non $\gamma=-30,15,30$	The results showed an increase in wind speed up to 1.77, as well as an increase in CP from (.76 2 - 26 .5).
K. Watanabe et al. 2021 [52]	EXP	L/D=0.18,1.7 H/D=0.13,0.69 $\Theta=12$ l/D=Non $\gamma=Non$	The results showed a clear increase in the power factor of about 2-5 compared with HAWT.
O. K. J. et al .2022 [53]	SIM	L/D=0.25 H/D=Non $\Theta=12$ l/D=Non $\gamma=Non$	The findings demonstrated that the turbine's location at the diffuser's beginning provides good energy by (20% -14%) compared to where it is at the beginning and conclusion.
B. Heyru et al .2022 [54]	SIM EXP	L/D=1.98 H/D=0.5 $\Theta=10$ l/D=1.5 $\gamma=90$	he results proved that the curved diffuser gives a higher speed than the straight diffuser by 7%
S. Sridhar et al.2022 [55]	SIM EXP	L/D=1.65 H/D=Non $\Theta=15$ l/D=2.7 $\gamma=Non$	The results showed an increase in speed by 46.8% and 27.4% compared to the un-drilled turbine.

NOTE: (R.M) Research method, (EXP) experimental, (SIM) simulation, (G.P)geometrical parameters.

Table 2-2: The summary of ESAWT for the previous literature

References	Remarks	Figures
O. Igra et al. 1981[5]	Increased shroud strength by up to 80%, and energy increase by approximately 25%	
D. Gysling et al. 2014 [56]	multi-slot diffusers are created to re-energize the flow that has expanded inside them, allowing for greater expansions while preventing the flow from separating from the inner surface.	
W. Han et al. 2015 [32]	The results showed that at low wind speeds between 2 and 6 m/s, the suggested wind turbine's wind energy utilization efficiency climbed to 66 to 73%	
F. A. Al-Sulaiman 2017[18]	The results show that as the ejector inlet area ratio rises, the wind turbine's performance increases, and as wind speed rises, the cost per kWh of the electricity produced falls noticeably, from around 2 \$/kWh at 5 m/s to roughly 0.1	
N.K. Siavasha et al. 2017[57]	The results showed an increase in energy by 14%.	

<p>E. Koc et al.2019 [58]</p>	<p>The flow speed is increased by 1.2 times using a concentrator with a flap.</p>	
<p>S. K. Thangavelu et al. 2020 [48]</p>	<p>Results revealed an exceptional increase in wind speed over the 4 m/s beginning wind speed in a modified diffuser (Model 3 Air vents with splitter), which is 8.56 m/s (2.14 times increment).</p>	
<p>J. Chai et al .2021 [59]</p>	<p>Multi objective optimization improves turbine chamber geometry, increasing output uniformity and reducing flow loss.</p>	
<p>J. Presz et al. 2022 [60]</p>	<p>It was discovered that thinner and more cambered flaps generate greater wind turbine performance, with power enhancements of up to 2.5 when compared to a naked turbine.</p>	
<p>L. Ramayee et al. 2022[61]</p>	<p>The findings indicate that the lobe height is the primary determinant of throat speed.</p>	

2.3 Summary

In this chapter, an extensive review of previous studies has been presented by researchers in the field of wind energy; the literature on aerodynamic power augmentation of HAWT was reviewed. The contributions were published in improving turbine power in two different techniques to augment the largest possible amount of power from HAWT. Therefore, reviews on different designs of diffuser-augmented wind turbines from previous studies included numerical and experimental procedures. Through many researches and studies in the field of DAWT and ESAWT, it is clear that the improvement of the efficiency of both DAWT and ESAWT depends heavily on the diffuser design, and the power of ducted wind turbines may be increased by 5 to 6 times compared to ordinary wind turbines. As a result, the focus of this study was to achieve the optimal diffuser design. Many experimental and simulation studies discussed in this chapter focused on achieving the highest increase in wind velocity at the inlet of the diffuser (place of the turbine installation).

Chapter Three

Methodology

3.1 Introduction

Low and erratic wind speeds are common, so using a wind turbine to generate power is no longer viable from an economic standpoint. The DAWT is a wind turbine augmentation device that might speed up the flow of wind that reaches the turbine blades. The diffuser's main operation mechanism is to alter the pressure within and outside the device. The diffuser's inlet will utilize a sharp rise in wind speed because the pressure inside the diffuser is lower than outside, causing the wind to be driven into the diffuser. To evaluate the turbine at various wind speeds, the study employed computational and experimental techniques.

The study conducted in two phases: the first phase included the fabrication of the previous publisher model and performance analysis using CFX. The second stage involved designing, producing, and evaluating a small diffuser with an ejector using the ANSYS R2. In this chapter, a flowchart that summarizes the study covered. Owing to the need for adequate preparation in the study as well as to give a summary of this research. Along with providing a micro level of planning, this chart is also designed to show the entire work's structure clearly, as shown in Figure 3-1.

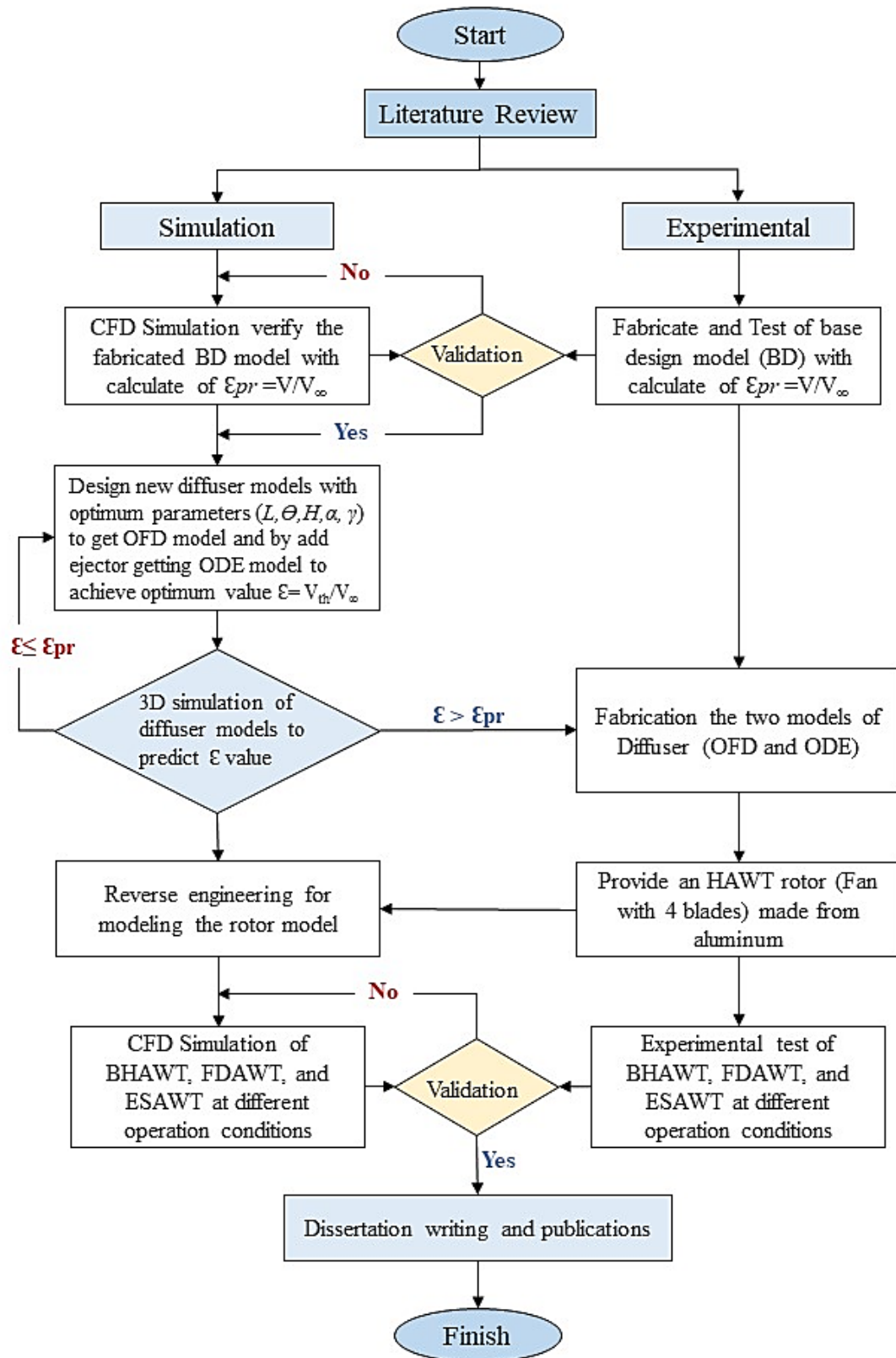


Figure 3-1: Present work flow chart

3.2 Fabrication of the Low-Speed Blower (LSB)

At the beginning, the blower was designed to fit various geometric shapes by using SOLIDWORKS software. As shown in خطأ! لم يتم العثور على مصدر المرجع. Then a wind tunnel was constructed to study the aerodynamics of DAWT and ESAWT in Department of Mechanical Engineering Techniques of Power Department of Mechanical Engineering Techniques of Power, Engineering Technical College of Najaf, Iraq, it is used for low speeds (3-5 m/s). The dimension of the tunnel is 0.55-m height, 0.55-m width, and 3 meters length, as shown in خطأ! لم يتم العثور على مصدر المرجع, and a centrifugal fan was used to drive the airflow up to 5 m/s. A Perforated air window has been manufactured. To obtain uniform air velocity. The intensity of the flow disturbance was very small. Figure 3-4 shows the stages of manufacturing the wind tunnel.

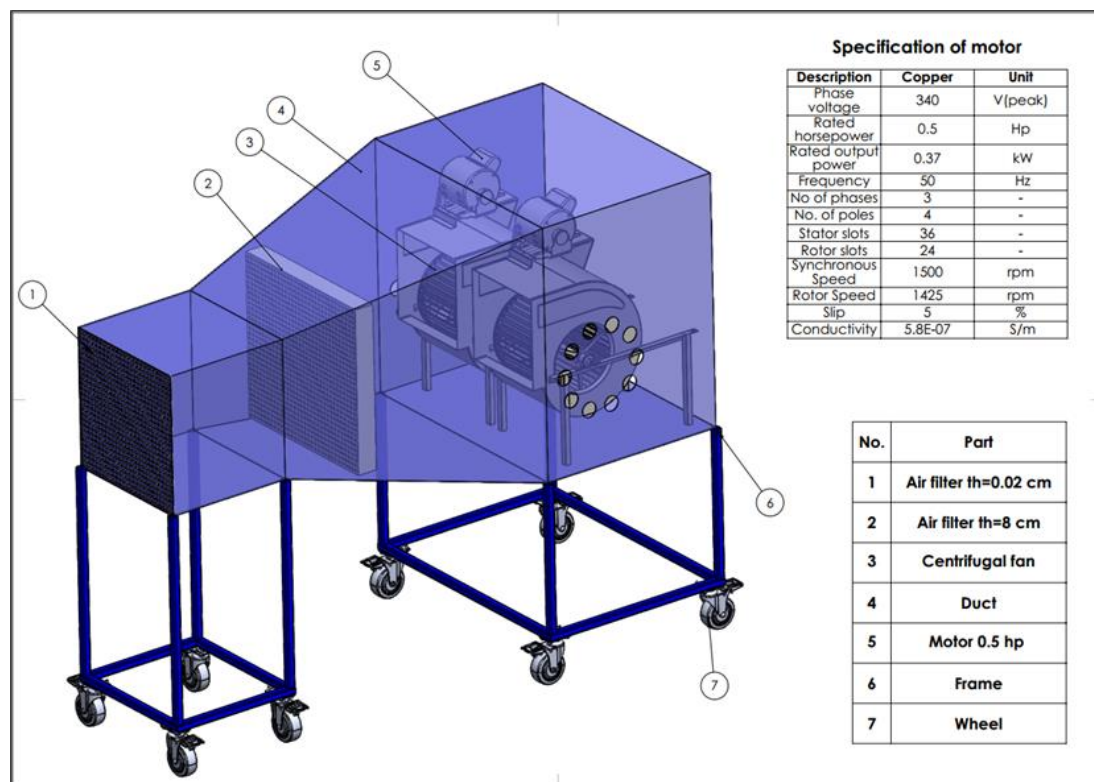


Figure 3-2: Low-Speed Blower with its compounds

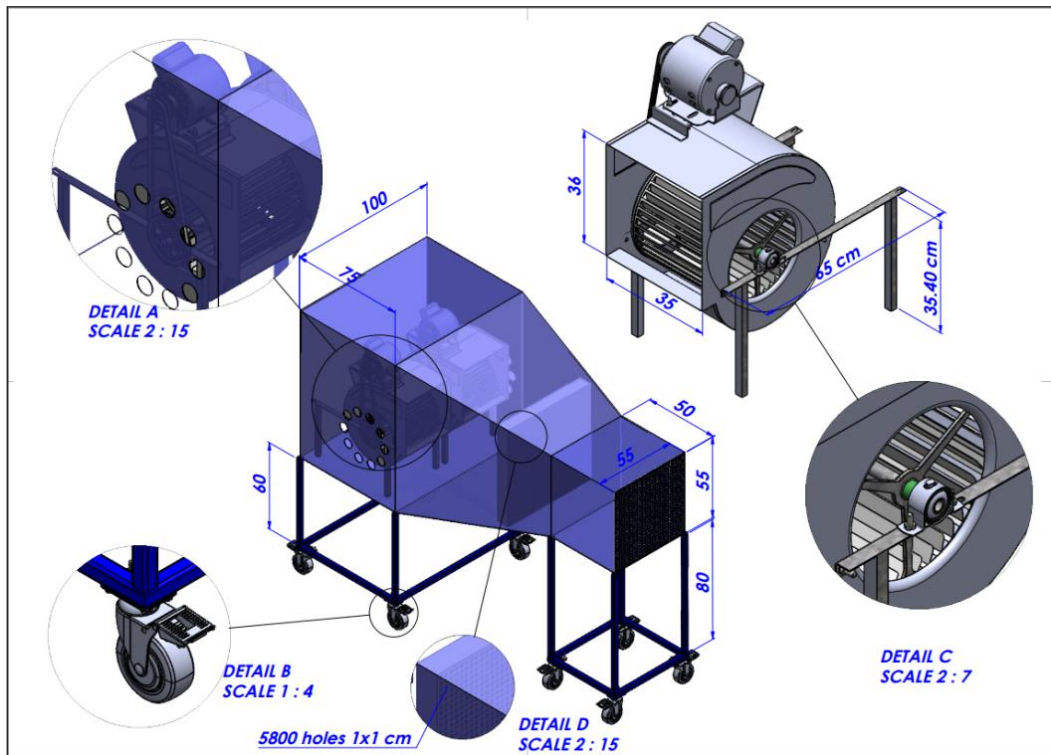


Figure 3-3: LSB compounds with dimensions



Figure 3-4: Stages of manufacturing LSB and testing of BD model.

3.3 Fabrication of diffuser (base design model)

The BD was made based on an empty flanged diffuser (EFD) that was presented by [19] using several steps. In the beginning, 2 mm thick galvanized sheets were selected based on aspects including price, toughness, and performance. The chosen material was then shaped utilizing a variety of production processes, including cutting, bending, and spot welding. Accurate dimensions and smooth surfaces were produced using manufacturing techniques. The basic parameters of the previous model were $D = 310$ mm, $l = 4.5$ mm, $L / D = 1$, $H / D = 0.35$, $\Theta = 10^0$. As shown in Figure 3-5, was calculated the speed increase ratio (\mathcal{E}) for the diffuser (BD) on the 7 points along the diffuser, Where the test was carried out using a Lower Speed air Blower (LSB) that was also manufactured in the Aerodynamics Lab, Department of Mechanical Engineering Techniques of Power Department of Mechanical Engineering Techniques of Power, Engineering Technical College of Najaf, Iraq, as detailed in the 3.2.1 paragraph.

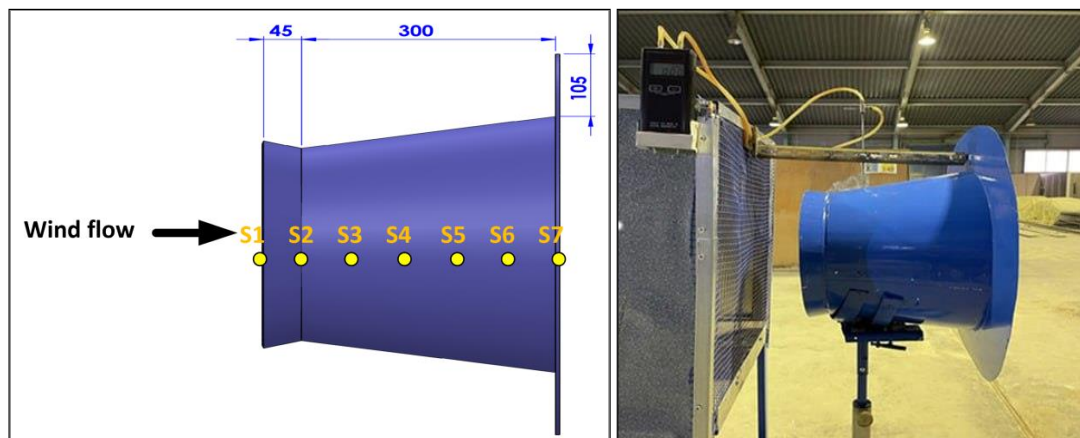


Figure 3-5: The BD model during the test

3.4 Simulation work

A numerical method was used to find the numerical approximation to the solution for the ordinary differential equations. The fluid flow in the bare diffuser, HAWT, and DAWT was simulated using the commercial computational fluid dynamics (CFD) software ANSYS-CFX processing, and post-processing were the three operations that made up the simulation.

3.4.1 Simulation of the diffuser model

The present study started with a 3D of BD model presented by Yu Yu[19]. ANSYS-CFX was used to create the computational domain for simulation in order to study the impacts of the diffuser on the airflow traveling through it. The computational domain used was as same as by [19], which has a cylindrical shape and a diameter of 310 cm, and its length 620 cm, as shown in Figure. 3-6. The outer domain and diffuser walls were specified as slip walls, while the inlet and outlet limits of the domain were defined as velocity inlet and pressure outlet, respectively. The domain is meshed with a tetrahedral unstructured mesh, as shown in Figure 3-7.

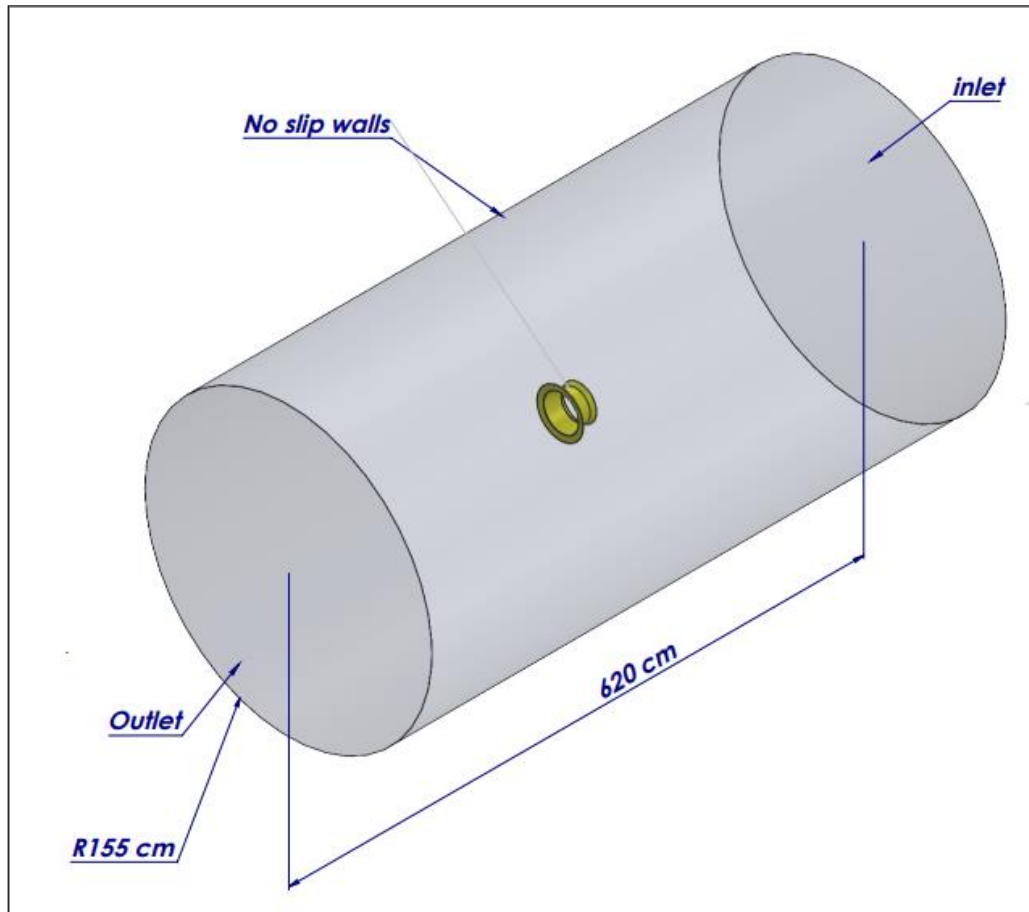


Figure 3-6: Computational Domain of BD model

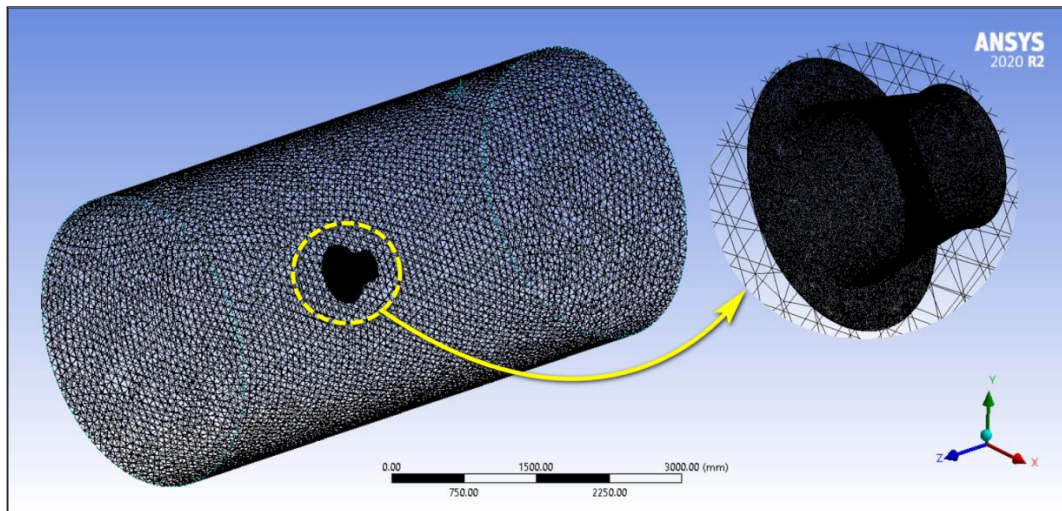


Figure 3-7: Mesh Generation for BD model

3.4.1.1 Grid independence test for diffuser domain

The whole geometry of the empty flanged diffuser model was numerically modeled in a 3D domain using CFX for high precision of flow study. Table 3-1 lists the grid independence for the 3D diffuser domain. The accuracy of the mesh in ANSYS is crucial in achieving reliable and precise simulation results. Numerous tests were undertaken in an effort to find the optimal mesh accuracy for a model. These tests assessed several mesh resolutions and configurations to determine the ideal balance between computing efficiency and precision.

The chosen mesh accuracy produced remarkable results, with an Orthogonal quality of 0.999. This implies that the mesh pieces are aligned with the local geometry with little distortion. However, it is important to note that the skewness value of 0.68 indicates element distortion or a non-ideal form, and from Figure 3-8, it is noted that it is within the good range [62]. In addition, to test the sensitivity of the mesh and to verify the validity of the model (skewing and orthogonally) by simulating the model by increasing the number of elements from (622588) to (2059872), it was found that after the value of (622588) the number of elements, the value of the velocity ratio remains approximately constant and this has been taken point as a point design to reduce time and good resolution.

Table 3-1: Statistic of grid independence for 3-D diffuser domain

Trial	No. of elements	No. of nodes	Skewness	Orthogonal quality	ϵ
1	622588	141516	0.8323	0.99	1.980
2	120179	324502	0.68	0.99	1.971
3	248610	730138	0.74258	0.99	1.959
4	4846758	1480055	0.698	0.99	1.967

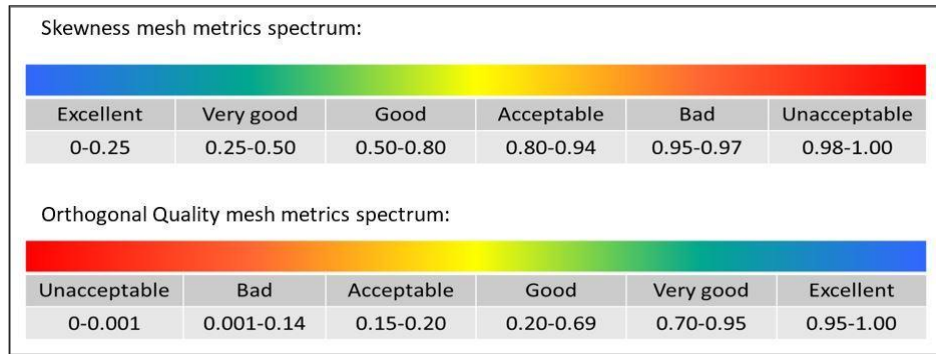


Figure 3-8: Skewness and orthogonal mesh spectrum [62]

3.4.1.2 Boundary conditions of diffuser domain

The commercial CFD code using ANSYS-CFX was used to explore numerical simulations under the steady state condition. The air was treated as an ideal gas with a temperature of 25 °C and a reference pressure of 1 atm throughout all domains. The flow was analyzed using an isothermal steady state convergence criterion of 10^{-4} with turbulent model *k- ω SST* which was give high prediction of the flow especially at the walls and improved the separation, moreover, it was used by [63, 64].The inlet stationary boundary at an inlet velocity of 5 m/s was applied, and the static pressure 0 Pa was set at the outlet stationary boundary.

3.4.2 Develop the Diffuser's Geometrical Specifications

In order to develop the previous diffuser (BD), the same previous domain (BD domain) was used, as shown in Figure 3-6. In order to investigate the effect of modifying the geometrical parameters on diffuser performance, the procedure of design modification of the diffuser in this study was based on achieving the best value of ϵ (ratio of maximum velocity at inlet diffuser to upstream velocity) at a different range of diffuser parameters (L , Θ , H , α) and flange angle (γ). Figure 1-5 shows

the geometrical parameters that have been investigated in this research with consideration of the optimum values of (L/D and H/D) mentioned by a previous study [19], as well as compacting the diffuser length to reduce the cost with optimum performance so the optimum values of geometrical parameters that achieved the highest value of ϵ are Model-16, as shown in Table 3-2 Compared to the BD model. Then the flange angle (γ) has been changed, as shown in Table 3-3 (all details and shapes for diffusers models illustrated in Appendix B). By adopting the optimum value of (γ) and by a little increase of L/D and H/D values, the best-flanged diffuser model was obtained in Model 8, which is called OFD of this study. The geometry with dimensions and Mesh of the best design has a skewness of 0.68, elements of 1932359, and nodes of 556368, as shown in Figure 3-9 and Figure 3-10, respectively. Thus, these parameters were considered in this study as the initial design. The results of comparing the geometrical parameters of previous and modified diffuser are laid out in Chapter 4.

Table 3-2: The achieved values of (ϵ) as a function of the geometrical parameters of an empty flanged diffuser

NO	V_{∞}	α (deg)	Θ (deg)	L/D	H/D	V_1^*	ϵ
1	5	10	10	1	0.33	9.93	1.986
2	5	10	10	0.87	0.33	7.70	1.54
3	5	10	10	1	0.2	8.12	1.62
4	5	11	10	1	0.33	8.14	1.63
5	5	12	12	1	0.2	8.66	1.73
6	5	12	12	0.9	0.2	8.53	1.71
7	5	12	12	0.5	0.2	7.77	1.55
8	5	15	10	1	0.35	9.19	1.84
9	5	32	12	0.3	0.2	8.37	1.67
10	5	16	12	0.5	0.2	8.55	1.71
11	5	18	12	0.5	0.2	8.84	1.77
12	5	19	12	0.5	0.2	8.96	1.79
13	5	20	12	0.5	0.2	9.06	1.81
14	5	25	12	0.5	0.2	9.06	1.81

15	5	29	12	0.5	0.2	9.53	1.91
16	5	30	12	0.5	0.2	9.73	1.95
17	5	30	12	0.4	0.2	9.05	1.81
18	5	31	12	0.5	0.2	9.52	1.90
19	5	32	12	0.5	0.2	9.50	1.90
20	5	33	12	0.5	0.2	9.45	1.89
21	5	35	12	0.5	0.2	9.37	1.87
22	5	35	12	0.2	0.2	7.71	1.54
23	5	36	12	0.5	0.2	9.28	1.86
24	5	37	12	0.5	0.2	9.21	1.84
25	5	38	12	0.5	0.2	9.15	1.83
26	5	39	12	0.5	0.2	9.01	1.80
27	5	40	12	0.5	0.2	9.38	1.88
28	5	41	12	0.5	0.2	8.82	1.76
29	5	45	12	0.5	0.2	8.37	1.67
30	5	30	12	0.4	0.2	9.05	1.81
31	5	0	12	0.5	0.2	5.09	1.02

Table 3-3: The OFD model with different ranges of flange angle.

N	V_{∞}	α	γ (deg)	Θ (deg)	L/D	H/D	V_{avr}	ϵ
1	5	30	50	12	0.5	0.2	10.4	2.08
2	5	30	55	12	0.5	0.2	10.33	2.066
3	5	30	60	12	0.5	0.2	10.10	2.02
4	5	30	40	12	0.5	0.2	10.28	2.056
5	5	30	35	12	0.5	0.2	10.27	2.054
6	5	30	47	12	0.5	0.2	10.34	2.068
7	5	30	-25	12	0.5	0.2	9.73	1.946
8	5	30	50	12	0.6	0.3	11.00	2.200
9	5	30	45	12	0.6	0.3	10.94	2.189
10	5	30	40	12	0.6	0.3	10.84	2.169
11	5	30	35	12	0.6	0.3	10.82	2.165
12	5	30	30	12	0.6	0.3	10.81	2.163
13	5	30	25	12	0.6	0.3	10.74	2.15
14	5	30	20	12	0.6	0.3	10.77	2.14

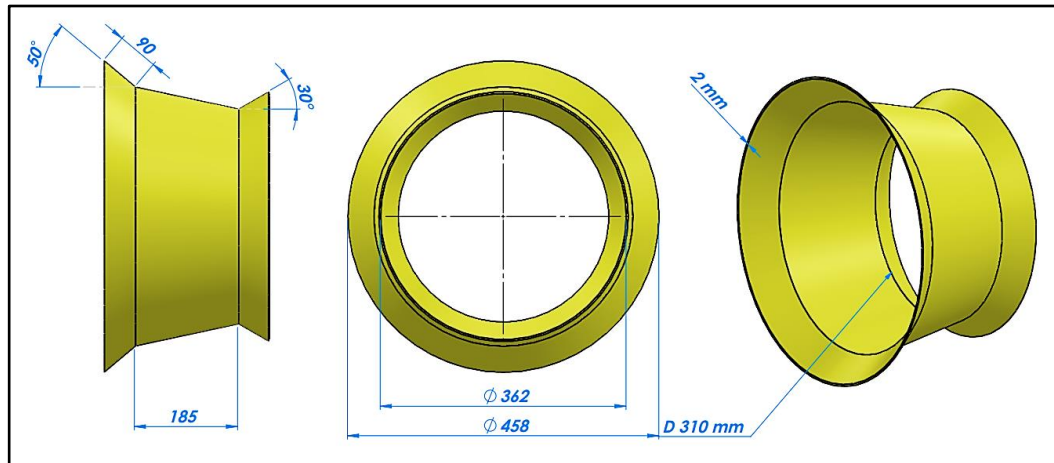


Figure 3-9: Optimum design of flanged diffuser OFD

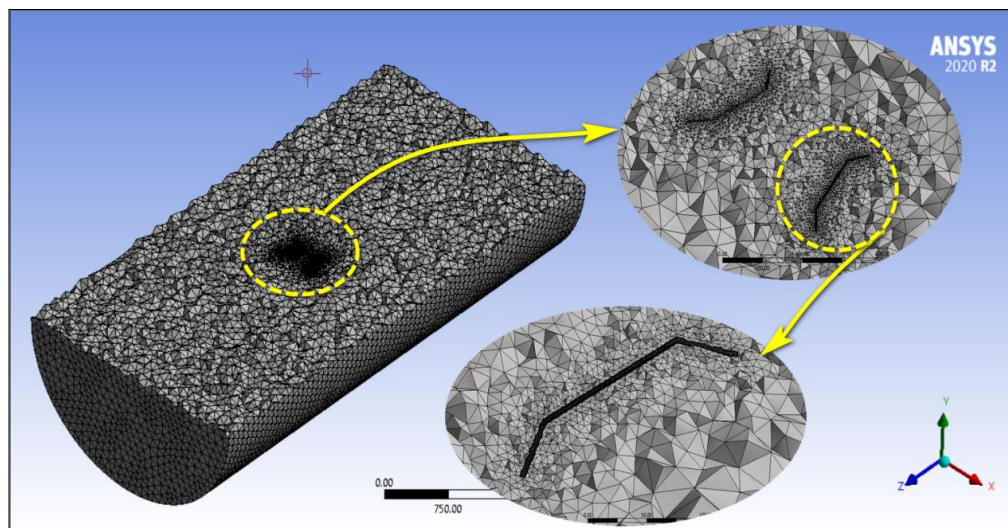


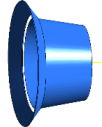
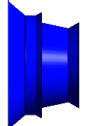
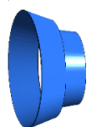
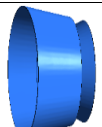
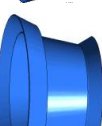
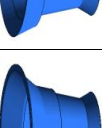
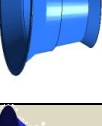
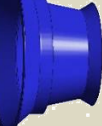
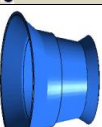
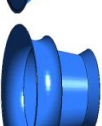
Figure 3-10: Mesh of OFD with domain

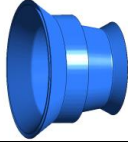
3.4.3 Optimum Diffuser with Ejector ODE

To improve the turbine's performance, an ejector was added to the OD, enabling it to achieve the maximum \mathcal{E} . Many attempts were made to obtain the best engineering parameters for the ejector using CFX. Table 3-4 shows the designed and simulated attempts to reach the maximum possible \mathcal{E} . The best model was obtained of ODE as shown in Figure 3-11, where the speed ratio reached up to 2.4 (model-7). The ODE incorporates an optimized pre-engineered diffuser without flange,

providing improved efficiency and sustainability in wind energy applications.

Table 3-4: The achieved values of (ϵ) as a function of the geometrical parameters of an empty flanged diffuser

Model No.	V_{∞} (m/s)	V_{ar} (m/s)	ϵ	Shape of Ejector
1	5	7.6	1.52	
2	5	11.79	2.35	
3	5	7.2	1.44	
4	5	8.02	1.604	
5	5	9.5	1.9	
6	5	11.3	2.26	
7	5	12.0028	2.4	
8	5	11	2.2	
10	5	11.95	2.39	
11	5	10.97	2.194	

12	5	10.95	2.19	
----	---	-------	------	---

After obtaining the best design of the ejector from the simulation process and the geometry of the best diffuser with ejector Mesh (Skewness 0.68, No. Of elements (2318116), No. Of nodes (689670) shown Fig 3.12, respectively. A suitable rotor will be sought for ODE model , in the next paragraph.

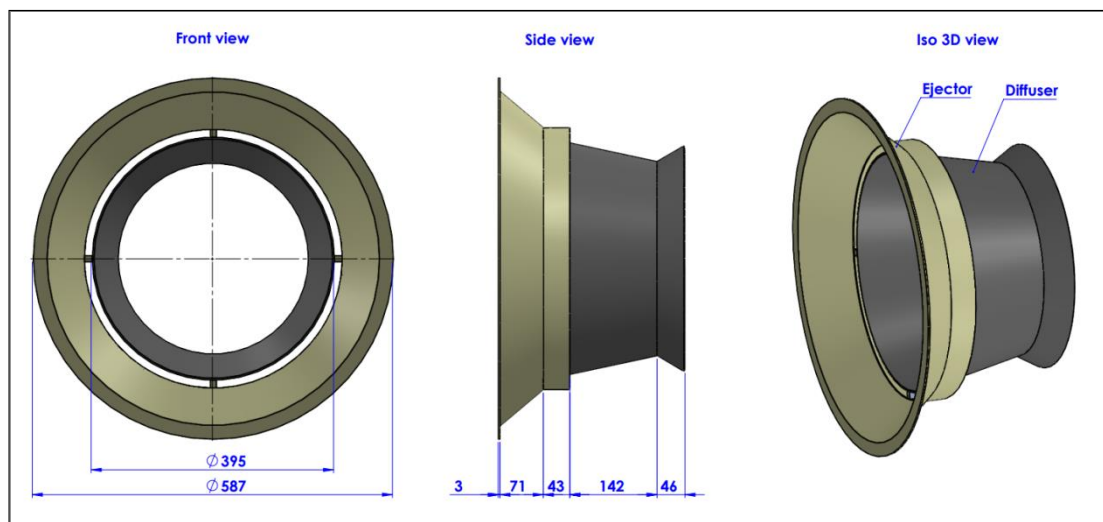


Figure 3-11: Optimum diffuser with ejector ODE

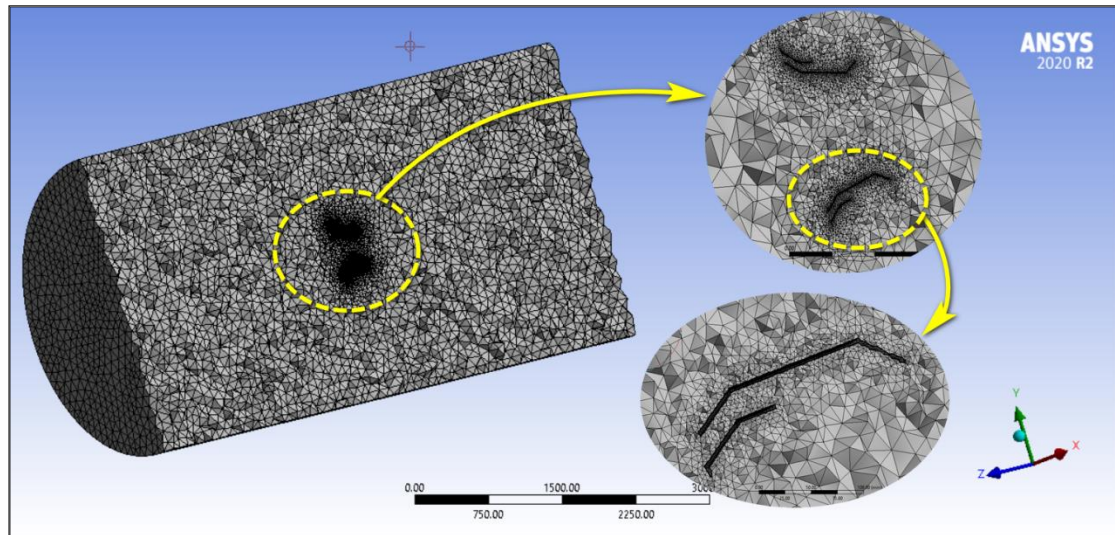


Figure 3-12: Mesh of Optimum diffuser with ejector ODE

3.4.4 Rotor model

HAWT are getting a lot of interest, research, and development by researchers. HAWT, due to its design that allows it to fully rotate the blades when placed in the wind flow, is highly efficient. In this section, a four-blade fan made of aluminum using engineering measurements to match the diameter of the diffuser.

3.4.4.1 Engineering measurements the fan model

Focus was placed particular emphasis on the design of its blade. Using a Venire scale, this precise measuring tool allowed capturing of detailed data, ensuring the accuracy of the analysis and subsequent modeling. The dimensions of the fan blades were precisely measured, with a radius of 150 mm and a thickness of 1 mm, as shown in خطأ! لم يتم. خطأ! لم يتم العثور على مصدر المرجع. and العثور على مصدر المرجع.



Figure 3-13: Fan engineering measurement process

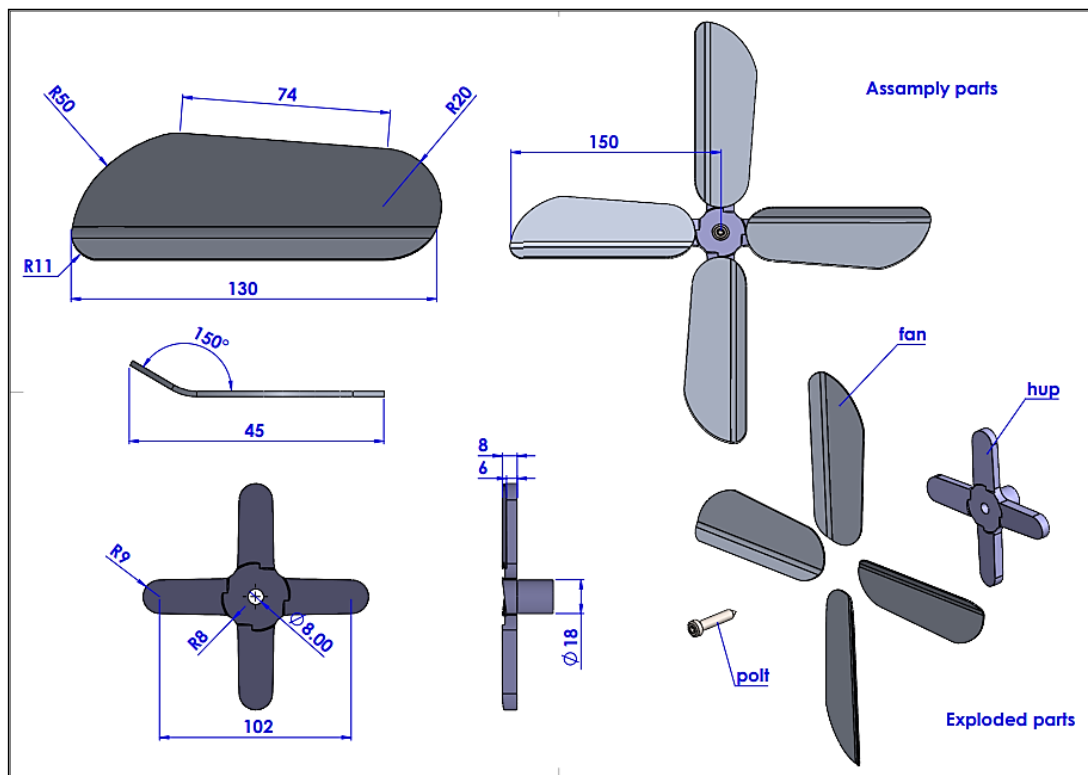


Figure 3-14: Details of the fan.

3.4.4.2 Simulation of bare and shrouded rotor

A 3D CFD Domain was used to explore numerical simulations of bare and shrouded rotors (FDAWT and ESAWT) under the steady state condition of isothermal flow with $K-\omega$ SST of the turbulent model. Isothermal flow was considered with a temperature of 25 °C and a reference pressure of 1 atm throughout all domains. The air was modeled as an ideal gas. The computational modeling of the governing equations in this study assumed the flow to be at a steady state and incompressible [63, 64]. The differential governing equations, which included the continuity equation and the Naviera-Stokes equations, were solved using the commercial Computational Fluid Dynamic (CFD) ANSYS CFX R2.

The CFD approach was employed to calculate the time-averaged performance coefficient of wind turbines. Assuming it as quasi-steady, the well-established Reynolds-Averaged Naviera Stokes (RANS) equations were adopted, which comprised of continuity equation and the Naviera-Stokes equations; they may be expressed in terms of mean quantities for Newtonian, turbulence, steady, incompressible flow as stated below [38].

$$\frac{\partial u_i}{\partial x_j} = 0 \quad (3.1)$$

$$u_j \frac{\partial u_i}{\partial x_j} = -\frac{1}{\rho} \frac{\partial p}{\partial x_i} + \frac{\mu}{\rho} \frac{\partial^2 u_i}{\partial x_j \partial x_j} - \frac{\partial}{\partial x_j} \overline{(u'_i u'_j)} \quad (3.2)$$

The term $\overline{(u'_i u'_j)}$ Represents the Reynolds stresses.

3.4.4.3 Boundary conditions and mesh

In this numerical inquiry, there are two domains: the rotating domain and the stationary domain, as shown in Figure 3-15. The stationary domain is the virtual cylindrical shape only in the case of the bare rotor, while in the case of DAWT, it consists of the virtual cylindrical shape and the diffuser walls. The rotating domain (in the two domains) consists of the HAWT rotor enclosed in the rotating frame (disc). Numerical simulations were considered. In the inlet stationary boundary, the inlet velocity 5 m/s is applied, and the static pressure 0 Pa is set at the outlet stationary boundary. The walls of the cylindrical domain and diffuser wall were considered as a no-slip wall, while the interface between the stationary and rotating frame was considered as a frozen rotor. The mesh was generated to the rotating domain HAWT and stationary domain (diffuser) for the three models using tetrahedral mesh type.

According to that the total elements of mesh for BHAWT was about 1348087 elements, whereas for FDAWT and ESAWT were 1066315 and 2320320 elements, respectively. As all domains have same dimensions, the mesh generation of the ESAWT domain is shown in Figure 3-16.

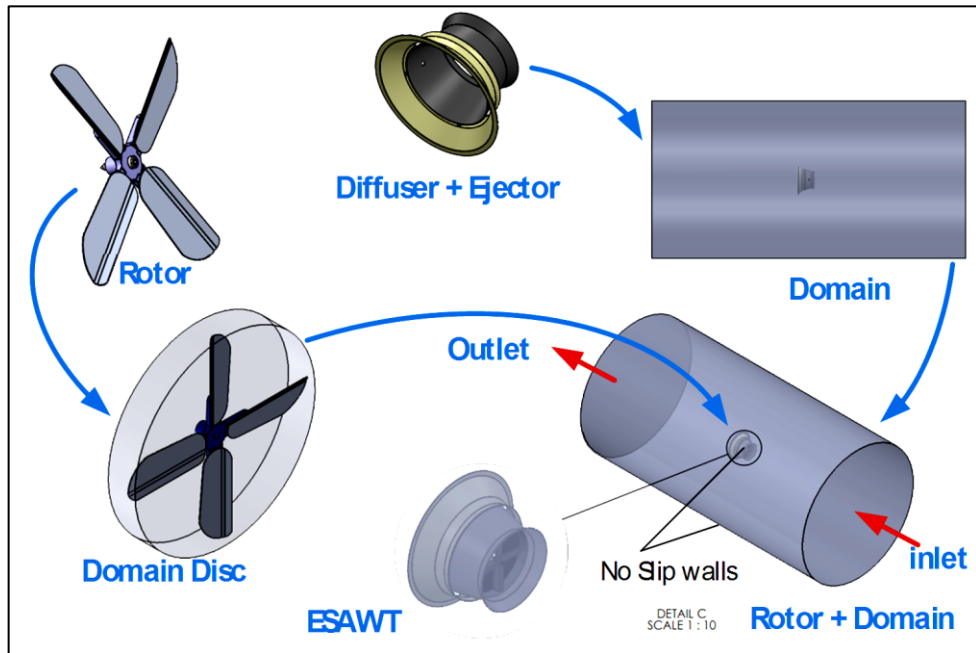


Figure 3-15: Procedures of CFX for ESAWT

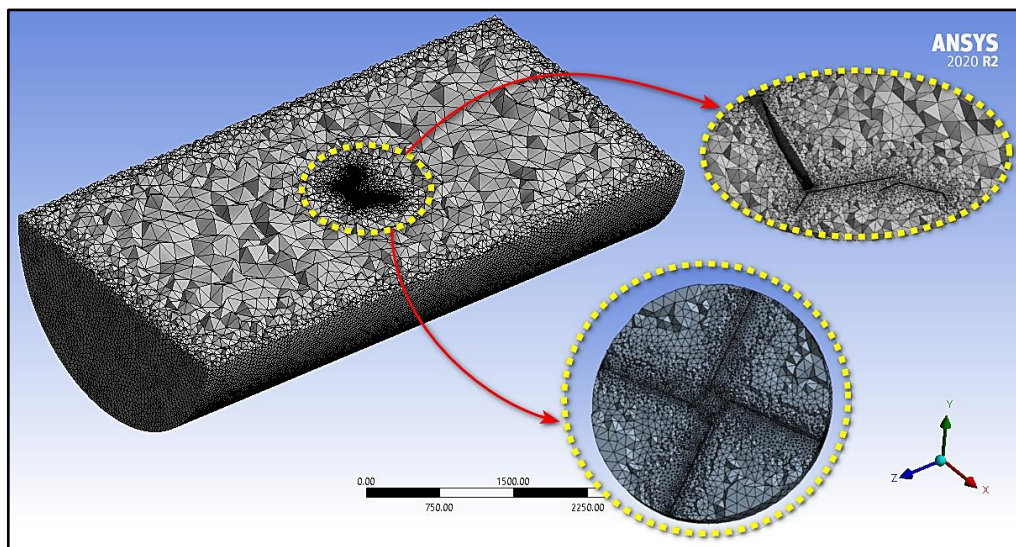


Figure 3-16: Mesh of ESAWT

3.5 Experimental work

3.5.1 Fabrication of Medium Speed Blower (MSB)

For the purpose of testing the diffuser at medium velocities from 5 m/s to 9 m/s, a blower with a centrifugal fan was designed and constructed to study the aerodynamics of (FDAWT and ESAWT). The

dimension of the tunnel is 1 meter high, 1 meter wide, and 2 meters length, as shown in. خطأ! لم يتم العثور على مصدر المرجع. An air grill has been manufactured with Square perforated holes. . The intensity of the flow disturbance was less than 5%, and the regularity of the flow was more than 95%. خطأ! لم يتم العثور على مصدر المرجع. shows the stages of manufacturing the wind tunnel.

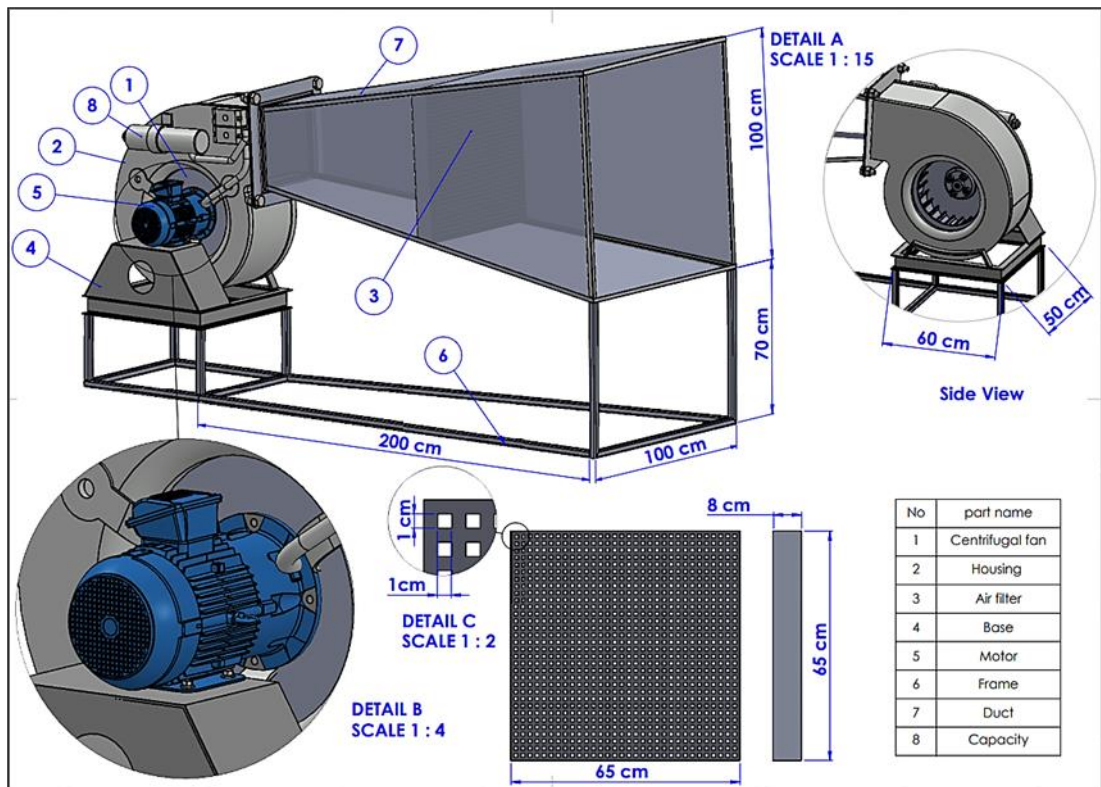


Figure 3-17: Medium Speed Blower with its compounds



Figure 3-18: Stages of fabrication of the MSB.

3.5.2 Fabrication the ODE model

The ejector was made using several steps. Initially, galvanized sheets with a thickness of 2 mm were selected based on aspects including price, rigidity, and performance. The selected material was then shaped using a variety of production processes, including cutting, bending, rolling, and spot welding. As shown in **خطأ! لم يتم العثور على مصدر المرجع.** Accurate dimensions and smooth surfaces were produced using precise manufacturing techniques. The dimensions used are shown in **خطأ! لم يتم العثور على مصدر المرجع.**



Figure 3-19: Stages of fabrication of ODE model

3.5.3 Fabrication the Load control panel

A load control board for the wind turbine power calculation was developed and built, as shown in Figure 3-20, to meet the challenge of measuring the HAWT power, especially for small sizes as well as the expensive torque sensor device. In this case, the measurable electrical power will be used to estimate the mechanical power of the turbine. The primary idea behind this board is to progressively increase reliable loads on the turbine while estimating its power at each round. 40 LED 12V, 1.5-Watt loads were used, as a result, connected together in a series of electrical circuits. The voltage, current, and resistance are all measured simultaneously using Voltmeter and ammeter.

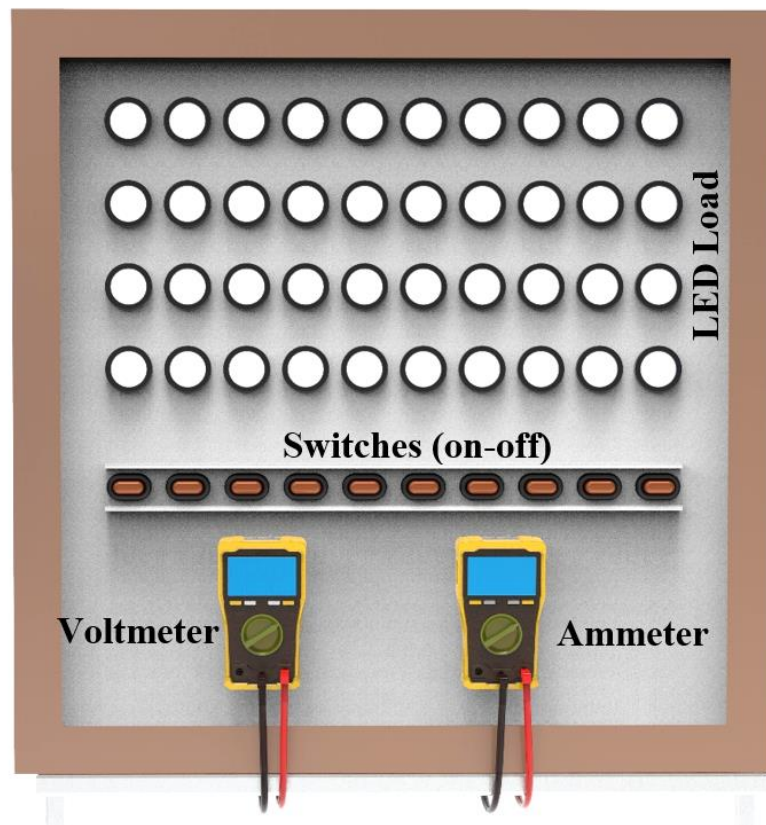


Figure 3-20: The load control board for calculating turbine power

3.5.4 Experimental setup for (BHAWT, FDAWT, and ESAWT)

The tests for wind turbines models (BHAWT, FDAWT, and ESAWT) were in the test section by air blower made the schematic diagram of the experiment's setup in Figure 3-21 and Figure 3-22, and the actual experimental setup is shown in Figure 3-23 respectively. The generator of the turbine was connected to the load. The voltmeters were used to measure the voltage and current across the load. The wind velocity was adjusted by the wind tunnel controller and measured by the Pitot tube installed upstream. By maintaining air velocity at a constant state, the load can be varied by operating more loads (lamps), and the voltage and current were recorded at each load. At the same time, the angular velocity was recorded at each load. The rotational speed of the rotor was measured by a tachometer. The experiment was repeated several times according to the cases of the models. The experiments for all models were conducted at wind speeds ranging from 5 to 9 m/sec (Re ranged from 7.431×10^3 to 1.337×10^4) [65], with an inlet air temperature at 25 C°

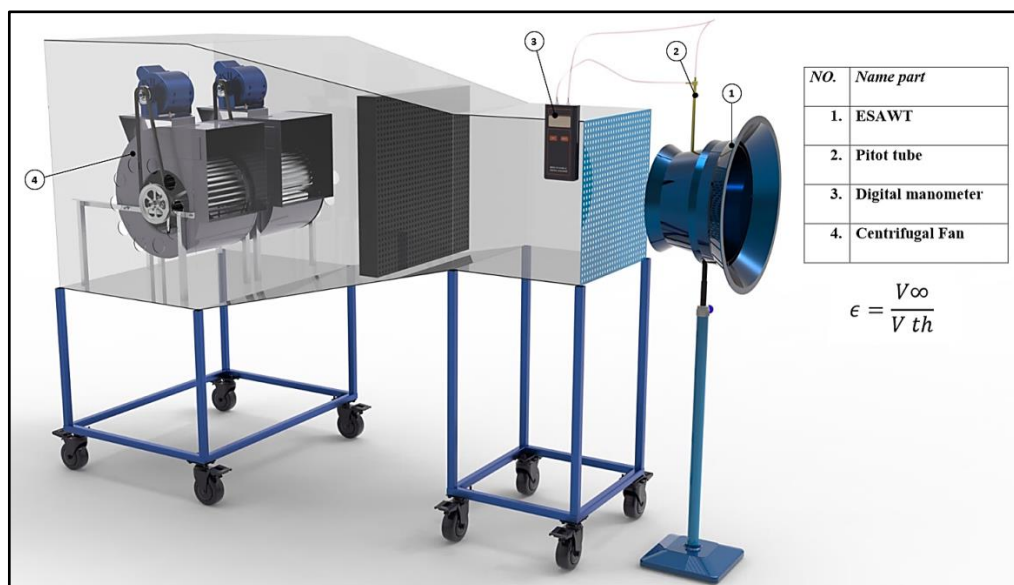


Figure 3-21: Virtual diagram of LSB rig for empty diffuser testing

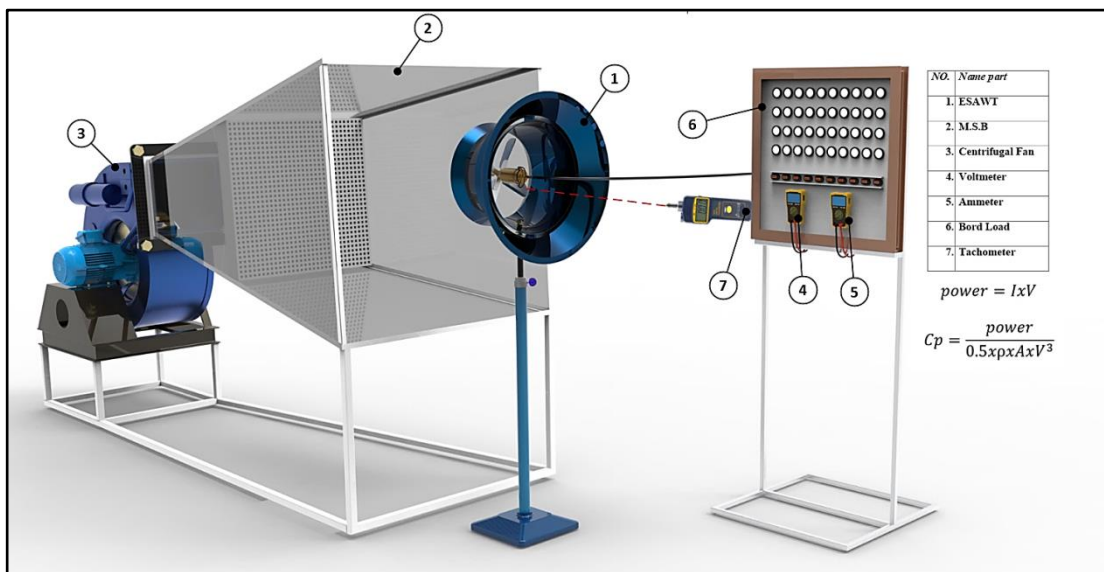


Figure 3-22: Virtual diagram of MSB for testing of FDAWT and ESAWT



Figure 3-23: Actual MSB for Experimental test of FDAWT and ESAWT

3.6 Wind turbine performance and power calculations

Because wind energy is a source of mechanical power for wind turbines, the following equation was used to compute the product of rotor torque and rotor angular velocity:

$$P_{out} = T\omega \quad (3.3)$$

The output power was estimated during an experimental power calculation utilizing a generator.

$$P_{out} = IV/\eta_g \quad (3.4)$$

Where I and V are the current and voltage generated by the generator, respectively. While η_g is generator efficiency and η_c is conversion efficiency.

The power coefficient, abbreviated (C_p), which measures the efficiency of a wind turbine, is as follows:

$$C_p = \frac{P_{out}}{0.5 \rho A V_\infty^3} \quad (3.5)$$

By plotting the power coefficient's values as a function of tip speed ratio (λ), the most popular technique was equivalent to:

$$\lambda = \frac{\omega R}{V_\infty} \quad (3.6)$$

In addition, torque coefficient (C_T), particularly for DAWT, may be thought of as a metric for analyzing turbine performance. In light of this, C_T as a function of:

$$C_T = \frac{\text{Actual torque}}{\text{Theoretical torque}} = \frac{T}{0.5 \rho A R V_\infty^2} = \frac{C_p}{\lambda} \quad (3.7)$$

CHAPTER FOUR

Results and Discussions

4.1 Introduction

This section of the theses covered the results of the FDAWT and ESAWT models using the methods described in Chapter 3. The process of presenting the results began with examining the diffuser model in a 3D simulation of CFD. Experimental verification of CFD data was carried out in order to measure the performance of diffuser (OFD, ODE) in terms of maximum increase in flow velocity. The performance results for whole turbine (BHAWT, FDAWT, and ESAWT) were discussed in terms of power, torque, and power coefficient. Validation of experimental results carried out using CFD for visualization

4.2 Diffuser results for OFD model

Since the amount of wind energy in the air transmitted through the rotor area is proportional to the cube of air velocity, any small increase in speed will result in a large increase in energy. The researchers found that covering the rotor with a diffuser with an edge improved the efficiency of HAWT, so obtaining the ideal model for the diffuser will lead to an increase in the flow velocity through the rotor, and this comes through the governing parameters of the diffuser. In this part, several attempts were made using CFX to develop the previous diffuser to determine the best flange angle, as well as reduce the size of the diffuser and obtain the maximum possible speed ratio, as shown in خطأ! لم يتم العثور على مصدر المرجع.

Table 4-1: The diffuser was specified by the variable values.

Variable	Minimum	Step	Maximum
L/D	0.3	0.1	1
h/D	0.2	0.05	0.3
Θ (deg)	9	1	15
γ (deg)	-10	5	60

α (deg)	5	1	50
----------------	---	---	----

On the geometry received from the parametric analysis, the optimization process is initiated by specifying the maximum number of iterations (81 Attempts) and precision of residuals 10^{-4} . خطأ! لم يتم العثور على مصدر المرجع. Illustrates how the optimizer arrived at the best design of the diffuser form after 81 attempts.

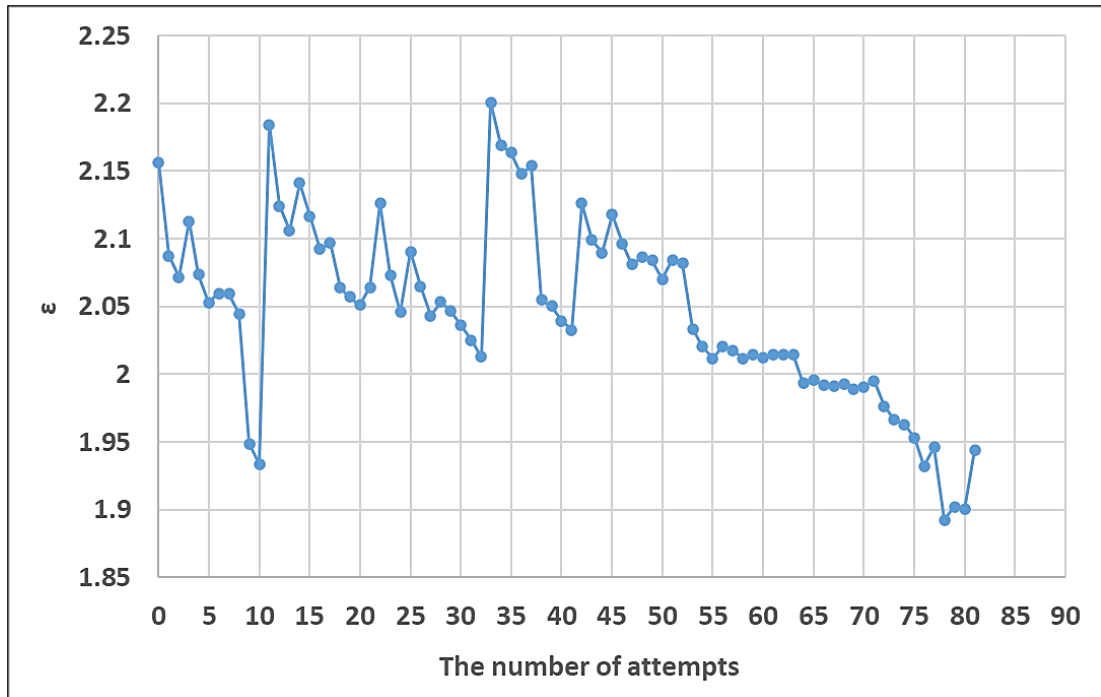


Figure 4-1: History of Optimization Diffuser

4.2.1 Effect of flange angle on velocity ratio

The angle of the flange can increase the average velocity at the throttle due to the creation of eddies behind the diffuser, which increases the pressure drop and, thus, increase the velocity flow. Figure 4-2 illustrates the impact of the diffuser flange angle on the average entrance velocity of the diffuser. The results demonstrate that a forward flange angle can significantly enhance the average entrance velocity, surpassing

the value obtained with zero flange angle, with a peak of $2.2 V_\infty$ achieved when utilizing a 50° forward flange angle.

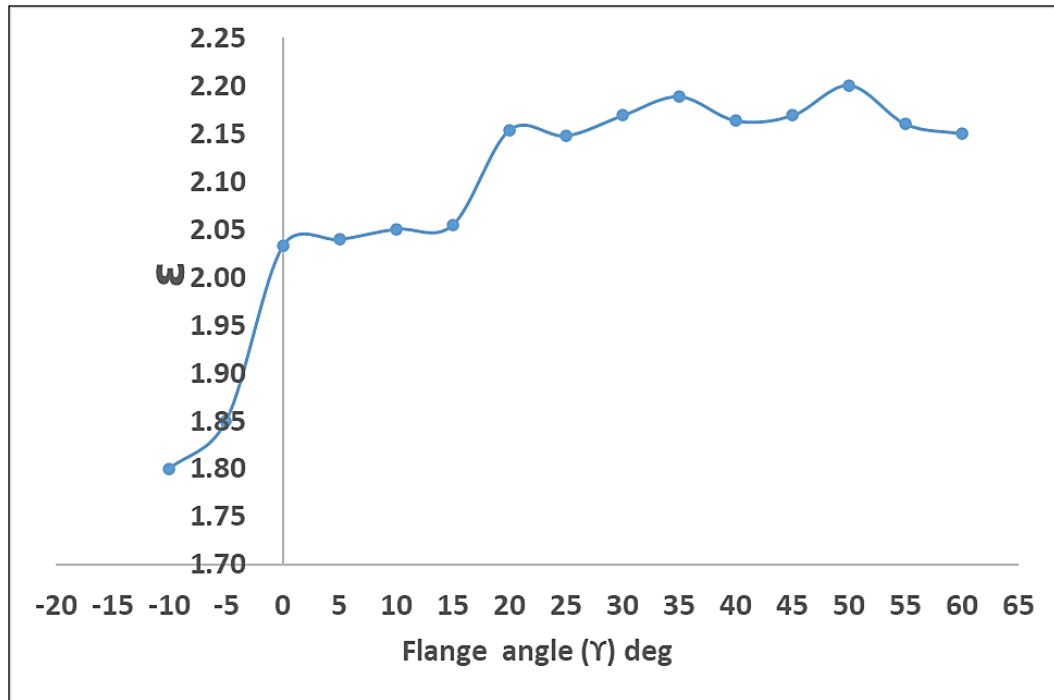


Figure 4-2: Effect of flange angle on velocity ratio.

4.2.2 Effect of Diffuser Flange Height

When a big flange is connected to the outside border of a diffuser exit, wind speed increases near the diffuser entry. The flow direction is left to right, and a vortex formation similar to the Karman vortex may be observed downstream of the flange. The static back pressure in the diffuser's flanged exit section decreases to relatively low pressure compared to the upstream flow, increasing the entry velocity. Figure 4-3 depicts the influence of flange height on velocity magnitude. The entry velocity is increased by raising the flange height to $h=0.3D$ when the flange angle is set at 50 to get the ideal flange height.

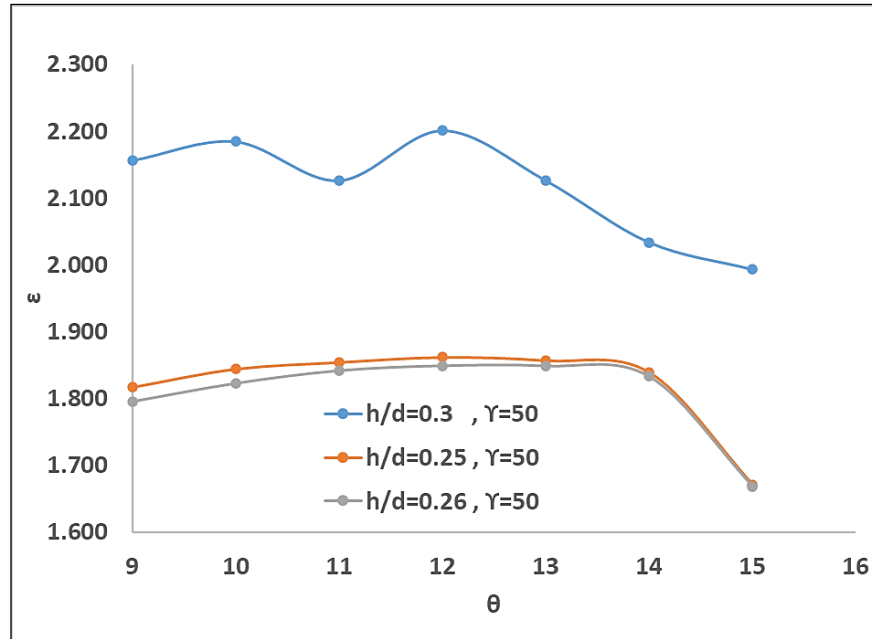


Figure 4-3: Effect of flange height on the mean entry velocity at a flange angle of 50 degree

4.3 Comparing of BD and OFD models

Since the amount of wind energy in the air transmitted through the rotor area is related to the mass flow rate, it can be optimized. Using a diffuser with flanged to surround the rotor is one of the most effective techniques. Since the diffuser geometric properties control the efficiency of the diffuser, many theoretical studies have been carried out by CFX. As mentioned in Chapter 3, the optimal values for the speed increase were determined to be $L = 0.6D$, $H = 0.3D$, and $\Theta = 12^\circ$, as shown in Table 4-2.

One of the most important elements of the work was the verification and validation of the results obtained from the experimental and numerical parts of the BD and OFD models measuring the velocity ratio. Figures 4-4 and 4-5 show the experimental part of the velocity measured by the Pitot tube in each section (divided into seven sections) of BD and OFD model, respectively.

The results obtained between the experimental part and the simulation showed a reasonable convergence in the velocity ratio with an error rate not exceeding 9%. Table 4-2 and Figure 4-6 also shows a comparison between the BD and OFD diffuser models, the results showed that the OFD model gives a higher speed ratio than BD and also the OFD model is characterized by a lower size than BD .

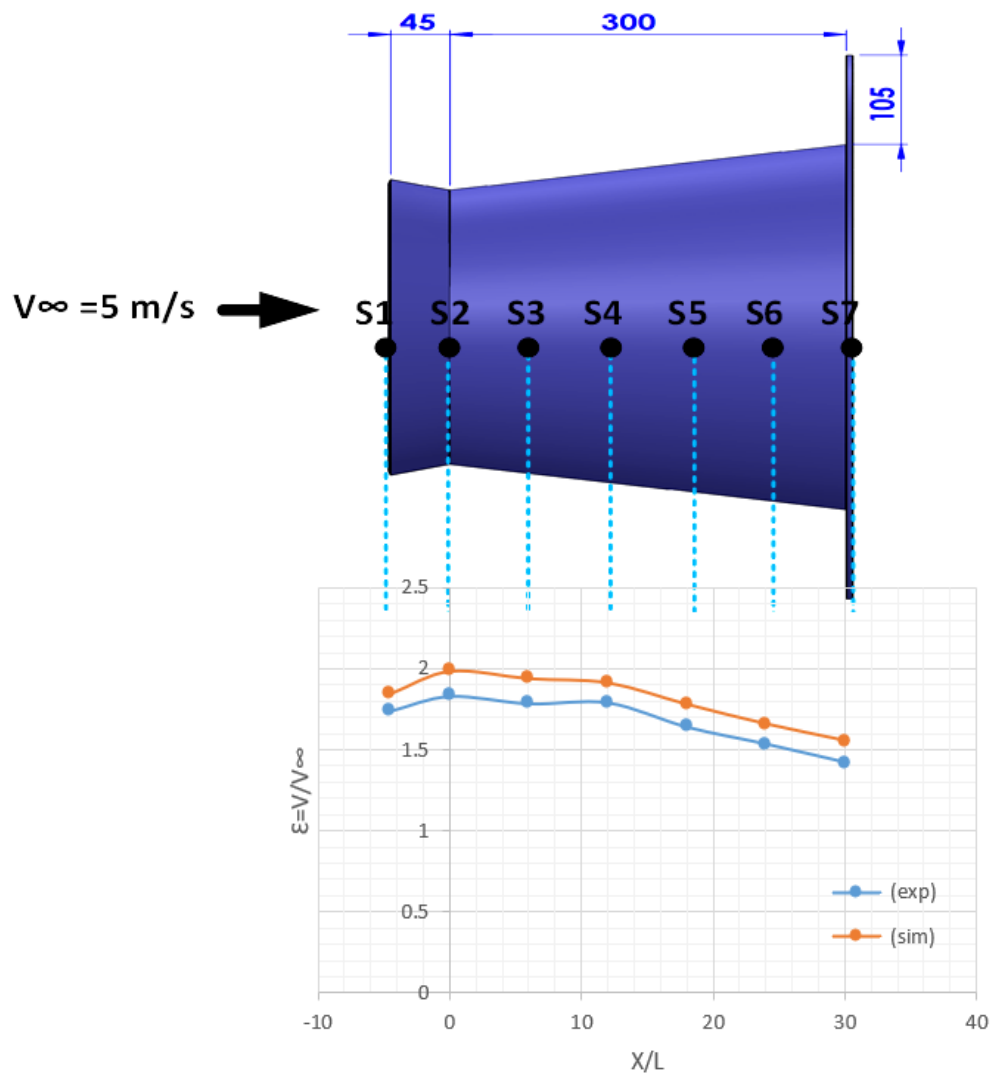


Figure 4-4: position of Pitot tube for readings taken at each section of the BD model.

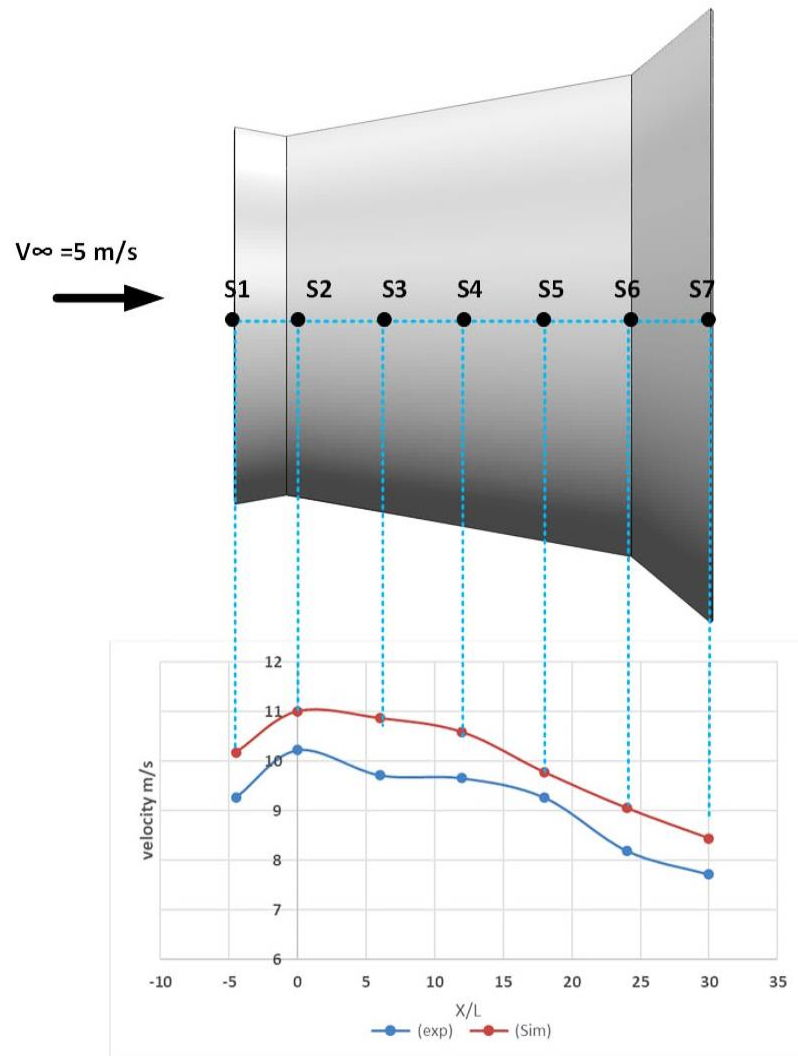


Figure 4-5: position of Pitot tube for readings taken at each section of the OFD model.

Table 4-2: Comparison of factors that distinguish two forms of diffuser.

Parameter study	Attempts	L/D	h/D	Θ (deg)	γ (deg)	α (deg)	\square
BD [19]	15	1	0.35	10	0	10	1.986
OFD	81	0.65	0.3	12	50	30	2.2

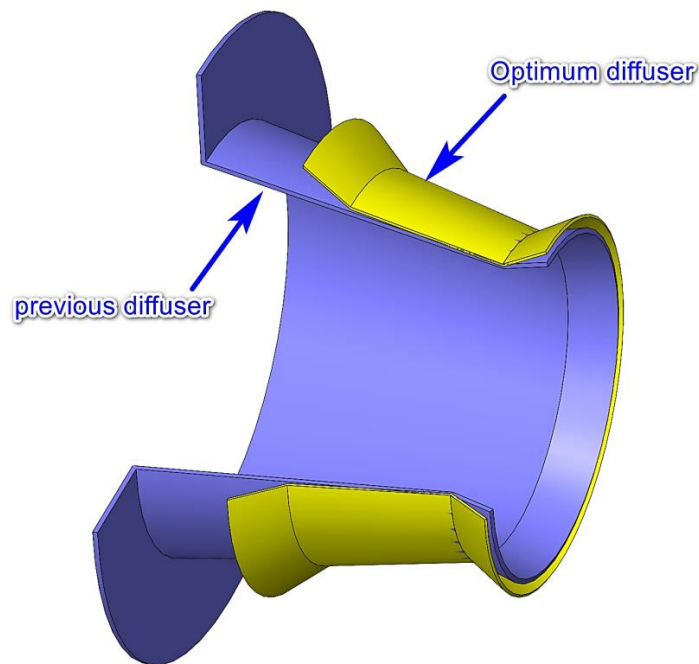


Figure 4-6: Comparison between the two diffuser models

4.3.1 Results of ODE

Many attempts were performed utilizing CFX to find the optimal technical specifications for the ejector. Figure 4-7 depicts the intended and simulated attempts to achieve the highest feasible velocity ratio. Model-7 was the best model of an optimal diffuser with an ejector (ODE), with a speed ratio of up to 2.4. The ODE has an optimized pre-engineered diffuser with no flange, which improves efficiency and sustainability in wind energy applications. This increase in velocity of wind for OED model was due to the presence of an ejector at an appropriate height at the outlet of the diffuser, which caused the generation of vortices behind the flange that produced a pressure drop at the outlet of the ejector.

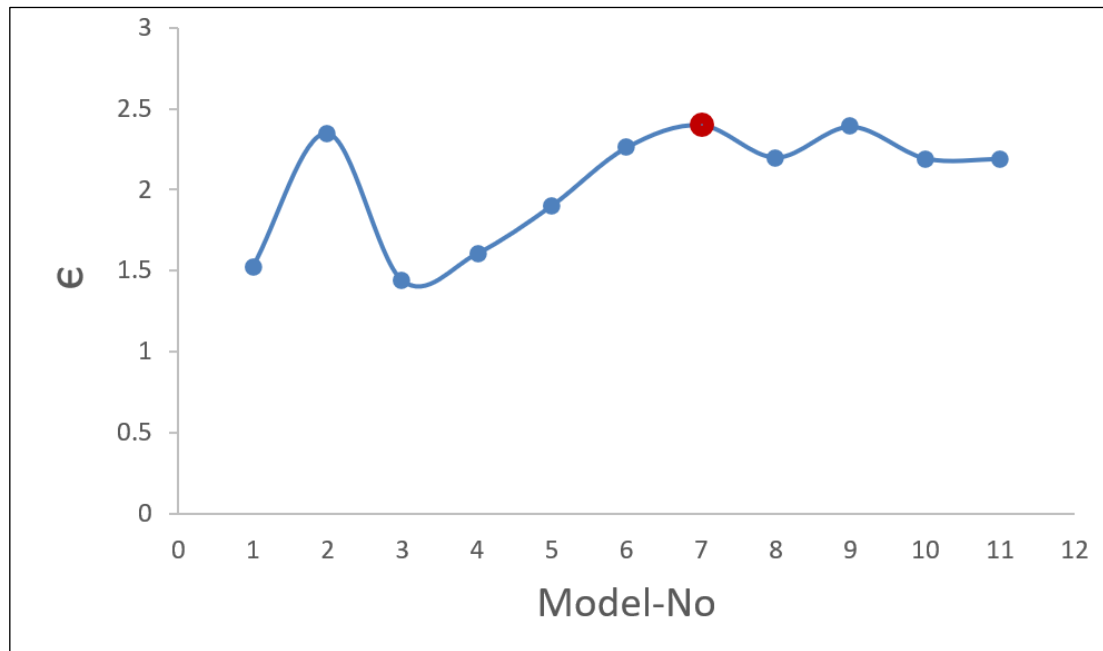
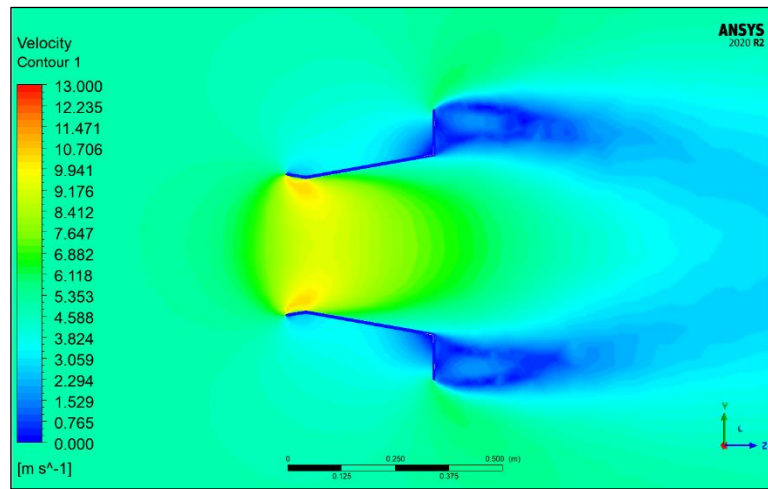


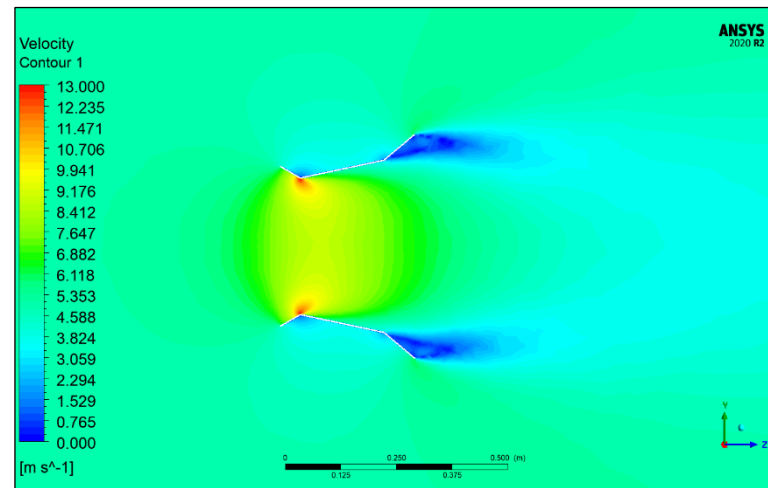
Figure 4-7: Velocity ratio for different ODE models

4.3.2 Visualization of diffuser models

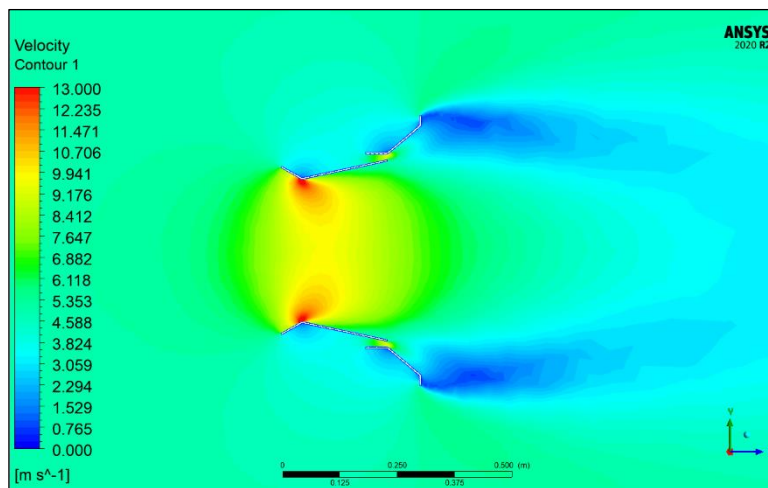
The simulated visualization for the three diffuser types was shown in terms of velocity contour, velocity streamlines, and pressure contour at a specified wind velocity of 5 m/s. The streamlines flow smoothly inside the diffuser, and the streamline velocity does not fluctuate considerably in the radial direction, Except for the boundary-layer region near the diffuser wall. As a result, the flow inside a diffuser is strongly connected to the surrounding flow, resulting in the formation of low pressure at the diffuser wake, which works as a vacuum, sucking in and speeding up the wind. In this regard, a flange placed at the diffuser outlet is critical for accelerating the oncoming flow. As seen in Figures 4-(8,9,10), a flange generates a massive separation behind it, where a very low-pressure region. (all contours velocity for other diffusers models illustrated in Appendix C).



(A)



(B)



(C)

Figure 4-8: Velocity contours at upstream wind flow of 5 m/s for (A): BD, (B): OFD, (C): ODE

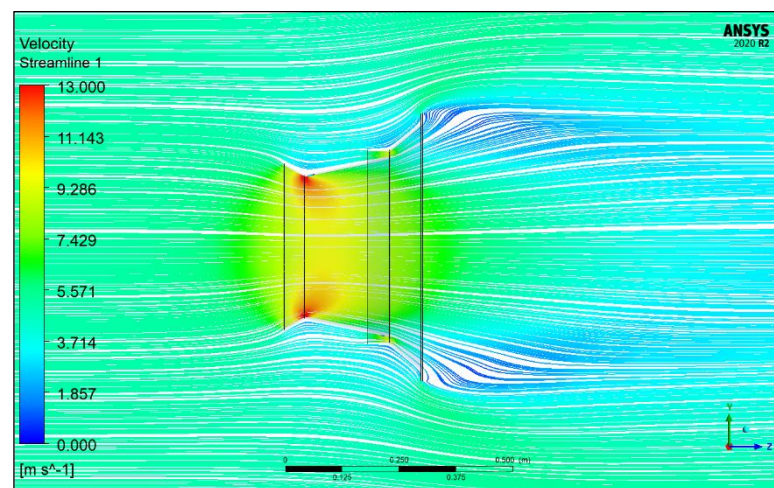
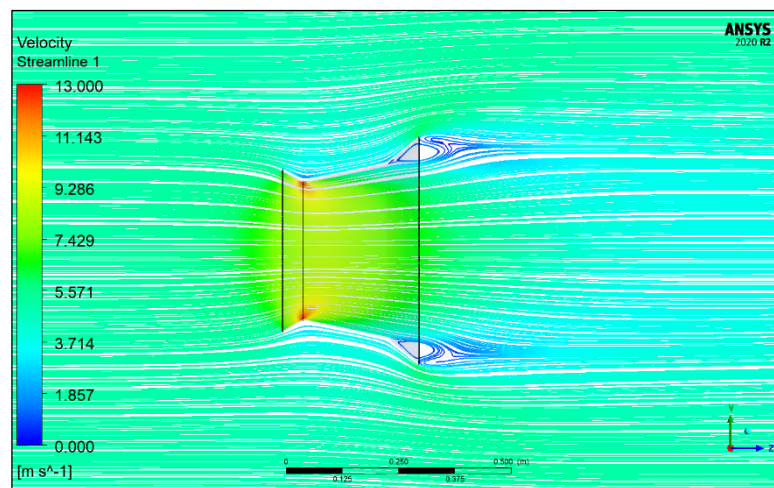
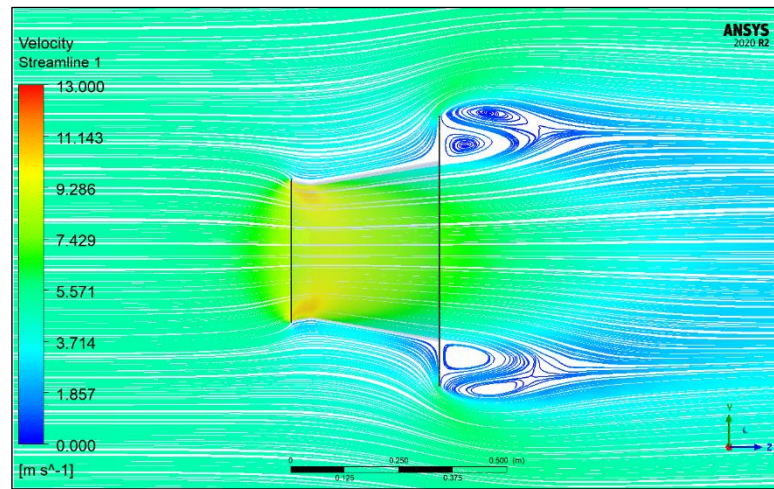
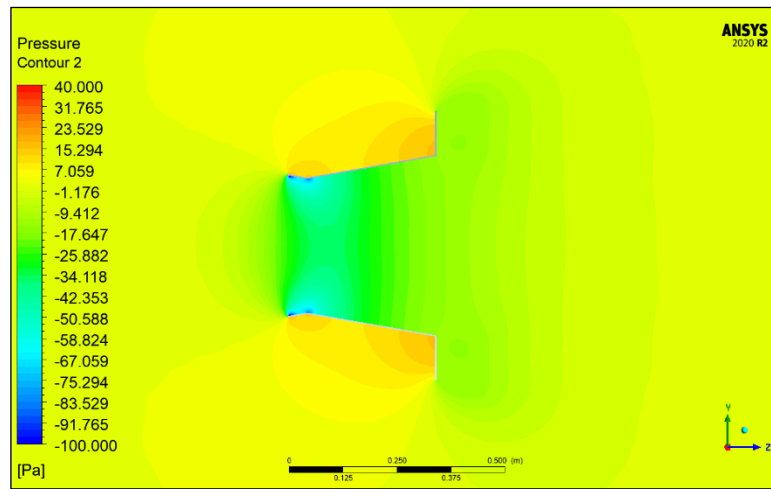
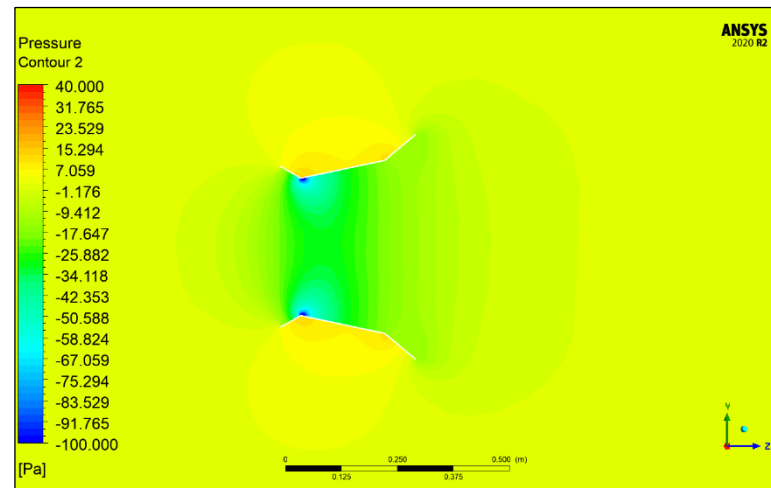


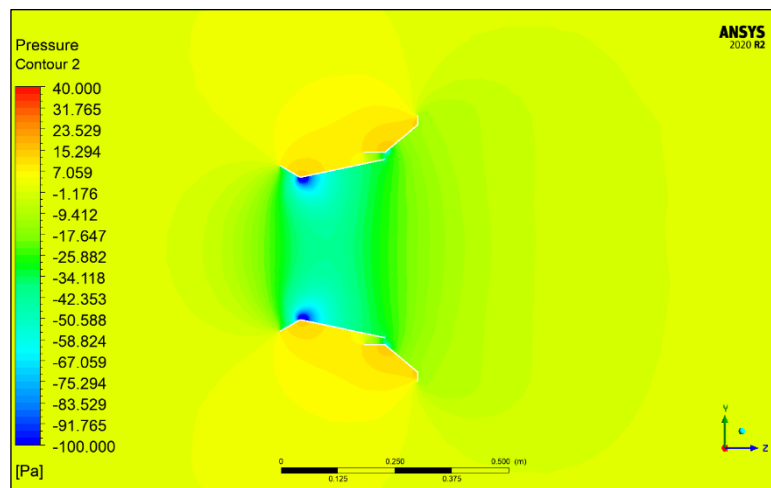
Figure 4-9: Velocity streamlines at upstream wind flow of 5 m/s for (A): BD, (B): OFD, (C): ODE



(A)



(B)



(C)

Figure 4-10: Pressure contours at upstream wind flow of 5 m/s for (A): BD, (B): OFD, (C): ODE

4.4 Validation of the diffuser models

The findings of the simulated diffuser models were confirmed by doing experiments on the two models; OFD and ODE. The experimental tests were conducted in the same range of wind speeds from 5 to 9 m/s, as indicated in Subsection 3.4.4. The experiments were performed three times for each velocity at each configuration (at throat) to ensure the correctness and precision of the data, which is critical for any experimental measurements. The mean value of several measurements, \bar{x} , best determines the accuracy of an experimental value, which is calculated as the following equation, where x_i represents a measurement and n is the number of measurements[66].

$$\bar{x} = \frac{\sum_{i=1}^n x_i}{n} \quad (4.1)$$

Table 4-3: The measured wind velocity values for diffuser configurations

V_{∞} (m/s)	OFD				ODE			
	x1	x2	x3	\bar{x}	x1	x2	x3	\bar{x}
5	10.86	10.92	10.89	10.89	11.63	11.84	11.77	11.75
6	11.75	11.89	11.99	11.88	12.56	12.79	12.71	12.69
7	12.93	13.08	13.19	12.94	13.82	14.07	13.98	13.96
8	15.20	15.29	15.25	15.25	16.28	16.58	16.48	16.45
9	17.03	17.12	17.08	17.08	18.24	18.57	18.46	18.42

The accuracy of a collection of measurements is expressed as σ to the root square of n , often known as standard deviation of the mean. σ and $\bar{\omega}$ are calculated using the following formulas:

$$\sigma = \sqrt{\frac{\sum_{i=1}^n (x_i - \bar{x})^2}{n-2}} \quad (4.2)$$

$$\bar{\omega} = \frac{\sigma}{\sqrt{n}} \quad (4.3)$$

Table 4.3 shows the data and mean measurements for all diffuser designs, with $\bar{\omega}$ values of ± 0.109 and ± 0.1197 for the flange diffuser and diffuser with ejector, respectively. The mean measurements used to validate findings showed a close agreement in experimental results, as shown in Figure 4-11.

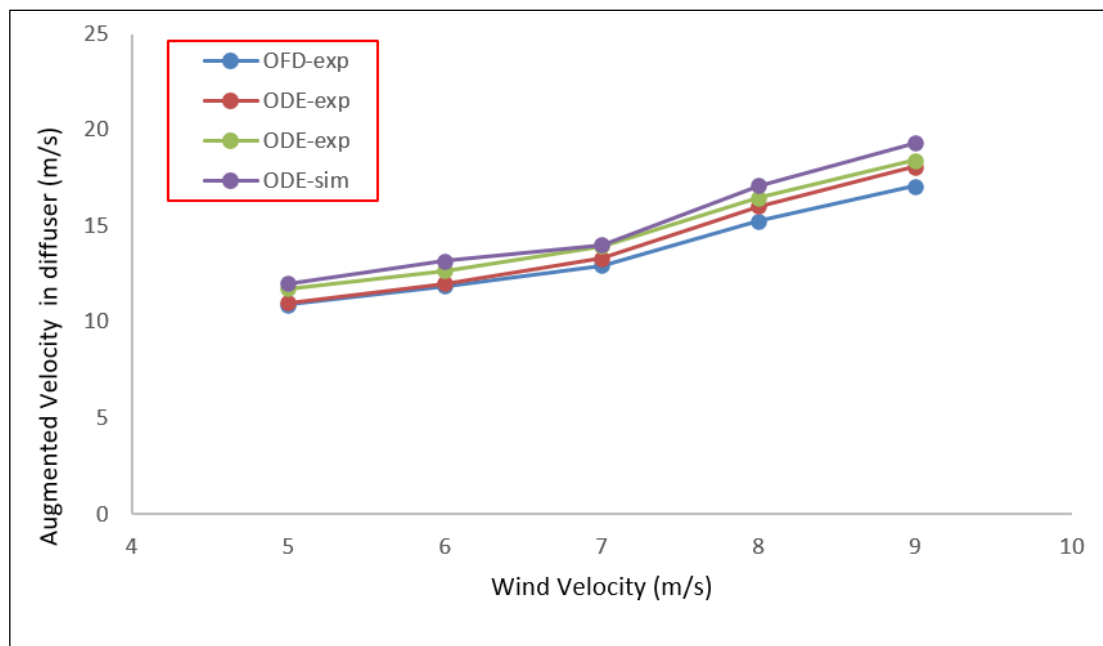


Figure 4-11: Validation of OFD and ODE models in range of wind velocity

4.5 Experimental analysis of FDAWT and ESAWT

Practical tests were carried out to calculate the aerodynamic performance characteristics of the turbine. Experimental tests were performed to calculate the aerodynamic performance characteristics of the turbine, especially power. The turbine model designed in this study worked over a range of upstream wind speeds, including low speeds, but was tested over a specific speed range of 5-9 m/s. Experimental test characteristics for BHAWT, FDAWT, and ESAWT are shown in Table 4-4. All configurations are listed in the table in terms of maximum rotational speed and maximum power at the average reading of all wind speeds used.

Table 4-4: Experimental the performance results of BHAWT, FDAWT and ESAWT

V_{∞} (m/s)	Rotational speed			Max Power output			Max Torque		
	(rpm)			(W)			(N.m)		
	BHAWT	FDAW	ESAWT	BHAWT	FDAWT	ESAWT	BHAWT	FDAWT	ESAWT
5	950	1030	1050	1.07	2.219	2.44	0.0107	0.0203	0.0222
6	1140	1236	1260	1.94	3.46	3.50	0.0162	0.0267	0.0265
7	1311	1446	1474	2.91	5.536	5.577	0.0212	0.0365	0.0361
8	1573	1633	1665	4.36	8.29	8.342	0.0264	0.0485	0.0478
9	1840	1832	1868	6.1	11.93	12.37	0.0316	0.0622	0.0632

Figures (4-12 and 4-13) show the maximum power recorded as a function of free stream wind velocity. As can be seen, as the wind speed increased, the power output increased for all configurations, starting at low power and increasing to a maximum power of 9 m/s. It can also be said that the variation in output increase was smaller at low wind speeds than at high wind speeds. There was a difference in performance improvement between BHAWT, FDAWT, and ESAWT. On the other hand, ESAWT and FDAWT achieved significant power enhancement compared to BHAWT, and this was because the diffuser flange created a larger pressure drop at the manifold outlet, allowing the air to enter at a higher velocity.

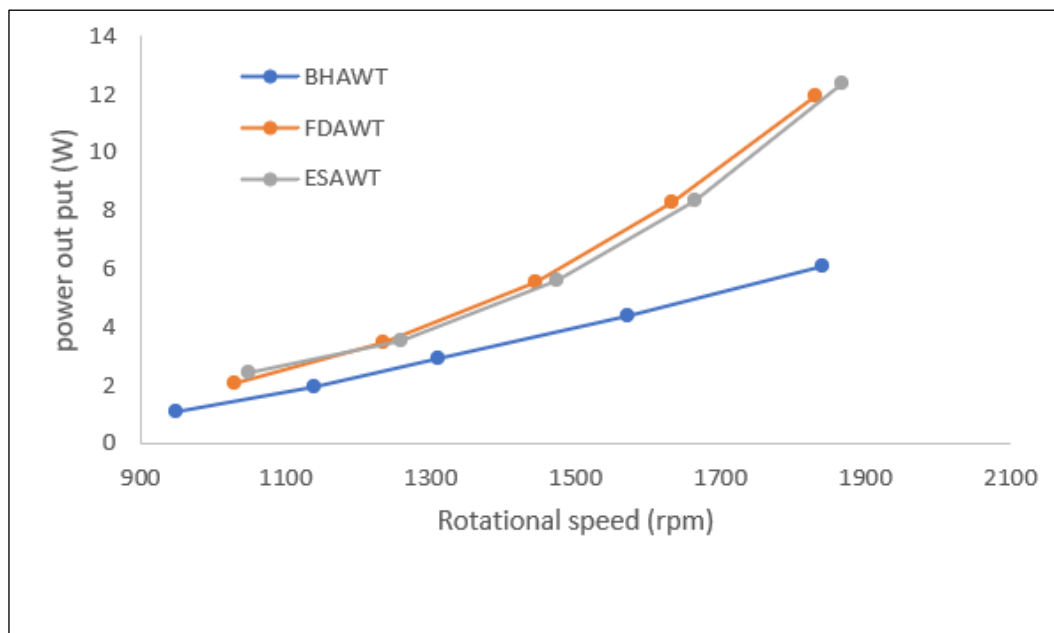


Figure 4-12: Comparing of max power output for (BHAWT, FDAWT, and ESAWT) in terms of rotational speed

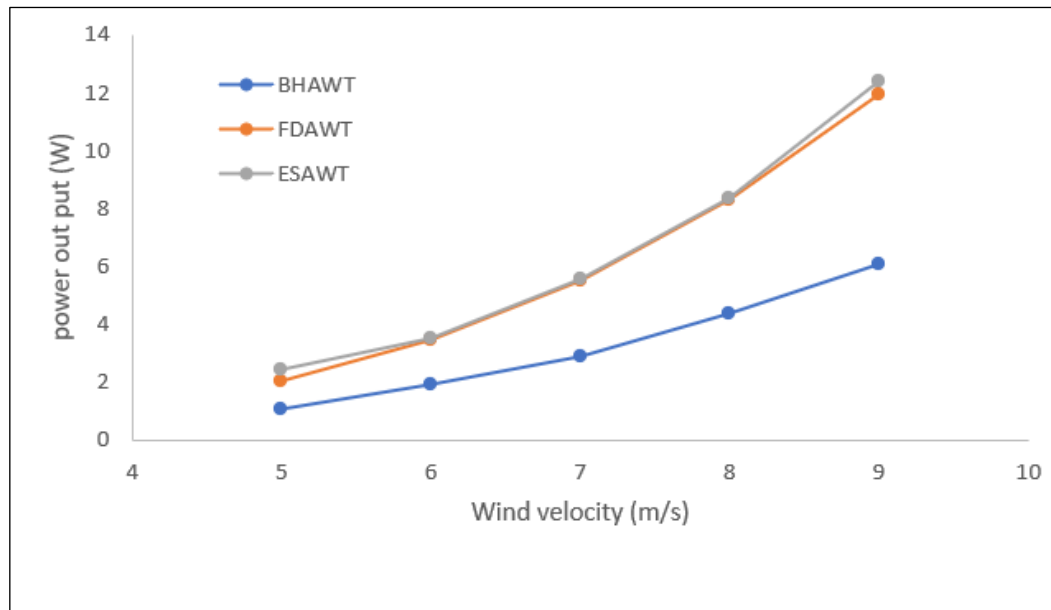


Figure 4-13: Comparing of max power output for (BHAWT, FDAWT, and ESAWT) in terms of wind velocity.

4.6 Evaluation of mechanical torque

In order to illustrate the effectiveness of the submitted designs, the mechanical torque for each of the three models (BHAWT, OFDAWT, and ESAWT) was assessed at varying wind speeds between 5 and 9 m/s. The information in Figure 4-14 results showed that, for all models, the mechanical torque tended to rise as free-stream wind velocity rose. However, the torque produced by BHAWT was less than that of DAWT in all of its forms, but it rose as the wind speed rose. For all configurations, the maximum torque was measured at a wind speed of 9 m/s. As a result, it was seen that the ESAWT had a significant; therefore, it was worth noting that there were benefits of enclosing the HAWT with an appropriate diffuser to form ESAWT for increasing the torque.

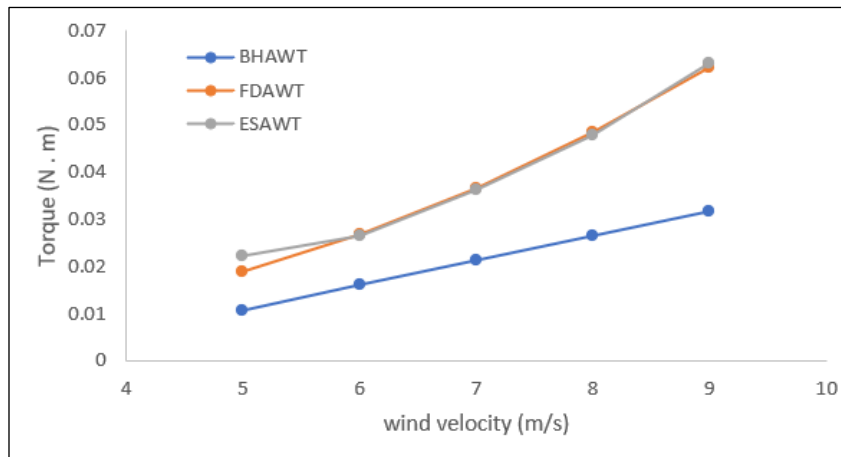


Figure 4-14: Comparing of max torque output for (BHAWT, FDAWT, and ESAWT) in terms of wind velocity

As previously stated, the criterion for representing power coefficient were the highest values of C_p . In the case of wind speeds ranging from 5 to 9 m/s, as illustrated in Figure 4-15, By examining the numbers one by one, it is possible to see that the value of the C_p was approximate stabile. The ESAWT model maintained the highest average C_p value at 0.407, while was approximately 0.395 for FDAWT where they higher than C_p for BHAWT that was 0.207 in average.

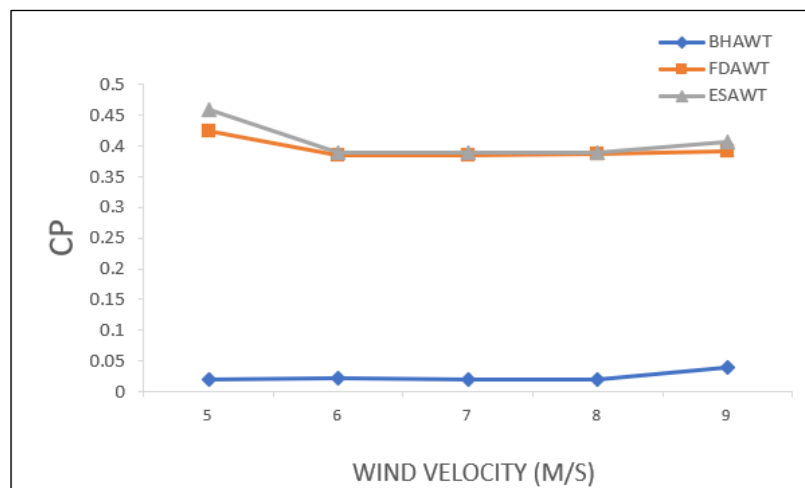


Figure 4-15: Comparing of max power coefficient for (BHAWT, FDAWT, and ESAWT) in terms of wind velocity

4.7 Evaluate of aerodynamic coefficients

The aerodynamic performance of three wind turbine models (BHAWT, FDAWT, ESAWT) was analyzed using the aerodynamic criterion, which represents the turbine's efficiency and is known as the power coefficient (C_p) and torque coefficient (C_T) as a function of the tip speed ratio λ . As a result, as shown in Figure. 4-16, the power coefficient increased as the tip speed ratio increased until reaching a maximum value, then experienced a diminishing trend because when the rotor rotated quickly, will increase the pressure level inside the turbine it appeared like an air disk, so air passed through it with less effect. The results also revealed that when the rotor is surrounded by DAWT and ESAWT, the power increases dramatically Due to the pressure drop behind the diffuser, as illustrated in Figure 4-17. Experimental test characteristics for BHAWT, FDAWT, and ESAWT are shown in Tables 4-(5,6,7). All configurations are listed in the table in terms of maximum rotational speed (RPM) and maximum power at the velocity of 5 m/s.

Table 4-5: BHAWT Torque, Power and C_p Data at V_∞ of 5 m/s

N (rpm)	ω (rad/sec)	λ (-)	I-exp (A)	V-exp (V)	P-exp (W)	C_p exp	C_T exp
172	18.0026	0.54008	0.0073	8.10	0.131912	0.0253	0.046852396
320	33.4933	1.0048	0.0076	16.50	0.279312	0.0535	0.053323122
440	46.0533	1.3816	0.0113	18.50	0.46552	0.0892	0.064634087
541	56.6246	1.69874	0.013	20.00	0.59637	0.1144	0.07324665
650	68.0333	2.041	0.0171	21.00	0.798424	0.1531	0.075040579
790	82.687	2.4806	0.0182	22.25	0.902088	0.1730	0.069758602
860	90.0133	2.7004	0.020	22.00	1.024496	0.1965	0.072775931
950	99.4333	2.983	0.0208	23.3	1.078176	0.2068	0.069333322
1022	106.969	3.20908	0.015	27.00	0.923208	0.1770	0.055185453
1100	115.133	3.454	0.0089	30.24	0.60456	0.1159	0.033575514

Table 4-6: FDAWT Torque, Power and C_p Data at V_∞ of 5 m/s

N (rpm)	ω (red/sec)	λ (-)	I-exp (A)	V-exp (V)	P-exp (W)	C_p exp	C_T exp
193	20.20066	0.6060	0.0079	8.10	0.14328	0.0274	0.0453
372	38.936	1.1680	0.009	16.50	0.3382	0.0648	0.0555
502	52.54266	1.5762	0.0105	25.00	0.58346	0.1119	0.0710
627	65.626	1.9687	0.0138	27.00	0.83044	0.1593	0.0809
710	74.3133	2.2293	0.0157	35.50	1.24012	0.2378	0.1067
762	79.756	2.3926	0.0146	44.90	1.46664	0.2813	0.1175
820	85.8266	2.5747	0.0126	60.3	1.69701	0.3255	0.1264
1030	107.8066	3.2341	0.0203	62.00	2.198	0.4216	0.1300
1180	123.5066	3.7051	0.0116	71.60	1.85324	0.3555	0.0959
1330	139.2066	4.1761	0.0084	77.40	1.45914	0.2799	0.0670

Table 4-7: ESAWT Torque, Power and C_p Data at V_∞ of 5 m/s

N (rpm)	ω (red/sec)	λ (-)	I-exp (A)	V-exp (V)	P-exp (W)	C_p exp	C_T exp
196	20.5146	0.61544	0.0116	8.5	0.2191	0.042	0.0682
380	39.7733	1.1932	0.0124	16.8	0.4634	0.0888	0.0744
510	53.38	1.6014	0.0136	25	0.7565	0.1451	0.0906
635	66.4633	1.9939	0.0155	33.3	1.1506	0.2207	0.1106
715	74.8366	2.2451	0.02	35.5	1.5749	0.3021	0.1345
770	80.5933	2.4178	0.0197	44.3	1.9424	0.3726	0.1541
825	86.35	2.5905	0.0199	51	2.2552	0.4326	0.1669
1050	109.9	3.297	0.021	52.3	2.44	0.4681	0.1420
1200	125.6	3.768	0.0178	60.5	2.3943	0.4592	0.1218
1358	142.137	4.26412	0.019	74.4	2.0439	0.392	0.0919

As predicted, increasing the quantity of flow across the rotor plane increased the torque of the rotor, resulting in a considerable increase in power for all models at all wind speeds. As shown in Figure 4-16 and 4-17, the updated design of the (ESAWT) has boosted the power compared to HAWT and FDAWT.

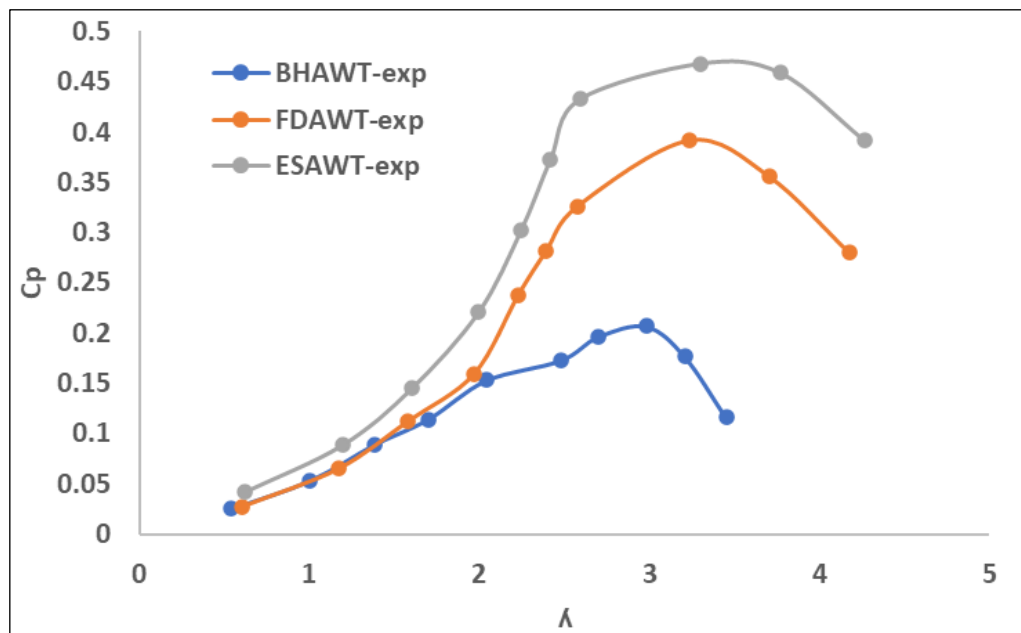


Figure 4-16: Power coefficient's validity as a function of tip speed at $V = 5$ m/s.

To explain the reason why the curve reaches the highest point and then begins to decrease when the rotational speed increases. Increasing the rotational speed at the optimum point will increase the pressure level inside the turbine, and this leads to an increase in the output power, but at the expense of the turbine's efficiency. There is a maximum limit to the rotational speed that the turbine can bear without being damaged. When the speed exceeds this limit, the curve begins to decrease, due to the increase in pressure and losses in efficiency due to excess pressure, and the increase in power .

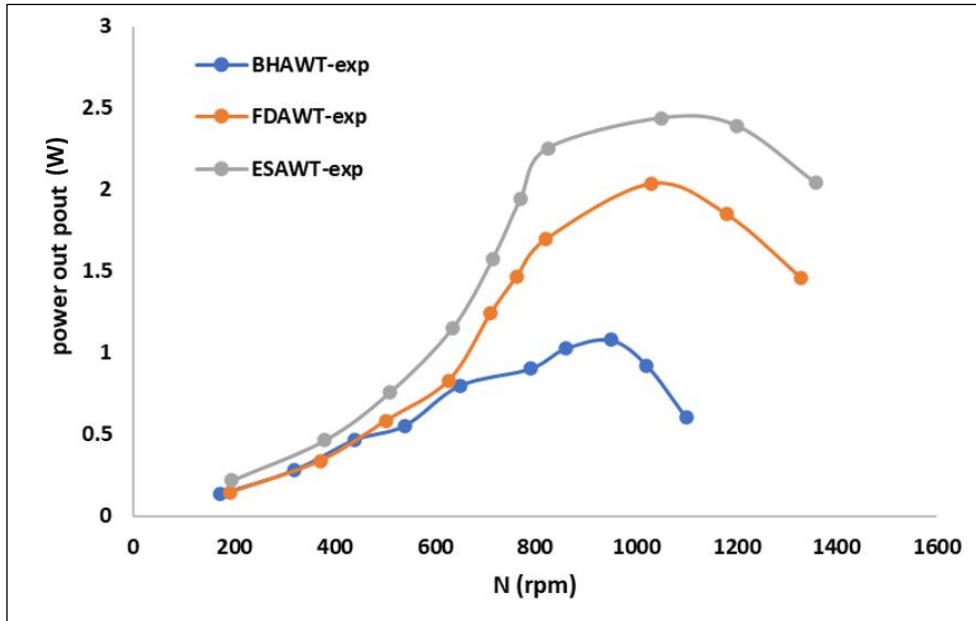


Figure 4-17: Power validity as a function of rotational speed at $V=5$ m/s

4.8 Simulation evaluation the shrouded turbines performance.

The efficiency and performance of wind turbines are better analyzed using the dimensionless aerodynamic coefficient criterion, which represents the aerodynamic efficiency of the turbine model. Turbine coefficients are usually expressed as a function of the tip speed ratio, λ , which varies with rotor speed. Therefore, in this study, performance is expressed by C_P and C_T . To determine the coefficient of performance as a function of tip speed ratio for all configurations BHAWT, FDAWT, and ESAWT, 5 m/s was chosen as shown in Tables 4-(8,9,10) data validation of the three models simulation. As can be seen from these graphs in Figures 4-(18,19,20) the coefficient of performance increased with increasing tip speed ratio until reaching a maximum value, after which it showed a decreasing trend. This is because when the rotor spins at high speed, it looks like an air disc and, therefore, has less airflow effect. The results also showed that the power increases significantly when the rotor is surrounded by DAWT and ESAWT.

Table 4-8: BHAWT Torque, Power, and Power coefficient Data at V_{∞} of 5 m/s

N (rpm)	\square (red/sec)	λ (-)	T (N.m)	P- sim (W)	C_p sim	C_T sim
172	18.0026	0.54008	0.00832	0.1499	0.0287	0.0531
320	33.4933	1.0048	0.00947	0.3174	0.0607	0.0604
440	46.0533	1.3816	0.01148	0.5290	0.1011	0.0731
541	56.6246	1.69874	0.01301	0.7371	0.1409	0.0829
650	68.0333	2.041	0.01331	0.9073	0.1734	0.0849
790	82.687	2.4806	0.01239	1.0251	0.1960	0.0790
860	90.0133	2.7004	0.01293	1.1642	0.2224	0.0823
950	99.4333	2.983	0.01232	1.2252	0.2342	0.0785
1022	106.969	3.20908	0.00980	1.0491	0.2012	0.0626
1100	115.133	3.454	0.00596	0.6870	0.1313	0.0380

Table 4-9: FDAWT Torque, Power, and Power coefficient Data at V_{∞} of 5 m/s

N (rpm)	\square (red/sec)	λ (-)	T (N.m)	P- sim (W)	C_p sim	C_T Sim
193	20.20066	0.6060198	0.009677432	0.195490505	0.0375	0.06187
372	38.936	1.16808	0.010630742	0.413918563	0.0794	0.0679
502	52.54266	1.5762798	0.012858412	0.675615185	0.1296	0.0822
627	65.626	1.96878	0.015648932	1.026976786	0.1970	0.1000
710	74.3133	2.229399	0.018919463	1.405967712	0.2697	0.1209
762	79.756	2.39268	0.021739687	1.733870452	0.3326	0.1390
820	85.8266	2.574798	0.023184335	1.989832687	0.3817	0.1482
1030	107.8066	3.234198	0.020401335	2.199398508	0.4219	0.1304
1180	123.5066	3.705198	0.017305657	2.137362855	0.4100	0.1106
1330	139.2066	4.176198	0.013106979	1.824578047	0.3500	0.0838

Table 4-10: ESAWT Torque, Power, and Power coefficient Data at V_{∞} of 5 m/s

N (rpm)	ω (red/sec)	λ (-)	T (N.m)	P- sim (W)	C_P sim	C_T sim
196	20.514	0.61544	0.011260237	0.231	0.0444	0.0719
380	39.773	1.1932	0.012307241	0.4895	0.0939	0.0786
510	53.38	1.6014	0.014970026	0.7991	0.1533	0.0957
635	66.463	1.9939	0.018282261	1.2151	0.2331	0.1168
715	74.836	2.2451	0.022220391	1.6629	0.3190	0.1420
770	80.593	2.4178	0.025452477	2.0513	0.3935	0.1627
825	86.35	2.5905	0.027257672	2.3537	0.4515	0.1742
1050	109.9	3.297	0.023674249	2.6018	0.4991	0.1513
1200	125.6	3.768	0.020129777	2.5283	0.4850	0.1287
1358	142.137	4.26412	0.015187424	2.1587	0.4141	0.0971

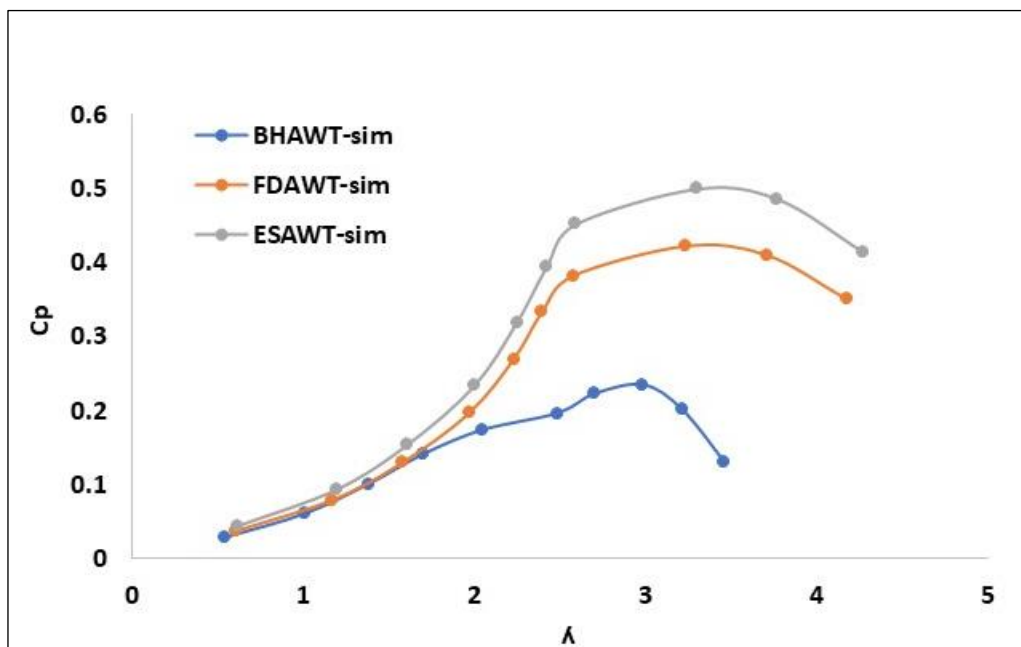


Figure 4-18: Power coefficient's validity as a function of tip speed ratio at $V = 5$ m/s

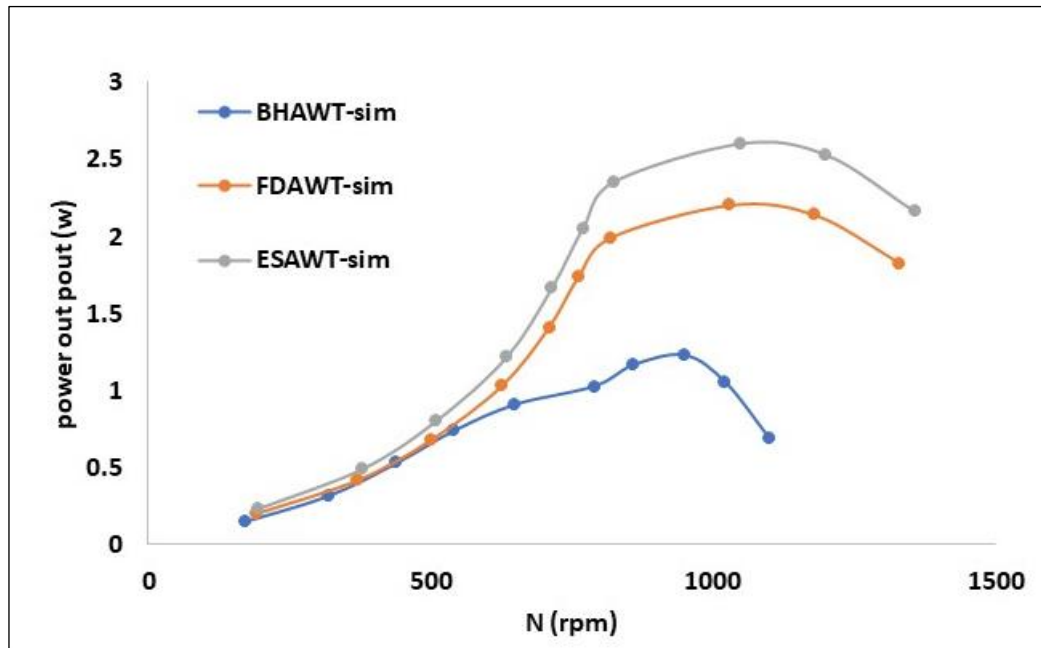


Figure 4-19: power validity as a function of rotational speed at V=5 m/s

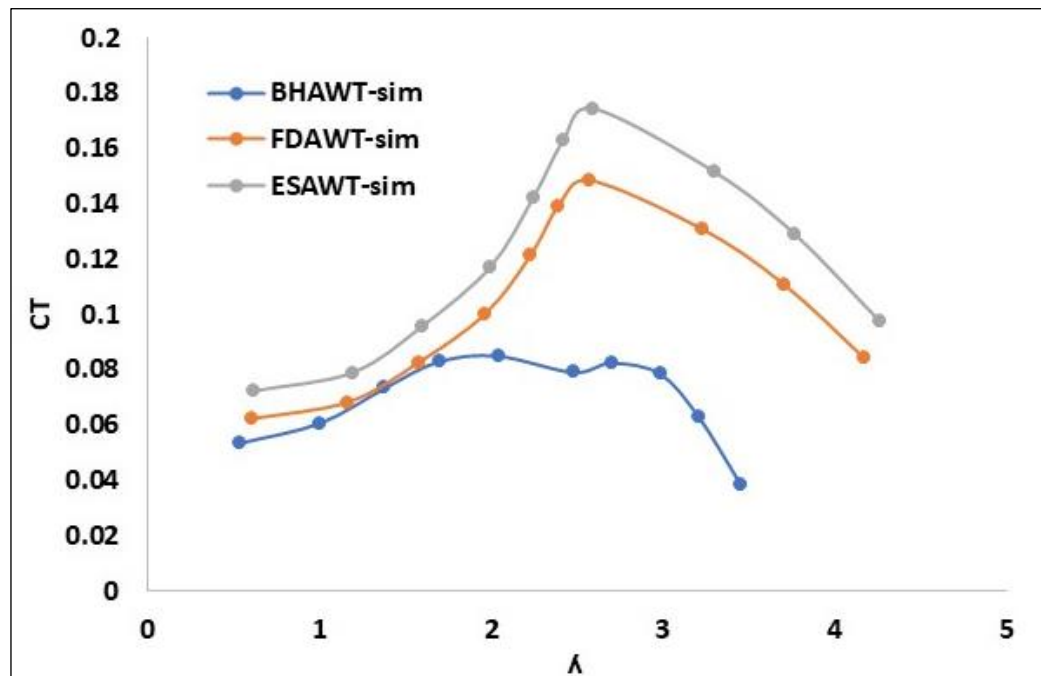


Figure 4-20: Torque coefficient's validity as a function of tip speed ratio at V=5 m/s.

4.9 CFD Simulation validation for the models

Prior to presenting the simulation results of the best DAWT models compared to BHAWT, the working domain should be validated. As a consequence, the validation approach was carried out by first adopting the best FDAWT, ESAWT models related to the BHAWT model by comparing experimental and simulation findings in terms of power coefficient as a function of tip speed ratio.

The initial validation used the power coefficient as a function of tip speed ratio for the best FDAWT, ESAWT, and BHAWT models at 5 m/s wind speed, as shown in Figure 4-21. This chart shows that there was good convergence between experimental and simulation findings within the permitted range about 10.3% on average. (All details of visualization for velocity contours, streamlines, and pressure contours for BHAWT, FDAWT, and ESAWT models were illustrated in Appendix D).

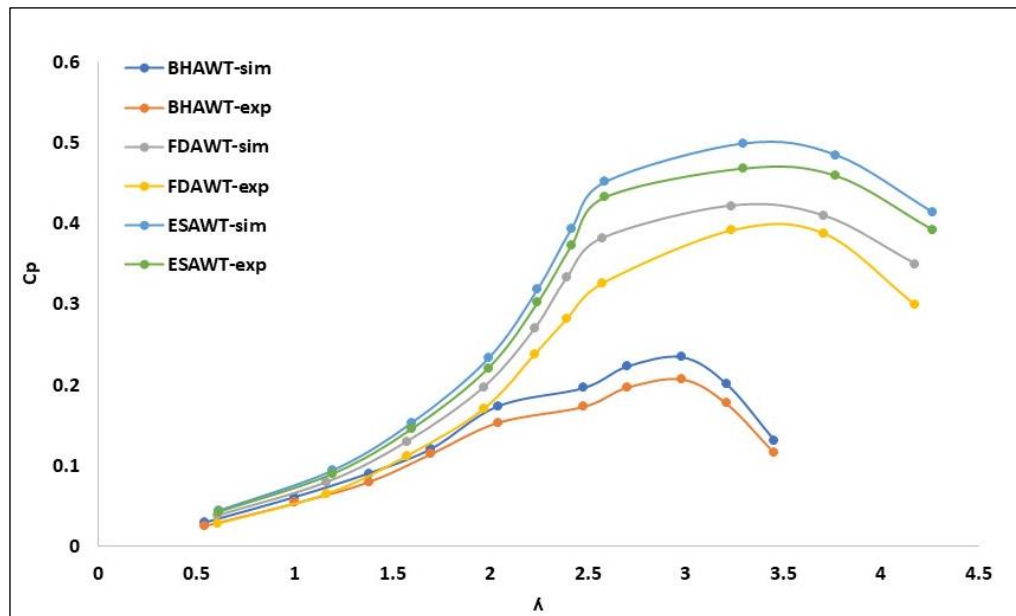


Figure 4-5: Validation of power coefficient as a function of tip speed at $V_{\infty} = 5\text{m/s}$.

4.10 Summary

This chapter aimed to show and debate the outcomes of two methodological techniques, simulation and experiments, that were achieved via planning. The findings were given in stages, beginning with simulation results of the diffuser in a 3D model and progressing to experimental validation. The experimental part was carried on by presenting and discussing the findings of the experiments for the BHAWT, FDAWT, and ESAWT models in terms of power, torque, power coefficient, and torque coefficient.

The simulation was carried out to determine the optimal ESAWT model compared to BHAWT, beginning with validation to ensure the validity of the assumptions and methodologies used in the simulation. Furthermore, simulations have been carried out since they can cover a broad spectrum of research.

Chapter Five

Conclusion and Recommendations

5.1 Introduction

This chapter was organized to provide a summary and compilation of the major objectives raised in this study, as well as concluding remarks and recommendations for the future course of action. This chapter also presented the findings from the ESAWT design development and practical and simulated tests. It also highlighted the findings of the significant study in this field. This may aid researchers in the field of wind energy investment by suggesting a more efficient wind turbine and the adoption of acceptable methodologies for performing performance evaluations on ESAWT, particularly small scaled types.

5.2 Conclusion

This Work concentrated on the investigation of wind energy investment in urban areas using the DAWT technique., which included developing the diffuser with ejector for the enclosing of a small-scale bare HAWT, improving the performance of HAWT model by including it in a diffuser with ejector (ESAWT), and determining or comparing the performance of ESAWT with bare rotor. As a result, the key findings were summarized as follows in accordance with these objectives:

The implementation of the DAWT concept made a quantum jump in enhancing wind power generation compared to traditional wind turbines, particularly for small turbines in urban locations. Enclosing HAWT in a diffuser has been shown to greatly improve performance in terms of wind velocity augmentation and, thus, the C_p value. However, an optimal design for diffuser is necessary to ensure that.

Enveloping the geometry model of the diffuser augmented by an ejector, suitable for shrouding a small-scale model of a HAWT, has proven its ability to increase the flow velocity at the suggested place of the installed rotor. In this dissertation a two geometries models of an empty diffuser were developed they, OFD and ODE using CFD simulation and was validated experimentally. The OFD model was used to shrouded BHAWT to getting FDAWT model. while ESAWT produced from shrouding BHAWT in ODE.

Results of developing the diffusers models showed that, the overall average increase in flow velocity for OFD model was (11.1%), while it reached up to (21.2%) for ODE model comparing to BD model, as well as minimizing the size of model. This increase in velocity of wind for ODE model was due to the presence of an ejector at an appropriate height at the outlet of the diffuser, which caused the generation of vortices behind the flange that produced a pressure drop at the outlet of the ejector.

Increasing wind velocity at the throat of diffuser (for the two models OFD and ODE) led to increase the rotor torque, which boosted the coefficient of power produced for FDAWT by 91.5% over the BHAWT, while ESAWT achieved higher percent up to (98.3%) compare to BHAWT.

On the other hand, in a simulation of the model diffuser (OFD), it has been calculated that the maximum increase in flow velocity ratio at different positions for diffuser (seven positions) along diffuser locations. Also, the rate of increase in flow velocity was calculated experimentally. The practical and theoretical results were compared, and the results

showed a convergence between the practical and simulated results, which gives credibility to the CFD simulation.

5.3 Contribution of the Study

This work made a substantial contribution to the creation of a small scaled effective (ESAWT) model. The ESAWT model increased the power coefficient up to 98.3% compare to BHAWT.

1. The modified model of ESAWT offers various benefits, including high efficiency, a simple design, a compact size, and a low production cost, allowing it to be utilized anywhere under any conditions.
2. Provided a device (Blower) to experimental tests of wind turbines by measuring, wind speed and turbine power output
3. A simple load control board, which regulated the loads linked to the generator, as mentioned in Subsection 3.4.3

5.4 Suggestions for future work

The performance of a small-scale HAWT was enhanced in this work by using an ESAWT model. Further research should be conducted using relevant methodologies, such as simulation or experimentation. As a result, the findings of this study served as a foundation for further research into:

1. Changing the diffuser shape by including spiral lines within the diffuser, adding holes for the flange, modifying the curvature of the flange, or relocating the rotor, and then investigating the effect of these modifications on performance.

2. Examine the effect of modifying the rotor design by increasing the number of blades and adjusting the NACA airfoil profile.
3. Try using a Flying DAWT (Zeppelin).
4. Studying diffuser models and turbines by adding different shapes inside the diffuser to create additional vortices behind the rotor to help reduce pressure.

References

- [1] K. H. Wong, W. T. Chong, N. L. Sukiman, S. C. Poh, Y.-C. Shiah, and C.-T. Wang, "Performance enhancements on vertical axis wind turbines using flow augmentation systems: A review," *Renewable and Sustainable Energy Reviews*, vol. 73, pp. 904-921, 2017.
- [2] M. Chandrala, A. Choubey, and B. Gupta, "CFD analysis of horizontal axis wind turbine blade for optimum value of power," *International Journal of Energy and Environment*, vol. 4, no. 5, pp. 825-834, 2013.
- [3] M. A. Zefreh, "Design and CFD analysis of airborne wind turbine for boats and ships," *Int. J. Aerosp. Sci.*, vol. 4, no. 1, pp. 14-24, 2016.
- [4] W. Tong, *Wind power generation and wind turbine design*. WIT press, 2010.
- [5] O. Igra, "Research and development for shrouded wind turbines," *Energy Conversion and Management*, vol. 21, no. 1, pp. 13-48, 1981.
- [6] B. L. Gilbert, R. A. Oman, and K. M. Foreman, "Fluid dynamics of diffuser-augmented wind turbines," *Journal of Energy*, vol. 2, no. 6, pp. 368-374, 1978.
- [7] A. Dilimulati, T. Stathopoulos, and M. Paraschivoiu, "Wind turbine designs for urban applications: A case study of shrouded diffuser casing for turbines," *Journal of Wind Engineering and Industrial Aerodynamics*, vol. 175, pp. 179-192, 2018.
- [8] U. Nations. "what-is-renewable-energy." www.un.org/en/climatechange (accessed).
- [9] dorar-aliraq. "How to generate electricity from wind." Iraq. <https://www.dorar-aliraq.net/threads/938896> (accessed).
- [10] N. Winter, "Renewables 2023 Global Status Report collection Economic & Social Value Creation Employment Factsheet," 2023.
- [11] M. K. Johari, M. Jalil, and M. F. M. Shariff, "Comparison of horizontal axis wind turbine (HAWT) and vertical axis wind turbine (VAWT)," *International Journal of Engineering and Technology*, vol. 7, no. 4.13, pp. 74-80, 2018.
- [12] A. W. Abas, F. A. Mohd, and H. I. Mohd, "The influence of roughness and obstacle on wind power map," 2006.
- [13] A. R. Winslow, "Urban wind generation: comparing horizontal and vertical axis wind turbines at Clark University in Worcester, Massachusetts," 2.017
- [14] M. Ebrahimpour, R. Shafaghat, R. Alamian, and M. Safdari Shadloo, "Numerical investigation of the savonius vertical axis wind turbine and evaluation of the effect of the overlap parameter in both horizontal and vertical directions on its performance," *Symmetry*, vol. 11, no. 6, p. 821, 2019.
- [15] A. V. Da Rosa and J. C. Ordóñez, *Fundamentals of renewable energy processes*. Academic Press, 2021.
- [16] J. N. Sørensen, *General momentum theory for horizontal axis wind turbines*. Springer, 2016.
- [17] Y. NASEER, "DESIGN AND OPTIMIZATION OF HAWT USING AUGMENTED," University Of Engineering and Technology LAHORE, 2012 .
- [18] F. A. Al-Sulaiman, "Exergoeconomic analysis of ejector-augmented shrouded wind turbines," *Energy*, vol. 128, pp. 264-270, 2017.

- [19] Y .Y. Maw and M. T. Tun, "SENSITIVITY ANALYSIS OF ANGLE, LENGTH AND BRIM HEIGHT OF THE DIFFUSER FOR THE SMALL DIFFUSER AUGMENTED WIND TURBIN," *ASEAN Engineering Journal*, vol. 11, no. 4, pp. 280-291, 2021.
- [20] Y. Ohya and T. Karasudani, "A shrouded wind turbine generating high output power with wind-lens technology," *Energies*, vol. 3, no. 4, pp. 634-649, 2010.
- [21] G. Lilley and W. Rainbird, "A preliminary report on the design and performance of ducted windmills," 1956.
- [22] O. Igra, "Compact shrouds for wind turbines," *Energy conversion*, vol. 16, no. 4, pp. 149-157, 1977.
- [23] M. O. L. Hansen, N. N. Sørensen, and R. Flay, "Effect of placing a diffuser around a wind turbine," *Wind Energy: An International Journal for Progress and Applications in Wind Power Conversion Technology*, vol. 3, no. 4, pp. 207-213, 2000.
- [24] N. Maftouni and H. Parsa, "Effects of Implementing a Diffuser around the Wind Turbine," in *2019 International Conference on Power Generation Systems and Renewable Energy Technologies (PGSRET)*, 2 :019IEEE, pp. 1-4 .
- [25] S. Mertens, "Wind energy in the built environment: concentrator effects of buildings," 2006.
- [26] T. Rezek, R. Camacho, N. Manzanares Filho, and E. Limacher, "Design of a hydrokinetic turbine diffuser based on optimization and computational fluid dynamics," *Applied Ocean Research*, vol. 107, p. 102484, 2021.
- [27] S. Jafari, F. Safaei, B. Kosasih, and K. C. Kwok, "Power generation analysis of PowerWindow, a linear wind generator, using computational fluid dynamic simulations," *Journal of Wind Engineering and Industrial Aerodynamics*, vol. 147, pp. 226-238, 2015.
- [28] M. Takeyeldein, T. M. Lazim, N. Nik Mohd, I. S. Ishak, and E. A. Ali, "Wind turbine design using thin airfoil sd2030," 2019.
- [29] M. Lipian, M. Karczewski, and K. Olasek, "Sensitivity study of diffuser angle and brim height parameters for the design of 3 kW Diffuser Augmented Wind Turbine," *Open Engineering*, vol. 5, no. 1, 2015.
- [30] H. M. Elbakry, A. A. Attia, O. E. Abdelatif, and M. Zahran, "Simulation of Diffuser augmented wind turbine performance," in *2016 World Congress on Sustainable Technologies (WCST)*, 2016: IEEE, pp. 40-48 .
- [31] M. Werle and W. Presz Jr, "Shroud and ejector augmenters for subsonic propulsion and power systems," *Journal of Propulsion and Power* ,vol. 25, no. 1, pp. 228-236, 2009.
- [32] W. Han, P. Yan, W. Han, and Y. He, "Design of wind turbines with shroud and lobed ejectors for efficient utilization of low-grade wind energy," *Energy*, vol. 89, pp. 687-701, 2015.
- [33] R. Schmidt and A. Hupfer, "Design and numerical simulation of ejector nozzles for very small turbojet engines," *CEAS Aeronautical Journal*, vol. 12, no. 4, pp. 923-940, 2021.
- [34] M. M. Nunes, A. C. B. Junior, and T. F. Oliveira, "Systematic review of diffuser-augmented horizontal-axis turbines," *Renewable and Sustainable Energy Reviews*, vol. 133, p. 110075, 2020.
- [35] N. A. Pambudi *et al.*, "The performance of shrouded wind turbine at low wind speed condition," *Energy Procedia*, vol. 158, pp. 260-265, 2019.

- [36] D. Lokesharun, S. Rameshkumar, B. Navaneeth, and R. Kirubakaran, "Design and Analysis of Diffuser Augmented Wind Turbine using CFD," *International Journal of Mechanical and Industrial Technology*, vol. 7, no. 1, pp. 1-13, 2019.
- [37] R. K. Chhetri, D. B. Upadhyay, and N. Ghimire, "Comparative Analysis of Diffusers for Micro Wind Turbine," *Nepal Journal of Science and Technology*, vol. 20, no. 2, pp. 103-112, 2021.
- [38] M. Takeyeldein, T. M. Lazim, I. S. Ishak, N. Nik Mohd, and E. A. Ali, "Wind lens performance investigation at lowwind speed," 2020.
- [39] W.-X. Wang *et al.*, "Experimental investigation into the influence of the flanged diffuser on the dynamic behavior of CFRP blade of a shrouded wind turbine," *Renewable Energy*, vol. 78, pp. 386-397, 2015.
- [40] T. A. Khamlaj and M. Rumpfkeil, "Optimization study of shrouded horizontal axis wind turbine," in *2018 wind energy symposium*, 2018, p. 0996 .
- [41] F. Q. Putra, D. Rifai, K. Suryoprato, and R. Budiarto, "Multilevel Diffuser Augmented for Horizontal Axis Wind Turbine," in *E3SWeb of Conferences*, 2018, vol. 42: EDP Sciences, p. 01001 .
- [42] M. I. Maulana, A. Syuhada, and M. Nawawi, "Analysis of diffuser augmented wind turbine (DAWT) with flange and curved interior using CFD," in *AIP Conference Proceedings*, 2018, vol. 1984, no. :1 .AIP Publishing LLC, p. 020025 .
- [43] F. Mardiansah, A. D. Putranto, and H. R. Hapsari, "Computational Fluid Dynamics Studies on the Wind Speed Characteristics of an Improved Diffuser Design," in *2018 International Conference and Utility Exhibition on Green Energy for Sustainable Development (ICUE)*, 2018: IEEE, pp. 1-4 .
- [44] S. A. Kale, R. V. Godse, and G. P. Haribhau, "Performance Evaluation of Small Wind Turbine Diffuser with Different Diameters," *International Journal of Innovative Technology and Exploring Engineering*, vol. 8, pp. 1077-1080.
- [45] X. Wang, K. Wong, W. Chong, J. Ng, X. Xiang, and C. Wang, "Experimental investigation of a diffuser-integrated vertical axis wind turbine," in *IOP Conference Series: Earth and Environmental Science*, 2020, vol. 463, no. 1: IOP Publishing, p. 012153 .
- [46] M. Anbarsooz, M. Mazloum, and D. Moghadam, "Converging–diverging ducts for efficient utilization of low-grade wind energy: numerical and experimental studies," *Journal of Renewable and Sustainable Energy*, vol. 12, no. 2, p. 023304, 2020.
- [47] S. Surya, A. A. Gaonkar, and R. Jayakrishnan, "Design and analysis of diffuser casings for diffuser augmented wind turbines," in *2020 4th International Conference on Green Energy and Applications (ICGEA)*, 2020: IEEE, pp. 28-31 .
- [48] S. K. Thangavelu, T. G. L. Wan, and C. Piraiarasi, "Flow simulations of modified diffuser augmented wind turbine," in *IOP Conference Series: Materials Science and Engineering*, 2020, vol. 886, no. 1: IOP Publishing, p. 012023 .
- [49] A. Susandi, F. Arifin, and R. Kusumanto, "Simulation of Diffuser Parameters in the Performance of Horizontal Axis Wind Turbine using Computational Fluid Dynamics," *Technology Reports of Kansai University*, vol. 63, no. 06, 2021.

- [50] J. R. Vaz, V. L. Okulov, and D. H. Wood, "Finite blade functions and blade element optimization for diffuser-augmented wind turbines," *Renewable Energy*, vol. 165, pp. 812-822, 2021.
- [51] A. M. Elsayed, "Design Optimization of Diffuser Augmented Wind Turbine," *CFD Letters*, vol. 13, no. 8, pp. 45-59, 2021.
- [52] K. Watanabe and Y. Ohya, "A simple theory and performance prediction for a shrouded wind turbine with a brimmed diffuser," *Energies*, vol. 14, no. 12, p. 3661, 2021.
- [53] O. K. J. Mohammed Mohsin Shkhair 1, 2, and Salih Meri Al Absi 3, "Effect of Rotor Blades Number and Rotor Position on the Performance of a Diffuser Augmented Wind Turbine," *International Journal of Mechanical Engineering and Robotics Research Vol. 11*, 2022.
- [54] B. Heyru and W. Bogale, "Flow field analysis and testing of curved shroud wind turbine with different flange angle," *Cogent Engineering*, vol. 9, no. 1, p. 2095951, 2022.
- [55] S. Sridhar, M. Zuber, S. Shenoy, A. Kumar, E. Y. Ng, and J. Radhakrishnan, "Aerodynamic comparison of slotted and non-slotted diffuser casings for Diffuser Augmented Wind Turbines (DAWT)," *Renewable and Sustainable Energy Reviews*, vol. 161, p. 112316, 2022.
- [56] D. Gysling and E. Dumlupinar, "Mixer-ejector turbine with annular airfoils," ed: Google Patents, 2014.
- [57] N. Keramat Siavasha, G. Najafi, T. Tavakoli, B. Ghobadian, and E. Mahmoodi, "An investigation on performance of shrouding a small wind turbine with a simple ring in a wind tunnel," *Journal of Renewable Energy and Environment*, vol. 4, no. 4, pp. 49-56, 2017.
- [58] E. Kocand T. Yavuz, "Effect of flap on the wind turbine-concentrator combination," *International Journal of Renewable Energy Research (IJRER)*, vol. 9, no. 2, pp. 551-560, 2019.
- [59] J. Chai, Z. Wang, X. Zhao, and C. Wang, "Multiobjective Optimization of Turbine Coolant Collection/Distribution Plenum Based on the Surrogate Model," *International Journal of Aerospace Engineering*, vol. 2021, pp. 1-12, 2021.
- [60] A. García Auyanet and P. G. Verdin, "Numerical study of the effect of flap geometry in a multi-slot ducted wind turbine," *Sustainability*, vol. 14, no. 19, p. 12032, 2022.
- [61] L. Ramayee, K. Supradeepan, S. Sreejith, and A. Priyadarshini, "Multi-Objective Optimization of Lobed Enclosure for Wind Turbine Applications Using Gray Relation Analysis," *Journal of Energy Resources Technology*, vol. 144, no. 11, p. 111302, 2022.
- [62] M. Ozen. "Mesh Metric Spectrum Quality." Ozen Engineering. https://www.ozeninc.com/wpcontent/uploads/2014/11/MESHING_WORKS_HOP_2014.pdf (accessed).
- [63] A. Tournlidakis, K. Vafiadis, V. Andrianopoulos, and I. Kalogeropoulos, "Aerodynamic design and analysis of a flanged diffuser augmented wind turbine," in *Turbo Expo: Power for Land, Sea, and Air*, 2013, vol. 55294: American Society of Mechanical Engineers, p. V008T44A022 .
- [64] B. Kosasihand H. S. Hudin, "Influence of inflow turbulence intensity on the performance of bare and diffuser-augmented micro wind turbine model," *Renewable Energy*, vol. 87, pp. 154-167, 2016.

- [65] B. Kosasih and A. Tondelli, "Experimental study of shrouded micro-wind turbine," *Procedia Engineering*, vol. 49, pp. 92-98, 2012.
- [66] S. W. Holman, *Discussion of the Precision of Measurements: With Examples Taken Mainly from Physics and Electrical Engineering*. J. Wiley & sons, 1901.

APPENDIX A

List of publications

1. Mohanned Mohammad Naji and Balasem Abdulameer Jabbar ‘Diffuser Augmented Wind Turbine: a review study’ 3rd International Conference on Engineering and Science (ICES2023), Al-Samawa, Iraq 2023,



3rd International Conference on Engineering & Science (ICES2023)
3 -4 MAY 2023 | Al-SAMAWA | IRAQ

Final Acceptance Letter

Manuscript Number: 135_Naji_ICES2023 **Decision ID : 025_FAL_ICES**
Date : 31/3/2023

Dear Mohanned Mohammad Naji ,

Co-Authors : Balasem Abdulameer Jabbar .

Congratulations!

It's a great pleasure to inform you that, after the peer review process, your manuscript entitled **Diffuser Augmented Wind Turbine: a Review Study**

Has been **ACCEPTED** for participating in the **3rd International Conference on Engineering and Science**, and considered for publication in **AIP Conference Proceedings**.

Thank you for your valuable participation in the ICES2023 conference.


Prof. Dr. Sabah Mohammed Milkat
Head of ICES2023 Scientific Committee
Dean of Al-Samawa Technical Institute




Dr. Ahmed Razzaq H. Al-Manea
ICES2023 Scientific Committee
AIP Conference Proceedings Editor

- Mohanned Mohammad Naji and Balasem Abdulameer Jabbar ‘Develop an empty diffuser for enhance the performance of DAWT’ 3rd International Conference on Nanotechnology & Nanoscience, UTAIC, University of Tehran, Tehran, April 2023.




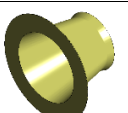
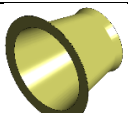
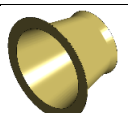
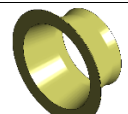
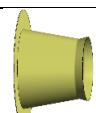
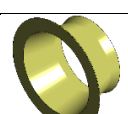
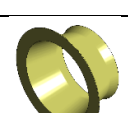
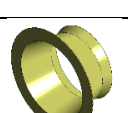


- Mohanned Mohammad Naji and Balasem Abdulameer Jabbar Analysis, ‘Manufacture And Performance Design Of A Diffuser-Augmented Wind Turbine’ International Conference of Sustainability Systems Development (ICSSD2023), Erbil, Iraq, July 2023.



APPENDIX B

Table 1: The achieved values of (ϵ) as a function of the geometrical parameters of an empty flanged diffuser at 5 m/s

Model No.	Θ (deg)	α (deg)	L/D	H/D	\square	Shape of diffuser
1-(BD)	10	10	1	0.33	1.986	
2	10	10	0.87	0.33	1.54	
3	10	10	1	0.2	1.62	
4	10	11	1	0.33	1.63	
5	12	12	1	0.2	1.73	
6	12	12	0.9	0.2	1.71	
7	12	12	0.5	0.2	1.55	
8	10	15	1	0.35	1.84	
9	12	32	0.3	0.2	1.67	
10	12	16	0.5	0.33	1.71	
11	12	18	0.5	0.2	1.77	






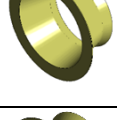
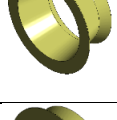
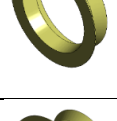
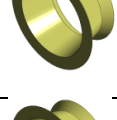
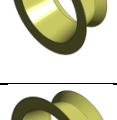
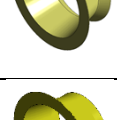
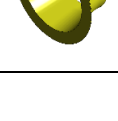



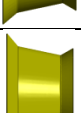


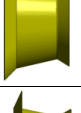


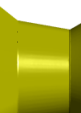
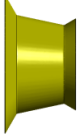
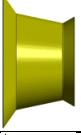

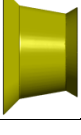
12	12	19	0.5	0.2	1.79	
13	12	20	0.5	0.2	1.81	
14	12	25	0.5	0.2	1.81	
15	12	29	0.5	0.2	1.91	
16	12	30	0.5	0.2	1.95	
17	12	30	0.4	0.2	1.81	
18	12	31	0.5	0.2	1.90	
19	12	32	0.5	0.2	1.90	
20	12	33	0.5	0.2	1.89	
21	12	35	0.5	0.2	1.87	
22	12	35	0.2	0.2	1.54	
23	12	36	0.5	0.2	1.86	

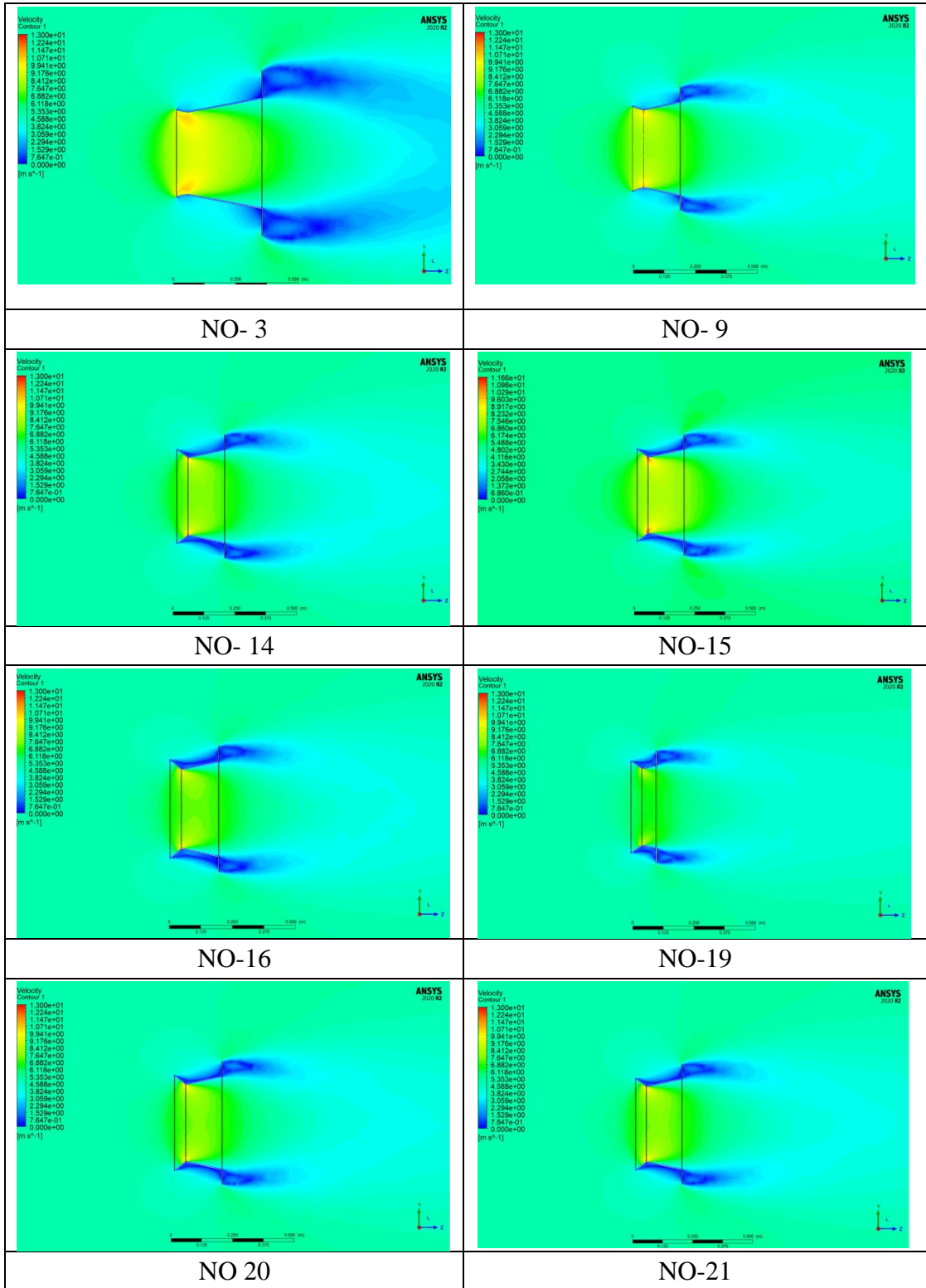
Table 2: The achieved values of (ϵ) as a function of the geometrical parameters of an empty flanged diffuser at $v=5$ m/s

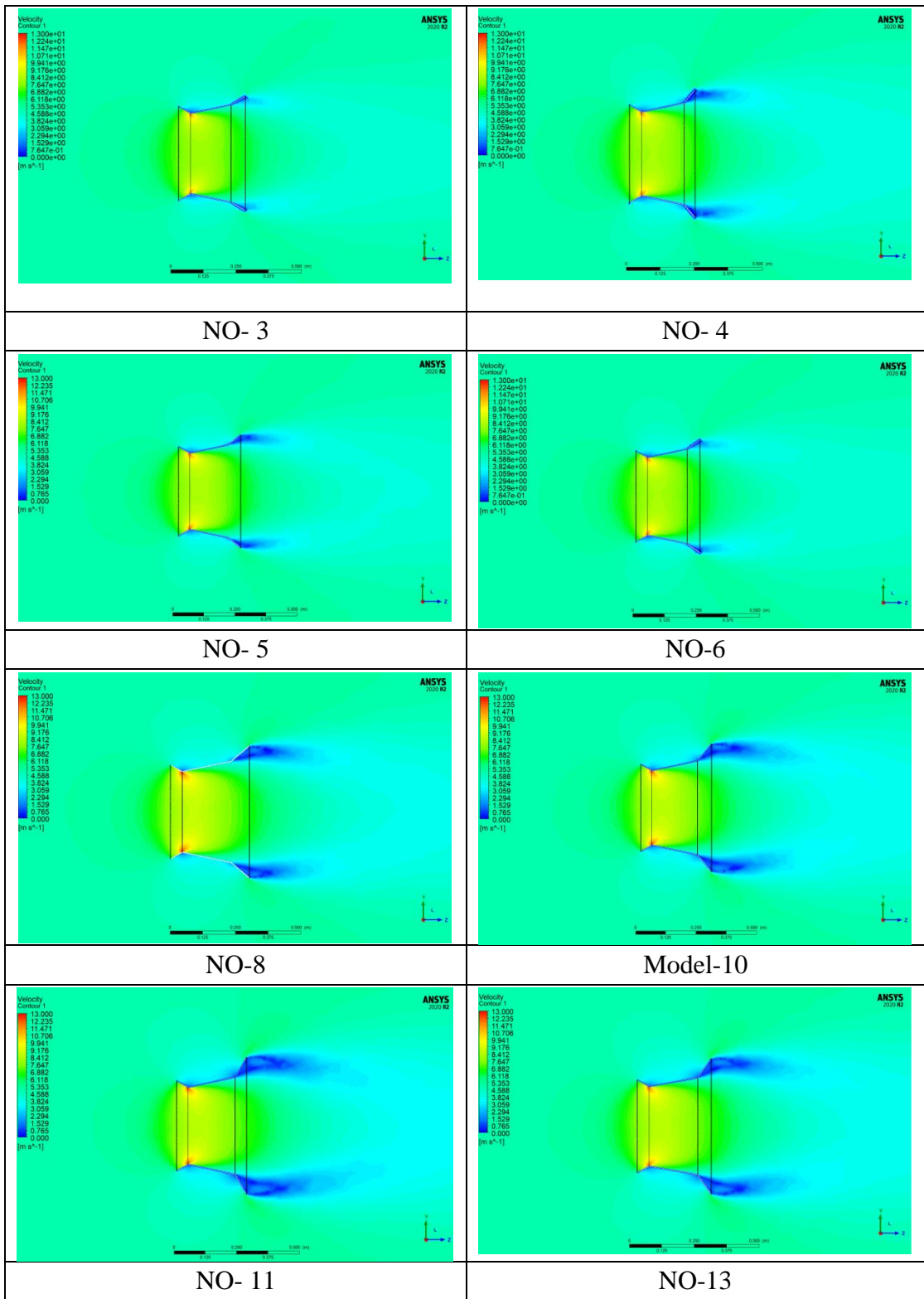
NO	α (deg)	γ (deg)	Θ (deg)	L/D	H/D	ϵ	Shape of diffuser
1	30	50	12	0.5	0.2	2.08	
2	30	55	12	0.5	0.2	2.066	
3	30	60	12	0.5	0.2	2.02	
4	30	40	12	0.5	0.2	2.056	
5	30	35	12	0.5	0.2	2.054	
6	30	47	12	0.5	0.2	2.068	
7	30	-25	12	0.5	0.2	1.946	
8	30	50	12	0.6	0.3	2.2	
9	30	45	12	0.6	0.3	2.189	
10	30	40	12	0.6	0.3	2.169	

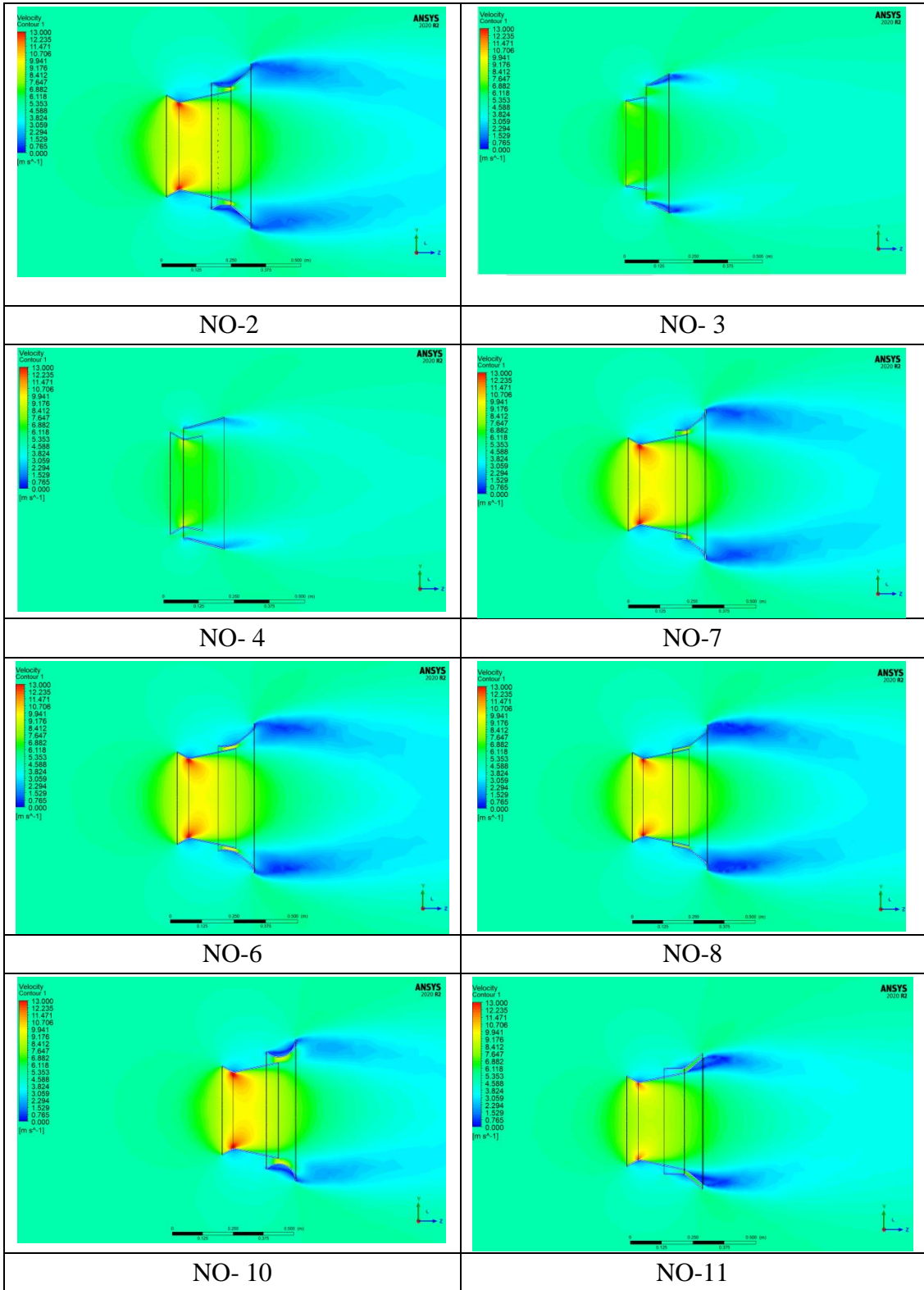
11	30	35	12	0.6	0.3	2.165	
12	30	30	12	0.6	0.3	2.163	
13	30	25	12	0.6	0.3	2.15	
14	30	20	12	0.6	0.3	2.14	

APPENDIX C

Velocity contour of geometrical diffuser parameters







APPENDIX D

Visualization of (BHAWT, FDAW and ESAWT) models

FigureC-1: Velocity contours at upstream wind flow of 5m/s for BHAWT, FDAW and ESAWT

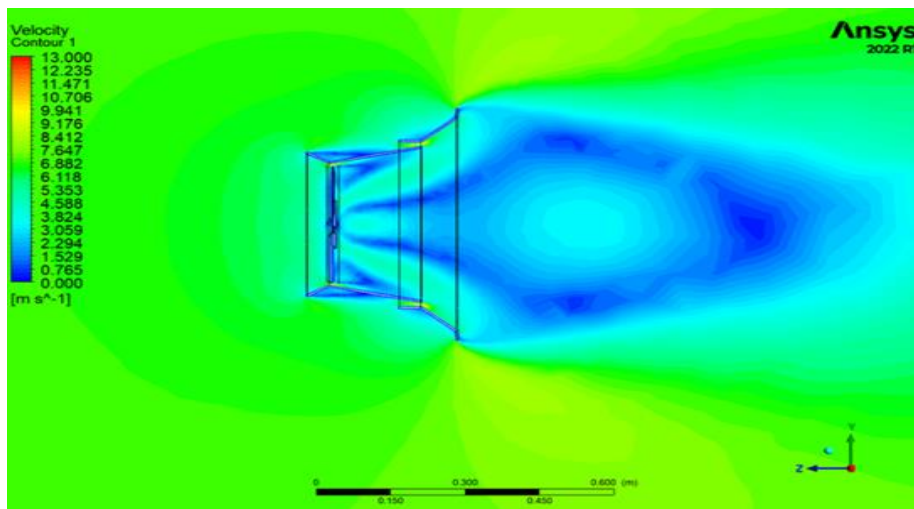
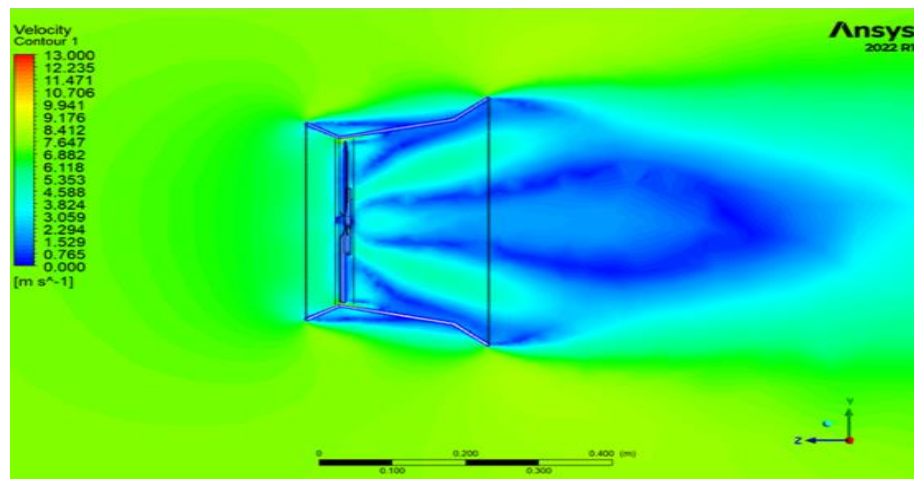
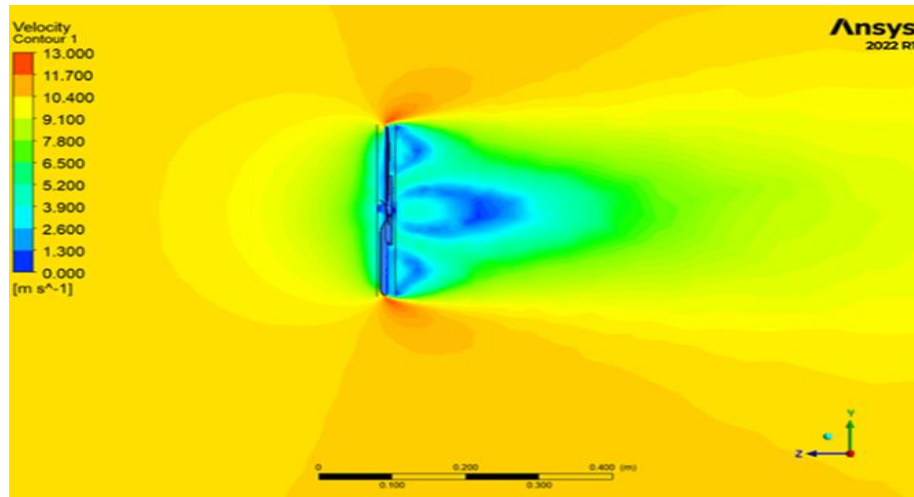


Figure C-2: Velocity streamlines at upstream wind flow of 5m/s for BHAWT, FDAWT and ESAWT

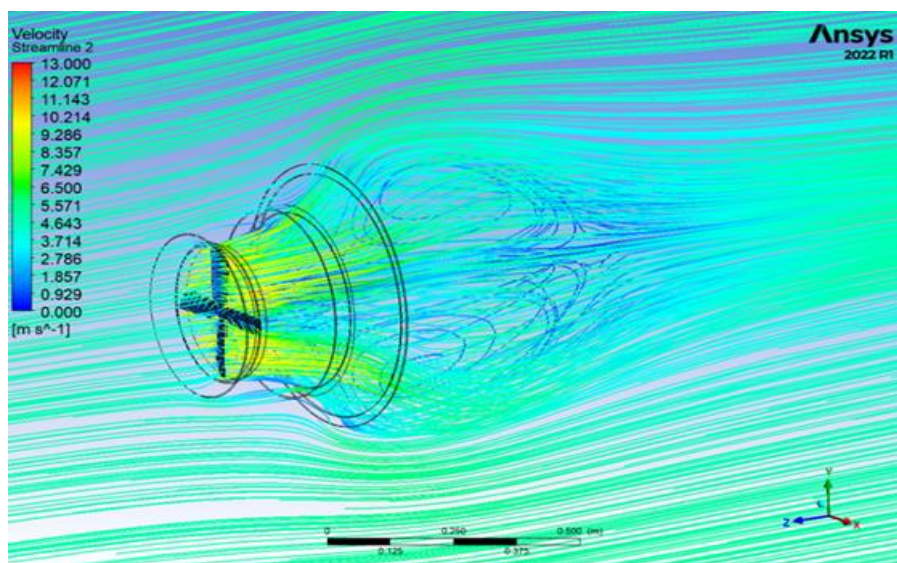
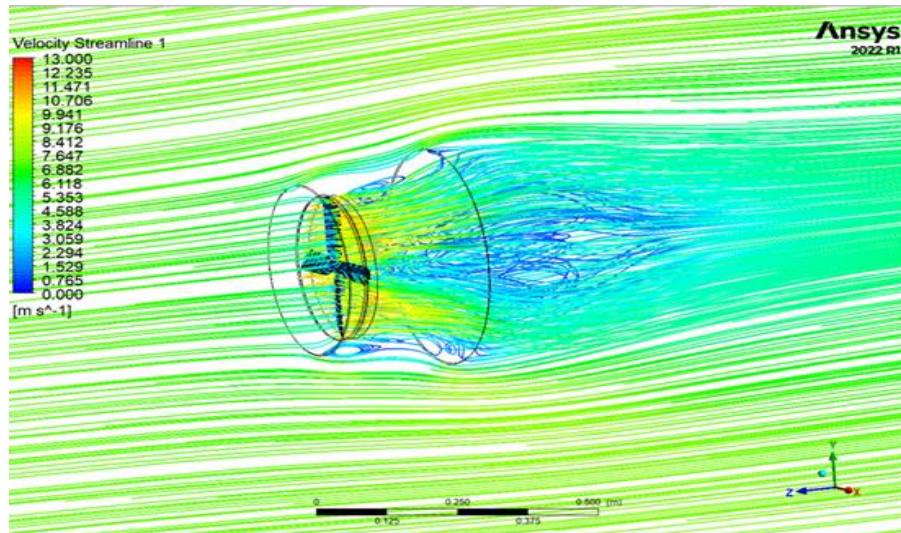
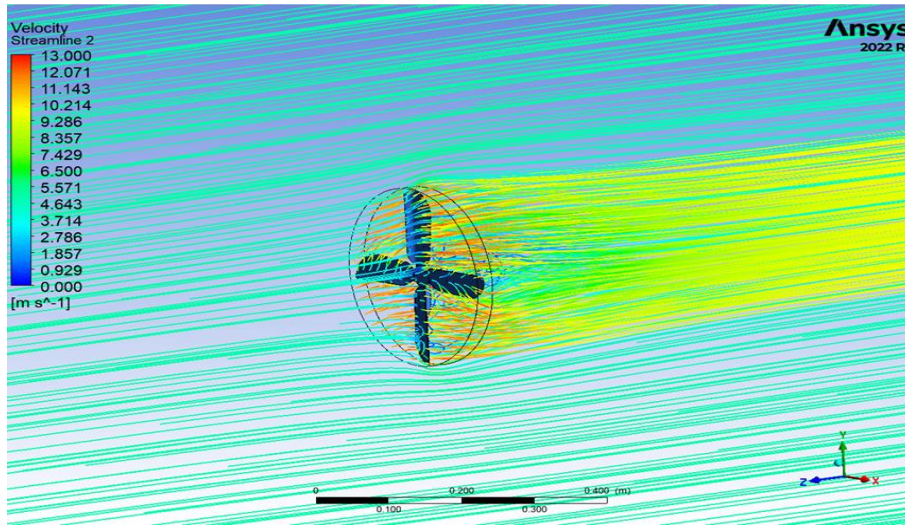
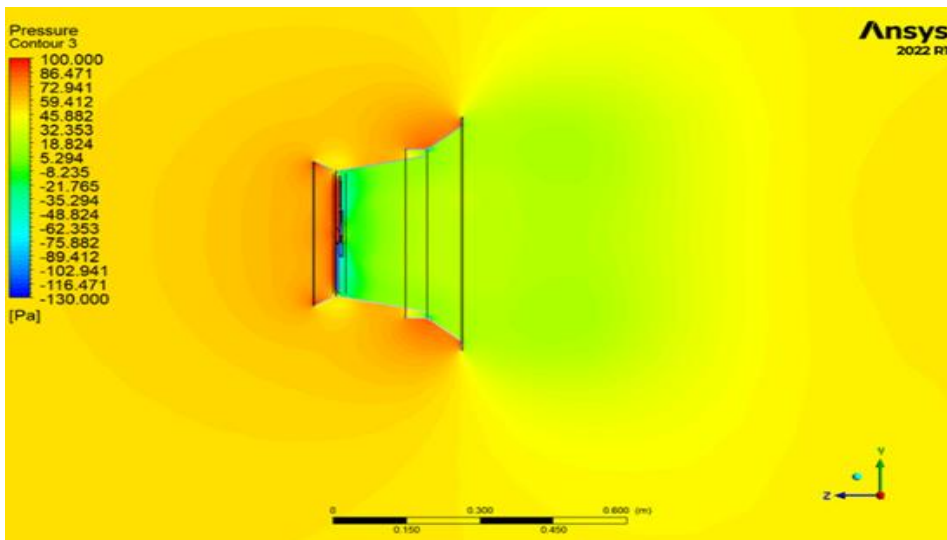
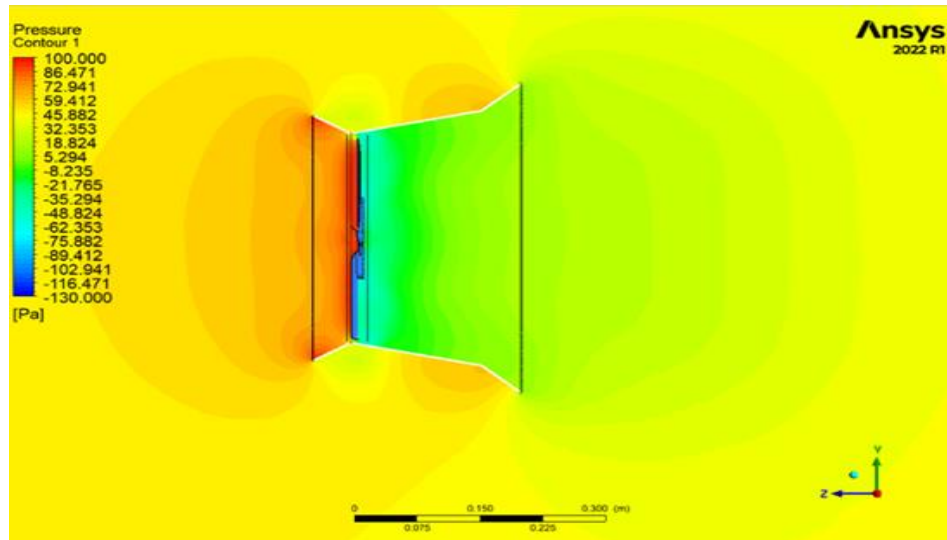
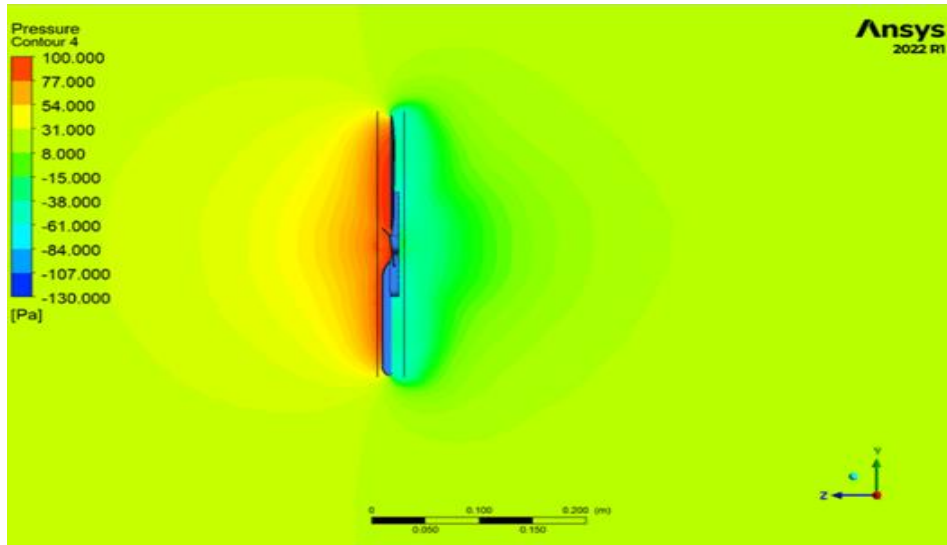


Figure C-3: Pressure contourat upstream wind flow of 5m/s for BHAWT, FDAWT and ESAWT




APPENDIX E

The specifications of measurements equipment


PHOTO/CONTACT TACHOMETER


Model : DT-2268 ISO-9001, CE, IEC1010



FEATURES

- * World's patent. Multi-functions, one instrument combine Photo Tach. (RPM) & Contact Tach. (RPM, m/min, ft/min.).
- * Wide measuring range from 0.5 to 100,000 RPM.
- * 0.1 RPM resolution for the measured value < 1000 RPM.
- * High precision with 0.05% accuracy.
- * The last value, max. value, min. value will be stored into the memory automatically & can be obtained by pressing MEMORY CALL BUTTON.
- * Laser light beam for photo tachometer, long measuring distance.
- * Large LCD display





LUTRON ELECTRONIC The Art of Measurement

PHOTO/CONTACT TACHOMETER


Model : DT-2268

FEATURES	
* World's patent, Multi-functions, one instrument combine Photo Tach. (RPM) & Contact Tach. (RPM, m/min., ft/min.).	* Large LCD display
* Wide measuring range from 0.5 to 100,000 RPM.	* High visible LCD display gives RPM reading exactly with no guessing or errors & saves battery energy.
* 0.1 RPM resolution for the measured value < 1000 RPM.	* This tachometer used the exclusive one chip MICRO-COMPUTER LSI circuit & crystal time base, offer the high accurate measurement & fast sampling time.
* High precision with 0.05% accuracy.	* The use of durable, long lasting components, including a strong, light weight ABS plastic housing, assures almost maintenance free performance for many years.
* The last value, max., value, min. value will be stored into the memory automatically & can be obtained by pressing MEMORY CALL BUTTON.	* The housing cabinet has been carefully shaped to fit comfortable in either hand.
* Laser light beam for photo tachometer, long measuring distance up to 50 cm at least.	

SPECIFICATIONS			
Measurement & Range	Photo Tachometer : 5 to 99,999 RPM.	Photo Tach. Laser light source	* Less than 1 mW.
	Contact Tachometer : 0.5 to 19,999 RPM.	Operating Temperature	* Class 2 laser diode. Red Wave length is 645 nm approximately.
Resolution	Surface Speed : m/min. - 0.05 to 1,999.9 m/min.	Operating Humidity	0 to 50 °C (32 to 122 °F).
	ft/min. - 0.2 to 6,560 ft/min.	Memory	Less than 80% R.H.
Display	RPM: 0.1 RPM (< 1,000 RPM).	Battery	Last/Max./Min. value.
	1 RPM (1,000 RPM).	Power Consumption	4 x 1.5V AA (UM-3) batteries.
Accuracy	m/min.: 0.01m/min. (< 100 m/min.).	Photo type : Contact type :	Approx. DC 153 mA.
	R/min.: 0.1 R/min. (< 100 R/min.).	Size	Approx. DC 10 mA.
Time base	ft/min.: 0.1 ft/min. (< 1,000 ft/min.).	Weight	215 x 65 x 38 mm. (8.5 x 2.6 x 1.5 inch).
	1 ft/min. (1,000 ft/min.).	Accessories Included	240 g (0.52 LB).
Circuit	LCD, size 60 mm x 30 mm. 5 digits with display unit.	Carrying case.....	1 PC.
	± (0.05% + 1 digit).	Reflecting tape marks (600 mm).....	1 PC.
Photo Tachometer detecting distance	Quartz crystal.	RPM adapter (CONE).....	1 PC.
	Exclusive one-chip of microcomputer LSI circuit.	RPM adapter (FUNEL).....	1 PC.
	50 to 500 mm typically.	Surface speed test wheel.....	1 PC.
		Operation manual.....	1 PC.

The DT-2258 had following countries patent & patent pending :
 USA - 4,823,080 GERMANY - G9015492.A, G8708922.0
 TAIWAN - 45478 & other countries patent pending.

* Appearance and specifications listed in this brochure are subject to change without notice. CAT-0209-DT2268



SPECIFICATIONS:

Service: Air and compatible gases.
 Wetted Materials: Consult Factory.
 Accuracy: ±0.5% F.S., 60 - 78°F (15.6 to 25.6°C); 1.5% F.S. from 32 to 60°F and 78 to 104°F (0 to 15.6°C and 25.6 to 40°C).
 Pressure Hysteresis: ±0.1% of full scale
 Pressure Limits: See chart.
 Temperature Limits: 0 to 140°F (-17.8 to 60°C)
 Compensated Temperature Limits: 32 to 104°F (0-40°C)
 Storage Temperature Limits: -4 to 176°F (-20 to 80°C)
 Display: 4-digit LCD (.425 H x .234 W digits)
 Power Requirements: 9 volt alkaline battery. Battery included but not connected.
 Weight: 10.8 oz. (306 g).
 Pressure Connections: Two barbed connections for use with 1/8" or 3/16" I.D. tubing. Two compression fittings for use with 1/8" I.D. x 1/4" O.D. tubing. (for 100 psi or higher pressure ranges)
 Agency Approvals: FM, CE.

MODEL/RANGE CHART

MODEL	PRESSURE RANGES	MAX. PRESSURE
475-000-FM	0-1.000 IN W.C. (0-.2491 kPa)	5 PSI (34.5 kPa)
475-00-FM	0-4.000 IN W.C. (0-0.996 kPa)	5 PSI (34.5 kPa)
475-0-FM	0-10.00 IN W.C. (0-2.491 kPa)	5 PSI (34.5 kPa)
475-1-FM	0-20.00 IN W.C. (0-4.982 kPa)	10 PSI (68.9 kPa)
475-2-FM	0-40.00 IN W.C. (0-9.96 kPa)	10 PSI (68.9 kPa)
475-3-FM	0-200.0 IN W.C. (0-49.82 kPa)	30 PSI (207 kPa)
475-4-FM	0-10.00 PSI (0-.6895 bar)	30 PSI (2.07 bar)
475-5-FM	0-20.00 PSI (0-1.379 bar)	60 PSI (4.14 bar)
475-6-FM	0-30.00 PSI (0-2.069 bar)	60 PSI (4.14 bar)
475-7-FM	0-100.0 PSI (0-6.895 bar)	150 PSI (10.3 bar)
475-8-FM	0-150.0 PSI (0-10.34 bar)	200 PSI (13.8 bar)



BRAND	INGCO
Model no.	DM200
Display	2000 counts
DC Voltage	200mV/2V/20V/200V/600V
AC Voltage	200V/600V
DC Current	20mA/200mA/10A
Resistance	200Ω / 2kΩ/ 20kΩ / 200kΩ / 2MΩ / 20MΩ
Packaging	Packed by Color Box



<https://www.aliexpress.com/item/4001214743522.html?gatewayAdapt=glo2ara>

Motor specifications: 43.9*50.9 MM
 Motor length: 82.7 MM (including front and rear bearing sleeves)
 Output shaft: 8 MM
 Output shaft length: 35 MM (from the front bearing sleeve)
 Motor weight: 507 g
 Motor power voltage: DC 230 V (AC220V rectification)
 Speed: 3400 RPM
 Actual power: around 35 W

When used as a generator: Reference power generation parameters:
 120 rpm: 6V
 240 rpm: 12V
 480 rpm: 48V
 1000 rpm: 96V
 2000 rpm: 192V

الخلاصة:

تعد تكنولوجيا طاقة الرياح ، كما تمثلها توربينات الرياح ، واحدة من أسرع تقنيات الطاقة البديلة توسعاً ، ولا سيما نوع توربينات الرياح ذات المحور الأفقي (HAWT) ، والتي تعد أكثر كفاءة من توربينات الرياح التقليدية الأخرى. ومع ذلك ، نظراً لسرعة الرياح المنخفضة نسبياً في المواقع الحضرية ، فهي أقل استخداماً. نتيجة لذلك ، تزايد الاهتمام بتطبيقات توربينات الرياح الصغيرة في المناطق منخفضة الرياح. الهدف الأساسي من هذا العمل هو تقديم وتطوير كفن HAWT صغير الحجم مناسب لمناطق سرعة الرياح المنخفضة والمتوسطة. تم تطوير مفهوم تقنية توربينات الرياح المعززة بالناشر (DAWT). اشتملت الدراسة على مرحلتين لتحسين الأداء ؛ أولاً ، تطوير تصميم الناشر (BD) عن طريق تحسين المعلمات الهندسية من أجل ضغطها للحصول على نموذج OFD. المرحلة الثانية ، تم تقديم ناشر مع قاذف عن طريق إرفاق OFD (بدون شفة) بقاذف للحصول على كفن يسمى نموذج ODE. تم تطوير نموذج الناشر باستخدام محاكاة CFD التي أثبتت صحة التجربة. من خلال الجمع بين OFD و ODE مع الدوار ، تم إنتاج نموذجين لتوربينات الرياح وهما نموذج FDAWT ونموذج ESAWT ، على التوالي.

تم اختبار نموذجي التوربينات في التجارب والتحقق من صحتها في طرق المحاكاة للتنبؤ بالأداء الديناميكي الهوائي ومقارنتها بنموذج BHAWT. أجريت الدراسة التجريبية في منفاخ هواء مفتوح الحلقة تم تصنيعه. تم إجراء المحاكاة باستخدام نماذج ANSYS R1 بواسطة نماذج CFD ثلاثية الأبعاد بناءً على نموذج الاضطراب SST k- ω . معاملات القوة والعزم والديناميكية الهوائية ، والتي كانت معامل القدرة ومعامل عزم الدوران ، عوامل لتقييم أداء النماذج.

تم الكشف عن الدراسة أن FDAWT التي لديها ناشر شفة بزواوية شفة 50 (OFD) تفوقت بشكل كبير على تكوينات FD الأخرى ، مما أدى إلى زيادة معامل القدرة بنسبة 91.5 % على BHAWT. بالإضافة إلى ذلك ، يتميز FDAWT مع OFD بشكل بسيط وغير مكلف ومضغوط عند مقارنته بتصميمات الفلنجات البديلة. بالإضافة إلى ذلك ، كشفت النتائج أن ESAWT حققت زيادة ملحوظة في معامل القدرة تصل إلى 7.5 % أكثر من FDAWT ، والتي كانت حوالي 98.3 % أكثر مقارنة بـ BHAWT.



دراسة تجريبية ومحاكاة للأداء الديناميكي الهوائي لتوربينات الرياح ذات المحور الأفقي ذات القاذف

رسالة مقدمة الى

قسم هندسة تقنيات ميكانيك القوى في الكلية التقنية الهندسية - النجف - جامعة
الفرات الاوسط التقنية كجزء من متطلبات نيل شهادة الماجستير في هندسة تقنيات
ميكانيك الحراريات

تقدم بها

مهند محمد ناجي

اشراف

الدكتور

بلاس م عبد الامير جبار القرشي

محرم ١٤٤٥